CHARLES UNIVERSITY
Faculty of mathematics
and physics

Critical phenomena and chaos in collective many-body systems

Habilitation thesis

Pavel Stránský

Institute of Particle and Nuclear Physics

Prague 2023

Acknowledgements

I would like to express my gratitude to all my colleagues and friends who have collaborated with me, helped me and shared their valuable experience and ideas, and to the institutes where most of the work of this thesis was carried out, for their hospitality and support. In particular, my thanks belong to Pavel Cejnar, Michal Macek, Michal Kloc, Jakub Novotný, František Knapp and the entire Institute of Particle and Nuclear Physics, Faculty of Mathematics and Physics, Prague, Czech Republic; Alejandro Frank, Irving Morales, Emmanuel Landa, Roelof Bijker, Ruben Fossion, Mirshod Ermamatov, Jorge Hirsch and his fantastic group, and the rest of the staff of the Instituto de Ciencias Nucleares, Universidad Nacional Autónoma de México, Mexico; Lea Santos from the University of Connecticut, USA; Sergio Lerma-Hernández from the Universidad Veracruzana, Mexico; Jorge Dukelsky and Rafael Molina at the Consejo Superior de Investigaciones Científicas, Madrid, Spain; Radim Filip from the Palacký University, Olomouc, Czech Republic; Maia Angelova at the Northumbria University, Newcastle, UK; Laura Muñoz and Alexis Dias-Torres, whom I met at the ECT* institute in Trento, Italy, during my second postdoc; and Milan Šindelka from the Institute of Plasma Physics, Czech Academy of Sciences.

Declaration of Authorship

I hereby confirm that this thesis is entirely my own unaided work. All direct or indirect sources used in its preparation are acknowledged as references. Apart from generating the petty epigraphs introducing each chapter, and employing Grammarly to check English spelling and grammar, no AI was used in writing this thesis.

Contents

Chapter 1

Introduction

What is a critical phenomenon in quantum mechanics, and what are its signatures? How does the criticality affect quantum states, their energies and average density of energy levels, their dynamics when the system's control parameters are varied, and the quantum thermodynamics? What is the connection between quantum criticality and quantum chaos? What are the ways to study quantum chaos in interacting nonintegrable systems that depend nontrivially on tunable parameters, such as the strength of an external field or intensity of internal coupling? And, finally, what shall we learn if we extend the control parameters or other inherently real quantities into the complex domain, making the quantum Hamiltonian non-Hermitian and the energy spectrum complex? I have been working on finding answers to these questions and elaborating the relevant theory during the last decade and this thesis is intended as a concise introduction to the research areas I have contributed to and as a summary of obtained results.

The thesis consists of two parts. The first part is divided into three main chapters (excluding the current introductory chapter and the Summary). Chapter 2 is focused on the critical phenomena in quantum systems, namely on the concept of the Excite-State Quantum Phase Transitions (abbreviated in the text as ESQPTs) as a natural extension of the Quantum Phase Transitions (QPTs). The presence of an ESQPT in the system leads to nonanalytic behaviour in the bulk spectral properties, especially in the smooth level density. The nonanalyticities are related to the stationary points in the classical limit of the quantum Hamiltonian and we expose a general theory of this connection. Besides static consequences imprinted in the spectral singularities, there are also dynamic consequences manifested, for instance, in quantum quench dynamics and parametric driving. Finally, Chapter 2 introduces miscellaneous models to demonstrate the theoretical conclusions and their consequences; the models are also used in later chapters.

Another broad branch of our research is quantum chaos, especially classical-quantum correspondence in chaos theory and the relation between the chaos theory and the presence of ESQPTs in systems whose chaoticity strongly depends both on energy and tunable parameters. This story is told in Chapter 3, the focus being laid on the recent results of the short-time and asymptotic behaviour of the Out-of-Time-Ordered Correlators (OTOCs) and their use as chaos indicators.

The third topic, discussed in Chapter 4, is related to various ways of extending quantum mechanics by introducing non-Hermitian interactions and by complexifying

1

some primarily real quantities. We connect the properties of complex degeneracies in the spectra of non-Hermitically extended Hamiltonians—the exceptional points—to the QPTs, both in bound systems with a discrete spectrum and in systems where the non-Hermiticity models an opening of decay channels into the continuum. We also extend the concept of the ESQPTs into unbound scattering systems, which brings along a nontrivial complex extension of the continuum level density, tightly related with complex phase shift and complex tunnelling time with a surprising classical interpretation.

The second part of this thesis contains 13 appendices that, for better reader comfort, reprint the most relevant publications written by the author. The appendices are referred to in appropriate places throughout the main chapters. All the papers that appear in the apendices have been published in international peer-reviewed journals, primarily in Physical Review journals (19 papers), Journal of Physics A: Mathematical and Theoretical (4 papers), Annals of Physics (3 papers), Physica Scripta (3 papers) and Physics Letters A (2 papers). Note that the Appendices contain selected original papers and do not provide an exhaustive list of publications that the author wrote during the period that the thesis covers; all the author's publications [1–57] (in chronological order) are listed in the List of Author's Publications.

The aim of the main text is not to explain the theory and all its consequences in detail. More likely, it intends to give a comprehensible overview of the research topics, supplemented by facts and bits of information and analyses that have not appeared in the published works. On one hand, it is complementary to the original papers given in the Appendices. On the other hand, it provides enough information and a taster of the author's research interests for those who only have access to the version of the thesis without embedded full versions of the articles in the Appendices.

The work presented here was performed within several working groups and in tight collaboration with other scientists ranging from students and junior researchers to senior researchers and recognised professors. A significant part of the results is a product of my long collaboration with the Instituto de Ciencias Nucleares in the Universidad Nacional Autónoma de México, where I spent two years as a postdoctoral fellow and later another year in a tenure-track position as an academic researcher, working tightly with the groups of Prof. Alejandro Frank and Prof. Jorge Hirsch. Another institution where I spent thirteen months as a postdoc and to which I am grateful for the generous support is the European Centre for Theoretical Studies in Nuclear Physics and Related Areas (ECT*), Trento, Italy. The rest of the work has been done in my alma mater, the Institute of Particle and Nuclear Physics at the Faculty of Mathematics and Physics, Charles University, Prague, in a working group centred around Prof. Pavel Cejnar. I have been working there full-time as an academic researcher since 2014.

Generally, the research summarised in this thesis can be described as purely theoretical, accompanied by extensive numerical demonstrations of the theoretical concepts and numerical analyses of phenomena unavailable to the analytical study. The systems and models employed in our studies are often simple toy models with a few degrees of freedom, whose initial purpose was to describe the essence of collective motion in many-body systems ranging from atomic nuclei and molecules to interacting optical systems, and we have often used them outside the range of their original physical

validity. It needs to be emphasised, however, that this research has become more and more experimentally relevant with the current boom of quantum technologies and quantum simulators (aptly dubbed quantum inspirators [58]) that allow for artificially constructing and measuring systems that behave according to pre-described, and usually simple, Hamiltonians. Possible or actual experimental realisation of the described phenomena will be given at corresponding places in the text.

Chapter 2

Excited-State Quantum Phase Transitions

> Listen up y'all, I got a story to tell
> 'Bout a quantum phenomenon, that's straight outta hell
> Excited-state quantum phase transition, that's the name
> A change so sudden, it's driving physics insane
>
> ——————————————————————————————
>
> ChatGPT, hip-hop style text on ESQPTs

An Excited-State Quantum Phase Transition (ESPQT) extends the concept of a quantum critical phenomenon called a Quantum Phase Transition (QPT). The QPT is related to an abrupt, nonanalytic change in the *ground-state properties* of an isolated bound quantum system at zero temperature, under a change of the nonthermal control parameters $\lambda = (\lambda_1, \ldots, \lambda_n)$, $n = 1, \ldots, N_\mathrm{p}$ (N_p denotes the total number of external tunable parameters) in the infinite-size limit $\mathcal{N} \to \infty$ [59, 60] (the size parameter $\mathcal{N}$ will be introduced in Section 2.1.3). The parameters λ can describe the strength of external fields or variations of internal coupling constants. We shall focus on systems whose Hamiltonians depend linearly on the control parameters,[1]

$$\hat{H}(\lambda) = \hat{H}_0 + \sum_{n=1}^{N_\mathrm{p}} \lambda_n \hat{V}_n, \tag{2.1}$$

where $\hat{H}_0$ is considered a free (non-interacting) Hamiltonian and operators $\hat{V}_n$ characterise perturbations, interactions between the constituents of the system, or interactions with external fields, and does not commute with the free Hamiltonian,

$$\left[\hat{H}_0, \hat{V}_n \right] = 0. \tag{2.2}$$

Often, the main essence of the critical phenomena can be demonstrated in systems with just one control parameter,[2]

$$\hat{H}(\lambda) = \hat{H}_0 + \lambda \hat{V}, \qquad \lambda \in \mathbb{R}. \tag{2.3}$$

---

[1]There will be some exceptions, for example, parameter χ in the Lipkin model (2.37).

[2]Multiparameter Hamiltonians have been a subject of our recent studies on an optimal quantum driving [53, 56].

Another possible and frequently used parametrisation is

$$\hat{H}(\lambda) = \lambda \hat{H}_1 + (1 - \lambda) \, \hat{H}_2, \qquad \lambda \in [0, 1], \tag{2.4}$$

which describes a transition between two different system configurations, each belonging to a different symmetry. The two parametrisations (2.3) and (2.4) are equivalent and can be mapped one onto the other by the simple transformation $\hat{H}_2 \equiv \hat{H}_0$, $\hat{H}_1 - \hat{H}_2 \equiv \hat{V}$.

The QPT occurs at a particular *critical* value of $\lambda \equiv \lambda_c$ and, following the standard Ehrenfest classification of the thermal phase transitions [61] based on the behaviour of the thermodynamic free energy, one can speak about a *first-order QPT* and a *second-order (or continuous) QPT*, if the ground-state function $E_{\text{gs}}(\lambda)$, in the infinite-size and zero-temperature limit of the system, exhibits a singularity in the first or second derivative, respectively [7, 59]. One can also study the behaviour of an order parameter o associated with the expectation value of an operator $\hat{O}$ in the ground state; the order parameter is discontinuous at the first-order QPT and has a discontinuous derivative at the second-order QPT. An example of an order parameter is the magnetisation in the ferromagnetic-paramagnetic phase transition, or the quadrupole deformation parameter in the nuclear shape transitions, given as an example later.

Another prominent feature of the QPTs is a tight gap between the ground state and the first excited state. The gap gets narrower rapidly as the system size grows and closes at $\mathcal{N} \to \infty$, diminishing exponentially in the case of a first-order QPT, and algebraically in a second-order QPT. A quantum level dynamics in a finite system is shown in Figures 2.2 and 2.3 as an illustration of the precursors of the first-order and second-order QPTs, respectively, where the closing gap is obvious. Note that the tight proximity of the states is a significant obstacle to the preparation of a desired quantum state via adiabatic driving, which consists of initiating the system in an eigenstate of the "free" Hamiltonian $\hat{H}_0$ (usually in the ground state), followed by a slow change of the parameters λ into the desired configuration $\hat{H}$. The driving must be sufficiently slow to avoid transitions into excited states, and, roughly, the driving time is proportional to the square of the minimum spectral gap, $T \propto (E_1 - E_{\text{gs}})^{-2}$, as the adiabatic theorem requires. This procedure of state preparation is the essence of the so-called *adiabatic quantum computer* [62].

In order to illustrate the phenomenon of the QPTs in an easily conceivable physical system, consider the shape phase transition in the ground-state deformation of atomic nuclei. A nucleus with a sufficiently high number of nucleons can be approximately described by collective coordinates, in which it is spherical near nuclear magic numbers and becomes deformed when the number of valence nucleons (or holes) is high enough. Hence, the number of valence nucleons can serve as the control parameter, whereas the (quadrupole) deformation parameter plays the role of the order parameter.

There are several pieces of experimental evidence for the nuclear ground-shape transition, two of which are presented in Figure 2.1. Panel (a) shows the two-neutron separation energies

$$S_{2\text{n}}(Z, N) = M(Z, N - 2)c^2 - M(Z, N)c^2 + 2M_{\text{n}}c^2, \tag{2.5}$$

relating masses M of second-neighbouring isotopes with proton number Z and neutron number N and $N - 2$ (M_{n} denotes the mass of the neutron and c is the speed
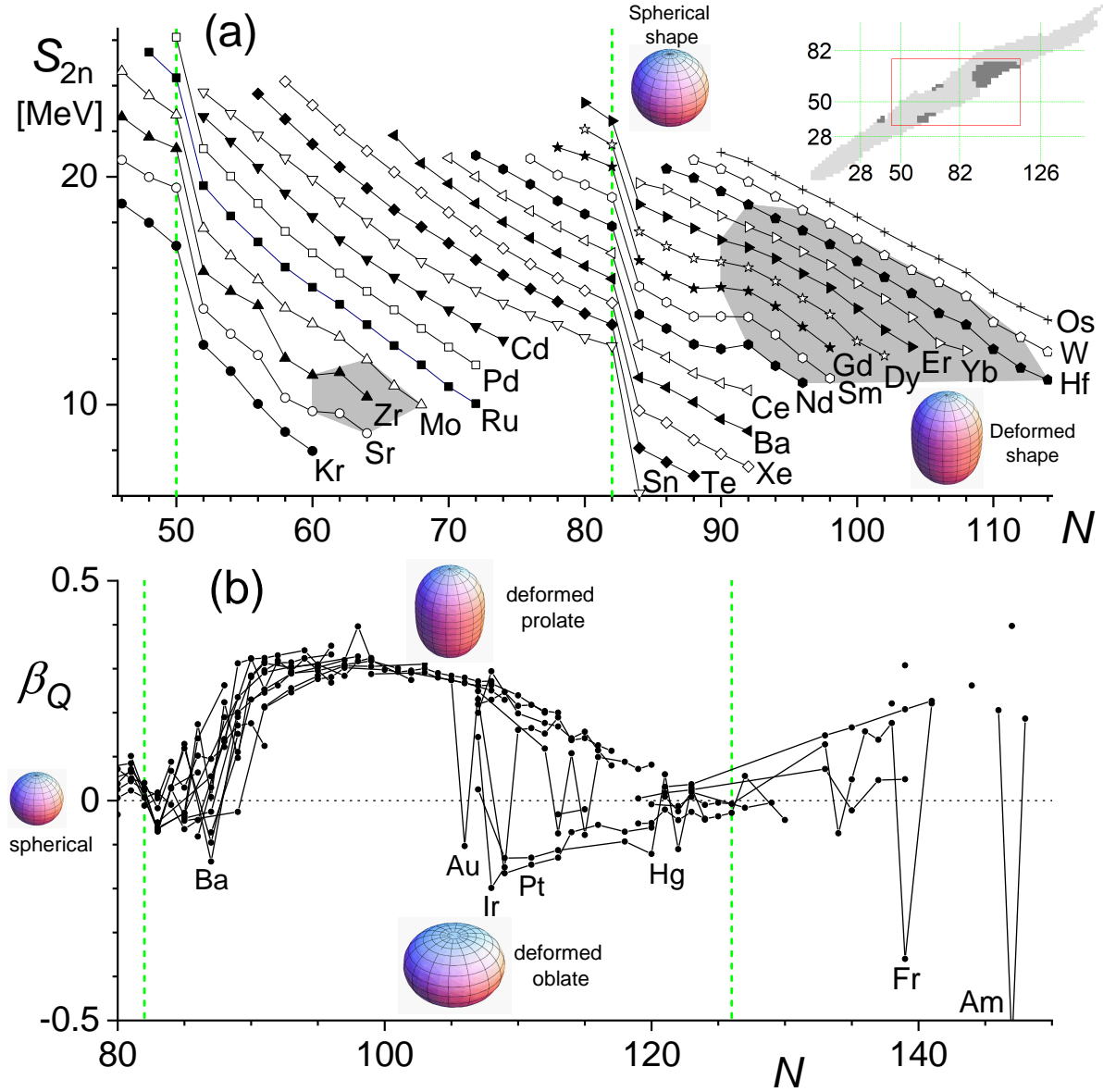
Figure 2.1: (a) Two-neutron separation energies for selected isotopic chains, calculated from the most recent Atomic Mass Evaluation AME 2020 [63, 64]. Regions of well-deformed nuclei are marked by a grey background. The inset indicates the region of the isotopes in the context of the whole nuclear chart. *Adapted from* [35]. (b) Deformation parameter for lanthanide and actinide nuclei. *Adapted from* [23]. The nuclear magic numbers are shown in green dashed lines.

of light). The general decreasing trend is explained by the symmetry term of the Bethe-Weizsäcker formula [65] and the sudden drops at magic numbers by shell effects. However, there are obvious irregularities where the spherical-deformed shape transitions for individual isotopic chains occur (the well-deformed nuclei are highlighted by the grey background) that have been explained by the presence of the shape transition [66].

Panel (b) shows the order parameter—the quadrupole deformation parameter β_Q—

calculated from the experimental electric quadrupole moments Q [67]. One observes an obvious transition from the spherical shapes at the neutron magic number $N = 82$ to the deformed shapes for $N \gtrsim 85$. This spherical-deformed phase transition is often modelled as the second-order QPT, whereas the prolate-oblate shape transition is of the first order with a discontinuous jump in the order parameter; see, for instance, the gold or iridium isotopic chains near $N \approx 110$. Why there are in general much fewer oblate nuclei than prolate, is another important and not yet fully-answered question [23].

A curious reader will find more information in the vast literature on various aspects of the QPTs in nuclei. For reviews and a rich source of original references, see [68] or Chapter 27 of [60]. Note, however, that due to the small number of valence nucleons, only smooth QPT precursors are observed instead of QPT nonanalyticities.

Let us turn now to the excited part of the quantum spectrum. As already mentioned, the ESQPT is an extension of the QPT critical phenomena to the excited domain, usually high above the system's ground state. Since the adequately rescaled energy spectrum in the infinite-size limit $\mathcal{N} \to \infty$ becomes infinitely dense, it is virtually impossible to study the properties of an individual excited state. Instead, it turns out that convenient quantities to study the ESQPT phenomenon are the density of quantum levels $\rho(\lambda; E)$, or more precisely, its smooth part $\bar{\rho}(\lambda; E)$, and the related smooth flow of the spectrum $\bar{\phi}(\lambda; E)$, both properly introduced later in Sections 2.1.1 and 2.1.2. The ESQPT occurs on the *critical borderline* $E_{\mathrm{c}}(\lambda)$ in the $\lambda \times E$ plane. The borderlines often, but not necessarily always, originate in the QPT of the system,[3] see Figures 2.2—2.5, and can be explained by the presence of stationary points in the classical Hamiltonian function (Section 2.1) or by the compactness of the classical phase space (Section C).

As for the history of the ESQPTs, their presence was described for the first time in the Interacting Boson Model [69] (IBM)—a model of collective nuclear motions based on the dynamical algebra u(6)—and later revealed in other algebraic models with $f = 1$ effective number of degrees of freedom [70], where also a firmer theoretical ground of the ESQPTs was established. The first contribution of the author of this thesis was the case study of simple $f = 1$ and $f = 2$ systems [7], which was elaborated, extended and systematised later [29] (reprinted in Appendix A), still for systems with a small number of degrees of freedom. The finite-size effects, manifesting when the characteristic frequencies of motion in individual degrees of freedom are strongly imbalanced, and the relation between the ESQPTs and chaos theory was studied in the follow-up paper [30] (reprinted in Appendix B). A key paper [34] (reprinted in Appendix D and summarised in Section 2.1) offers a rigorous classification of the ESQPT singularities based on the type of stationary points in the system's classical limit and the number of degrees of freedom. Canonical and microcanonical thermodynamics in the presence of the ESQPTs was analysed in [36] (reprinted in Appendix E).

The study of the ESQPTs was later extended to the optical Rabi model and Dicke model of atom-field interaction [37, 38, 52], which have been experimentally realised and extensively tested [71–75]. Within these models, we analysed the quantum quench dynamics [41, 50] and discovered a robust stabilising effect of particular ESQPTs on the quench dynamics [52]. The phase space border in compact systems as another source of

---

[3]Counterexamples are given in this thesis in Section 2.2.4 or Reference [52].

the ESQPT singularities was revealed and discussed in [43] (reprinted in Appendix C). The ESQPT concept was also applied to quantum tunnelling through multibarrier one-dimensional potentials, and the singularities in the complex continuum level density were connected to the singularities in the complex time shift [48, 51] (reprinted in Appendices J and K). Recently, a review has been published by our group [49], which contains updated and the most comprehensive information on ESQPTs and an exhaustive list of references. The latest result in this field is an attempt to find common ground for the ESQPT and the Dynamical Quantum Phase Transitions (DQPTs) [76] by analysing the distribution of zeros of the quantum survival amplitude for times extended into the complex domain [54].

This chapter introduces and summarises the theory of the ESQPTs (Section 2.1), especially their static properties, and demonstrates the manifestations of the ESQPT phenomenon on various systems with $f = 1$ and $f = 2$ degrees of freedom (Section 2.2).

2.1 Theory

Let us consider a bound quantum system with f degrees of freedom described by a time-independent Hamiltonian $\hat{H}(\lambda)$ that depends on a single control parameter λ. The discrete eigenenergies $E_n(\lambda), n = 0, 1, 2, \dots$ of the Hamiltonian are given by the solution of the stationary Schrödinger equation

$$\hat{H}(\lambda) |E_n(\lambda)\rangle = E_n(\lambda) |E_n(\lambda)\rangle, \tag{2.6}$$

where $|E_n(\lambda)\rangle$ are eigenstates corresponding to E_n. The eigenenergies are ordered: $E_n \leq E_m$ for $n < m$. The ground state E_0 will be usually denoted as E_{gs}.

2.1.1 Level density

The level density of the system is generally given by the formula

$$\rho(\lambda; E) = \sum_n \delta(E - E_n(\lambda)), \tag{2.7}$$

where E_n are the discrete eigenenergies of the system (2.6) and δ is the Dirac function. The level density can be written as a sum of a smooth and an oscillatory component [77]

$$\rho(\lambda; E) = \bar{\rho}(\lambda; E) + \tilde{\rho}(\lambda; E). \tag{2.8}$$

The smooth part of the level density $\bar{\rho}(\lambda; E)$ is given by an energy derivative of the Liouville measure of the classical phase space (volume function), attributed as the Thomas-Fermi formula or Weyl formula [78],

$$\bar{\rho}(\lambda; E) = \left(\frac{N}{2\pi}\right)^f \frac{\partial}{\partial E} \int_{H(\lambda; \boldsymbol{x}) < E} \mathrm{d}^{2f} \boldsymbol{x}, \tag{2.9}$$

where $H(\lambda; \boldsymbol{x})$ is the classical limit of the quantum Hamiltonian, $\boldsymbol{x} = (\boldsymbol{q}, \boldsymbol{p})$ specifies a point in the $2f$-dimensional phase space of canonically conjugated positions $\boldsymbol{q}$

and momenta p, and $\mathcal{N}$ is a size parameter of the system (more on that later in Section 2.1.3). In practice, the approximation of the smooth level density can be obtained from the quantum energy spectrum by blurring the δ functions in (2.7), for example, by replacing them with Gaussians of width larger than the local mean level spacing, see Appendices A and B.

The oscillatory level density is given by the trace formulae [79] and is crucial in the semiclassical theory of quantum chaos. Although the oscillations can be pretty wild and become faster with increasing system size, they have a zero mean and hence can be neglected in the $\mathcal{N} \to \infty$ limit.

The smooth component of the level density can develop singularities even if the classical Hamiltonian $H(x)$ is an analytic function on the phase-space manifold $\mathcal{M}$. It turns out that the singularities are caused by the presence of stationary points[4] $s^{(j)}$, $j = 1, \ldots, N_s$, where N_s is the number of isolated stationary points. In the following text, we shall assume that N_s is finite.[5,6]

The stationary points are given by a set of $2f$ algebraic equations

$$\left. \frac{\partial H(x)}{\partial x_k} \right|_{x=s^{(j)}} = 0, \quad k = 1, \ldots, 2f. \tag{2.11}$$

The stationary point at $s^{(j)}$ is called *nondegenerate* if

$$\det \mathsf{h}(s^{(j)}) \neq 0, \tag{2.12}$$

where

$$\mathsf{h}_{kl}(x) \equiv \frac{\partial^2 H(x)}{\partial x_k \partial x_l} \tag{2.13}$$

are the components of the Hessian matrix. Then, according to the Morse theory [80–83], the Hamiltonian function $H(x)$ can be expressed as a quadratic form in a new set of orthogonal coordinates constructed in the vicinity of the stationary point,

$$H_{s^{(j)}}(y) = H(s^{(j)}) - y_1^2 - \cdots - y_r^2 + y_{r+1}^2 + \cdots + y_{2f}^2. \tag{2.14}$$

The integer number $r \in \{0, 1, \ldots, 2f\}$, called *index* of the nondegenerate stationary point, counts the number of the negative eigenvalues of the Hessian matrix.

For a Hamiltonian in the standard form,

$$H(x) = \frac{p^2}{2M} + \mathcal{V}(x), \tag{2.15}$$

---

[4]These points are also called critical points in the literature. To avoid confusion, we shall reserve the attribute *critical* for situations when the system exhibits a critical behaviour at the QPTs or ESQPTs.

[5]Note that in the case of degenerate stationary points, there can even be a continuum of stationary points. An example is the standard-form Hamiltonian with the so-called Mexican hat (champagne bottle) potential

$$\mathcal{V}(x, y) = \left(x^2 + y^2\right)^2 - 2\left(x^2 + y^2\right), \tag{2.10}$$

where the whole unit circle $x^2 + y^2 = 1$ is a minimum of the potential. Still, due to the separability, this kind of stationary point can be counted as one.

[6]The dependence of the Hamiltonian on the external parameter(s) λ is not important here, and hence, for the sake of simplicity, it will not be explicitly written from now on.

quadratic in the momenta and with a potential depending on positions only, it is obvious that $r \leq f$. On the other hand, as we shall see later, in the case of algebraic models constructed from operators of some Lie algebra, the classical Hamiltonian function can be much more complicated, the positions and momenta cannot be separated into kinetic and potential terms, and the index r can range up to $r = 2f$; for an immediate example of such Hamiltonians see Subsections 2.2.3 and 2.2.4 or Reference [52].

Let us now sketch the derivation of the level density singularities connected with a nondegenerate stationary point s of the classical Hamiltonian function $H(x)$. In the vicinity of energy of the stationary point, $E_s \equiv H(s)$, the smooth level density can further be split into a sum of regular and irregular parts,

$$\bar{\rho}_s(\Delta) = \bar{\rho}_s^{\text{reg}}(\Delta) + \bar{\rho}_s^{\text{irr}}(\Delta), \tag{2.16}$$

where $\Delta \equiv E - E_s$ is small. The irregular part $\bar{\rho}^{\text{irr}}$ is calculated by integration over a small phase-space neighbourhood around the stationary point, whereas the regular part captures the smooth contribution to the level density given by the integration (2.9) over the rest of the phase space. Therefore, the nonanalytic properties of the smooth level density are entirely captured in the irregular part of the level density. Note that there may be several isolated stationary points of different types with the same energy, $E_{s^{(j)}} = E_{s^{(k)}}$ with $s^{(j)} \neq s^{(k)}$. However, let us not be bothered by this conspiracy, which will, in the end, lead only to more than one irregular part in the sum (2.16).

The integration of (2.14) can be performed explicitly (see Appendix D), yielding

$$\bar{\rho}_s^{\text{irr}}(\Delta) = \left(\frac{\mathcal{N}}{2\pi}\right)^f \frac{\sigma_{2f}}{2\sqrt{\det \mathsf{h}(s)}} \Theta(\Delta) \Delta^{f-1}, \qquad\qquad r = 0 \tag{2.17a}$$

$$\bar{\rho}_s^{\text{irr}}(\Delta) = \left(\frac{\mathcal{N}}{2\pi}\right)^f \frac{\sigma_r \sigma_{2f-r}}{r(2f-r)\sqrt{\det \mathsf{h}(s)}}$$

$$\times \frac{\partial}{\partial \Delta} \left\{ \Delta^{\frac{2f-r}{2}} \, {}_2F_1\left(\frac{r}{2}, -\frac{2f-r}{2}, 1 + \frac{r}{2}; -\frac{y_-^2}{\Delta}\right)\Bigg|_{y_- = \Theta(-\Delta)\sqrt{|\Delta|}}^{y_- = \sqrt{e}} \right\}, \quad r \neq 0, \tag{2.17b}$$

where $\sigma_d = 2\pi^{\frac{d}{2}}/\Gamma\frac{d}{2}$ is the surface area of a d-dimensional unit ball, Γ is the Euler gamma function, Θ is the Heaviside step function, ${}_2F_1(a, b, c; z)$ is the Gaussian hypergeometric function and e is a sufficiently small energy cutoff. The formulae (2.17) can be further elaborated for r even and odd,

$$\bar{\rho}_s^{\text{irr}}(\Delta) = g_s(\Delta) + C_s \frac{\mathcal{N}^f}{\sqrt{\det \mathsf{h}(s)}} \begin{cases} (-1)^{\frac{r}{2}} \Theta(\Delta) \Delta^{f-1}, & r \text{ even}, \\ (-1)^{\frac{r+1}{2}} \Delta^{f-1} \ln|\Delta|, & r \text{ odd}, \end{cases} \tag{2.18}$$

where g_s is a smooth function and C_s is a positive constant. From the last expression, it can be concluded that the lowest $f - 2$ derivatives of the smooth level density (2.16) are continuous, but the $(f-1)$-th derivative is singular with either an upward (downward) jump for r even and $r/2$ even (odd), or an upward-pointing (downward-pointing) logarithmic divergence for r even and $(r - 1)/2$ even (odd),

$$\frac{\mathrm{d}^{f-1}\bar{\rho}_s}{\mathrm{d}E^{f-1}} \propto \begin{cases} (-1)^{\frac{r}{2}} \Theta(\Delta), & r \text{ even}, \\ (-1)^{\frac{r+1}{2}} \ln|\Delta|, & r \text{ odd}. \end{cases} \tag{2.19}$$

If the system has just one degree of freedom, $f = 1$, the corresponding singularity induced by the nondegenerate stationary point appears in the level density itself and be either an upward jump, a downward jump or an upward-pointing logarithmic divergence.

Note that in some cases, for example in dispersion relations of lattice systems, f can formally attain a half-integer value [34, 84, 85]. Still, Formula (2.17) remains valid and leads to an algebraic divergence at the $\lceil f - 1 \rceil$-th derivative of the smooth level density, where $\lceil \bullet \rceil$ indicates the ceiling function.

The analysis of degenerate stationary points is far more involved and must be treated case by case. A classification can be developed for a particular class of separable stationary points (see Appendix D); unfortunately, they form only a small subset of all degenerate stationary points. The degenerate stationary points are often ignored as being structurally unstable, which means that almost any perturbation of the Hamiltonian transforms them into nondegenerate ones [84]. On top of that, functions with degenerate stationary points make a subset of measure zero in a set of all possible functions.

If a degenerate stationary point does appear in the model, its impact is usually stronger than in the case of the nondegenerate points and can bring the singularities to lower than $(f - 1)$-st derivatives of the level density. An example of a degenerate stationary point is the quartic global minimum, often connected with the second-order QPT, see, for instance, the CUSP model discussed in Section 2.2.1 and shown in Figure 2.3.

2.1.2 Level flow

Instead of analysing the ESQPTs as singularities along the energy axis, we can take advantage of the fact that our system is controlled by the parameter λ and turn from the level density to the properties of the *level dynamics* $E_n(\lambda)$—the dependence of the quantum spectral lines on λ (see, for example Figures 2.2 and 2.3).

Besides the smooth level density $\bar{\rho}(\lambda; E)$ we introduce the smooth *flow rate* $\bar{\phi}(\lambda; E)$ as an average slope of the energy levels at a given point in the $\lambda \times E$ plane. Both quantities are related via the continuity equation

$$\frac{\partial}{\partial \lambda} \bar{\rho}(\lambda; E) + \frac{\partial}{\partial E} \left[\bar{\rho}(\lambda; E) \bar{\phi}(\lambda; E) \right] = 0, \tag{2.20}$$

which guarantees that

$$\int \bar{\rho}(\lambda; E) \mathrm{d}E = 0, \tag{2.21}$$

reflecting the fact that the total number of energy levels is conserved as λ changes (the levels do not appear, split or disappear).

At the critical borderline $E_c(\lambda)(\lambda)$ connected with an ESQPT, the flow rate exhibits also a specific type of singularity. Its type can be derived from the continuity equation (2.20), see Appendix D. It turns out that, apart from some conspiratory cases when either $\bar{\rho} = 0$ or the flow-rate direction is parallel with the critical borderline, the singularity of both quantities at point (λ, E) is of the same type.

If the system is described by the Hamiltonian linear in the control parameter (2.3), then the smooth flow rate is, due to the Hellman-Feynman theorem, related to the average expectation value of the interaction $\hat{V}$,

$$\bar{\phi}(\lambda; E) = \overline{\left\langle E_n(\lambda)\left|\hat{V}\right|E_n(\lambda)\right\rangle}\bigg|_{E\simeq E_n(\lambda)}, \tag{2.22}$$

see Appendix A and Reference [45].

2.1.3   System size

The system size and the appropriate size parameter $\mathcal{N}$ are essential to properly approach the infinite-size limit in which critical phenomena occur. In simple algebraic models, represented, for instance, by the Lipkin u(2) model (Section 2.2.3) and the vibron u(3) model (Section 2.2.4), the system size is naturally quantified by the total number N of excitations, which mathematically corresponds to the label of the fully symmetric irreducible representation of the corresponding dynamical group U(2) and U(3), respectively. In a system obtained by the canonical quantisation of a classical Hamiltonian in the form (2.15), the size parameter is reciprocal to the Planck constant,

$$\mathcal{N} \propto \frac{1}{\hbar}. \tag{2.23}$$

More specifically, a dimensionless quantity is obtained by including the characteristic size and characteristic momentum of the system[7] into the formula:

$$\mathcal{N} = \frac{p_{\mathrm{ch}}q_{\mathrm{ch}}}{\hbar}. \tag{2.25}$$

A more careful approach is necessary if the studied system consists of several coupled subsystems with dramatically different sizes (an extremal case can be the Rabi model, in which a single spin is coupled to an electromagnetic field and the classical limit is performed in the field component only [52], or if the masses or frequencies in individual degrees of freedom are several orders of magnitude from each other, as is discussed in Appendix B.

2.2   Models

This section will present some simple low-dimensional models exhibiting the QPTs and ESQPTs. The list of models archetypal for the ESQPT theory is not exhaustive; the author of this thesis was also involved in studying the quantum criticality in the Dicke model of superradiance [37, 38, 41, 42, 47, 50], in the Rabi model of atom-field interaction [52] or the Interacting Boson Model (IBM) [43] of atomic nuclei, and there

---

[7]Or equivalently by considering the characteristic mass and energy

$$\mathcal{N} = \frac{\sqrt{ME_{\mathrm{ch}}}q_{\mathrm{ch}}}{\hbar}. \tag{2.24}$$

are various other models properly introduced and exhaustively discussed elsewhere, see the reviews on ESQPTs [49, 70]. The main aim of this chapter is to summarise the basic properties of the models used in the papers reprinted in Appendices A—F and L and to demonstrate the most prominent static aspects of the ESQPTs.

2.2.1 CUSP

The CUSP is a $f = 1$ integrable system, whose name originates in the catastrophe theory [86]. It has a standard Hamiltonian in the form (2.15). Its potential reads

$$\mathcal{V}(q) = q^4 - 2Bq^2 + Aq, \tag{2.26}$$

where two tunable parameters are $\lambda = (A, B)$ and the size parameter can be identified with

$$\mathcal{N} = \frac{\sqrt{M}}{\hbar}, \tag{2.27}$$

where M is the mass parameter of the kinetic term and $\hbar$ the Planck constant. As probably the simplest toy model to demonstrate the theoretical concepts of the ESQPTs, it was used firstly in Reference [7] and later in the paper reprinted in Appendix A. A separable multidimensional extension of this model was introduced in the papers reprinted in Appendices D and E.

First-order QPT

If we fix $B > 0$ and vary A, the system exhibits a first-order QPT at $A = 0$. The *level dynamics*—a set of curves $E_n(A)$ connecting individual eigenlevels in the studied range of A values—is shown, for this regime of the CUSP system, in the lower panel of Figure 2.2 by black and grey curves.

First, let us look at the ground state $E_{gs}(A)$, highlighted by a thicker black line. One immediately observes a change of direction (derivative) of $E_{gs}(A)$ at $A = 0$; the derivative $E'_{gs}(A) = \partial E_{gs}/\partial A$ is shown in the inset. This sudden change is a smooth precursor of the first-order QPT; the nonanalyticity—the discontinuous jump in E'_{gs}— will appear only in the infinite-size limit $\mathcal{N} \to \infty$.

Focusing on the excited part of the spectrum, we see that the energy levels flow smoothly far to the left, right and top in the graph of the level dynamics. However, they start to wiggle dramatically as they enter a well-defined approximate triangle in the middle of the graph. One can deduce from the figure that the average level flow and level density suddenly change when the edges of the triangle are crossed.

The edges of the triangle indicate the ESQPTs. Their exact location can be calculated by finding the stationary points of the potential (2.26) and their energies, as described in Section 2.1. The critical triangle is spanned between the spinodal and antispinodal points

$$A_s = \pm\sqrt{\frac{64B^3}{27}}, \tag{2.28}$$

marked in the graph by the red inverse-triangular points. At these points, the potential undergoes a structural change. Outside the critical triangle, it has one minimum only. However, inside the triangle, a pair of a local minimum and a local maximum appears,

Figure 2.2: **Lower panel:** Level dynamics $E_n(\lambda)$ for the CUSP system (2.26) with $B = 1$ and control parameter $\lambda \equiv A$. The ground state $E_{\text{gs}}(A)$ is highlighted by the thick black line; its derivative $E'_{\text{gs}} \equiv \partial E_{\text{gs}}/\partial A$ is displayed in the inset. The red dashed curves indicate the positions of all the local extremes of the classical Hamiltonian function. The red solid curve corresponds with the Hamiltonian global minimum. The first-order QPT is shown by the red bullet. The spinodal points are marked by the red inverse triangles. There are no real crossings of energy levels; all the apparent crossings observed inside the critical triangle are avoided, which is demonstrated by the evolution of the 6$^{\text{th}}$ excited state (yellow line). **Upper panels:** Classical potential (orange colour) and smooth level density (blue colour) for three particular values of the control parameter: $A \in \{-2, 0, 0.5\}$. System size is $\mathcal{N} = 20$.

see the potential plotted by the orange curves in the upper panels of Figure 2.2. The third vertex, highlighted by the red circle, is the QPT point $(A_c, E_c(\lambda)) = (0, -B^2)$, in which both of the potential minima coincide.

The ESQPT critical borderlines are plotted by the dashed red curves in the main panel of Figure 2.2. In the spinodal region $|A| < A_s$, the potential has a double-well structure with a global minimum and a local one separated with a local maximum at $q \approx 0$, $E \approx 0$. When $|A| \geq |A_s|$, however, there is only one minimum and the ESQPT structure is not present.

Due to finite-size quantum effects, the system's ground state is situated slightly above the critical borderlines. However, as the size of the quantum system grows, the ground-state line approaches the critical borderline, and both lines coincide when $\mathcal{N} \to \infty$.[8]

The levels inside the critical triangle form a mesh of seemingly intersecting lines. However, there are no real crossings; all crossings are *avoided* [7] with tight gaps between consecutive levels. The avoided crossings are demonstrated by the yellow curve in the level dynamics of Figure 2.2 indicating the dynamics of the sixth excited state: its evolution is monotonous outside the critical triangle, whereas inside the triangle, it exhibits up-and-down motion from one avoided crossing to another [7]. Note that the avoided crossings can be easily locally modelled by a two-level system with Hamiltonian $\hat{h} = \delta\hat{\sigma}_3 + \lambda\hat{\sigma}_1$, where $\hat{\sigma}_k, k = 1, 2, 3$ are Pauli matrices, $\delta \neq 0$ is the width of the minimal gap and λ the tunable parameter. The width of the gap exponentially diminishes with the height of the barrier separating both wells or with the increase of the system size, as can be explained by the semiclassical Wetzel-Kramers-Brillouin (WKB) approximation of the tunnelling from between the wells, see Appendix F.

All the stationary points of this model are nondegenerate. The minima have index $r = 0$, inducing jumps in the smooth level density, whereas the local maximum, if present, has index $r = 1$, leading to the logarithmic divergence. The smooth level density, calculated by the Thomas-Fermi formula (2.9), is shown by the blue curves for three values of the control parameter $A \in \{-2, 0, 0.5\}$ in the upper panels of Figure 2.2; one can also easily compare the positions of the nonanalyticities on the level dynamics with the positions of the potential stationary points.

The global minimum of the potential is indicated by the solid red curve. As was mentioned earlier, the global minimum corresponds to the ground state in the $\mathcal{N} \to \infty$ limit and its position can hence serve as the QPT order parameter. At the QPT, where both wells are equally deep (see the middle upper panel of Figure 2.2), the order parameter discontinuously changes from $q > 0$ for $A < 0$ to $q < 0$ for $A > 0$, which is consistent with the order of the QPT.

Second-order QPT

If, on the other hand, we fix $A = 0$ and vary parameter B, a second-order QPT is induced at $B = 0$. The level dynamics and the potentials at three values of $B \in \{-0.5, 0, 1\}$ are depicted in Figure 2.3. In this case, the potential is an even function,

---

[8]The same effect is observed in other systems; however, in some systems, the ground state can appear even below the critical borderline, as observed, for instance, in Figure 2.5 for the Lipkin model.

$V(q) = V(-q)$, so the parity is conserved; the even parity levels are drawn in a darker colour than the odd ones.
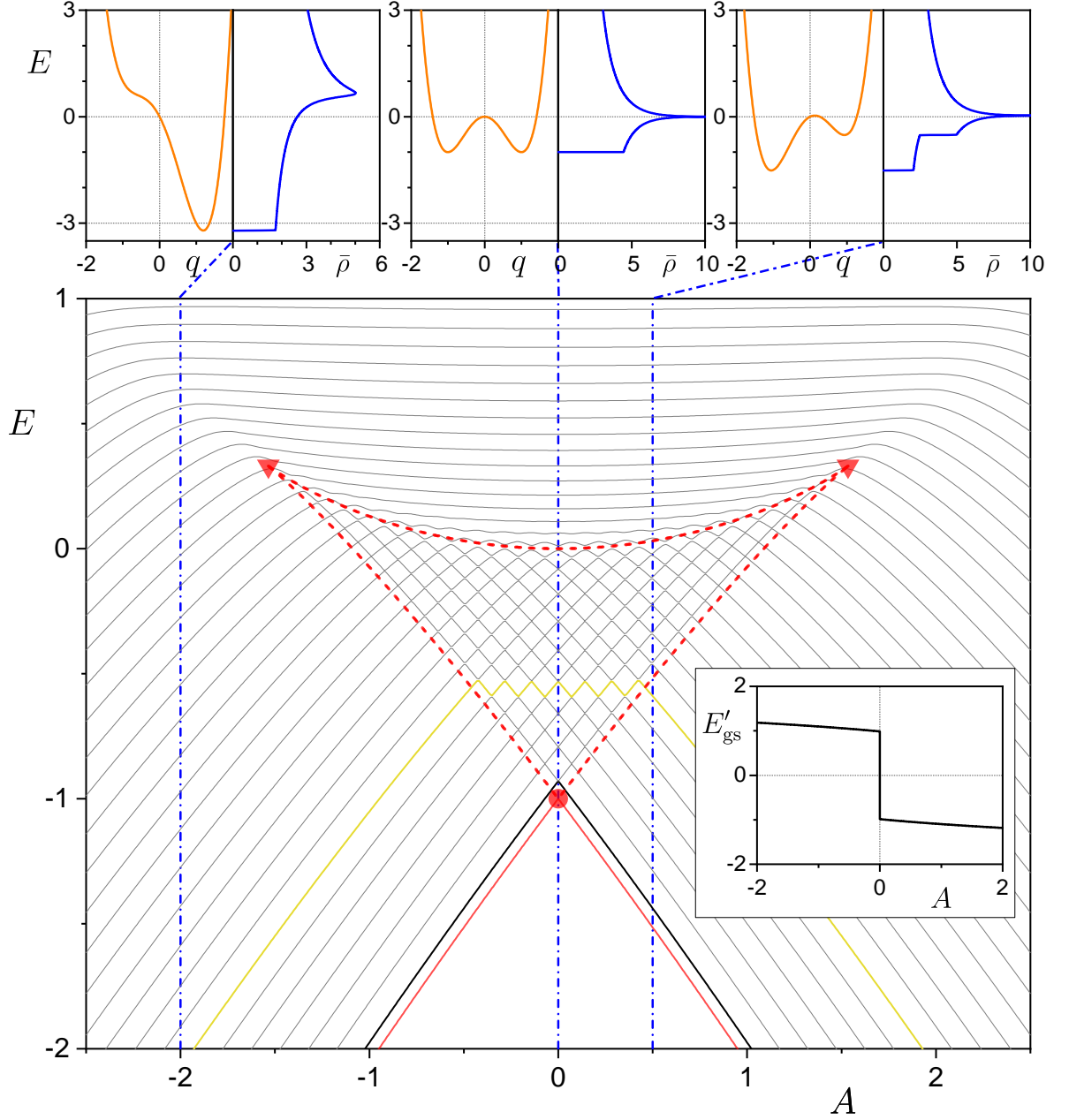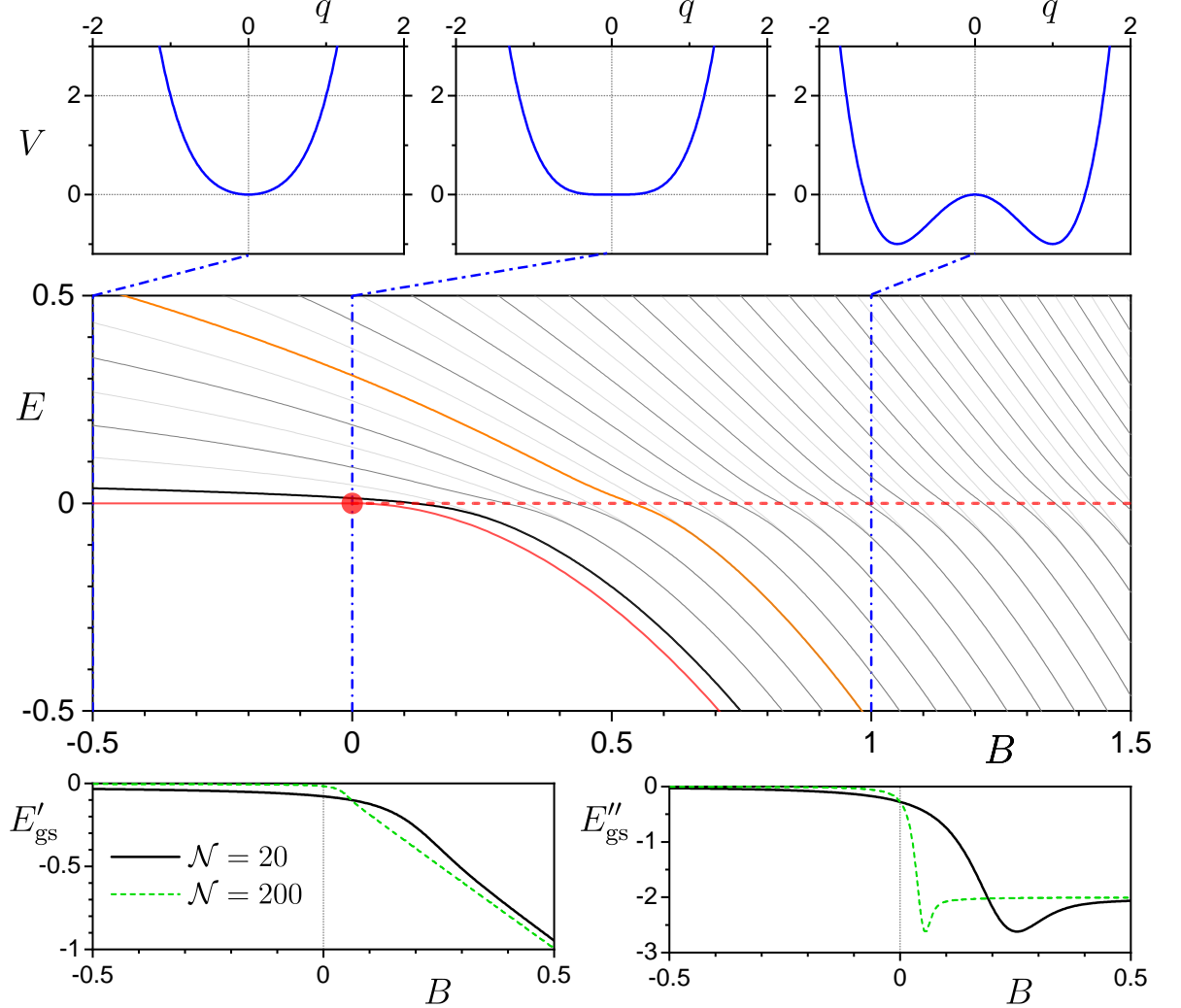

Figure 2.3: **Middle panel:** Level dynamics $E_n(\lambda)$ for the CUSP system (2.26) with $A = 0$ and control parameter $\lambda \equiv B$. The ground state $E_{gs}(B)$ is highlighted by the thick black line. The red dashed curves indicate the positions of all the stationary points of the classical Hamiltonian function. The second-order QPT is shown by the red bullet. States with even (odd) parity are plotted in black (grey). **Top panels:** Classical potential for three particular values of the control parameter: $B \in \{-0.5, 0, 1\}$. System size is $\mathcal{N} = 20$. **Bottom panels:** The first and the second derivative of the ground-state function $E_{gs}(B)$ for two system sizes.

The second-order QPT is often related to the transition from a single-well potential with the global minimum at $q = 0$ (usually called the *normal* or *non-deformed phase*) to a symmetric double-well potential with two equally deep minima at $|q| > 0$ (the *deformed phase*), separated by a local maximum at $q = 0, V = 0$. At the critical point $B_c = 0$, the stationary point of the global minimum is degenerate (quartic); see the middle upper panel in Figure 2.3. The ground-state curve $E_{gs}(B)$ and its first derivative

$E'_{\text{gs}}(B) = \partial E_{\text{gs}}/\partial B$ seem rather smooth; however, the second derivative E''_{gs} exhibit a precursor of a jump at $B = 0$. The jump becomes more prominent towards the infinite-size limit, see the bottom panels in Figure 2.3.

There is an ESQPT at $E = 0$ in the deformed phase, $B > 0$, connected with the local maximum between the two wells, inducing the logarithmic divergence in the smooth level density (see the upper middle panel in Figure 2.2 that corresponds to the same configuration as the upper right panel in Figure 2.3). This ESQPT separates a region of quasi-degenerate parity dublets for $E < 0$, which become fully degenerate in the limit $\mathcal{N} \to \infty$, from a positive-energy region with parity states well separated in energy.

2.2.2 Creagh-Whelan model

This model is a $f = 2$ nonintegrable extension of the simple CUSP model (2.26). It is obtained by introducing a simple harmonic oscillator degree of freedom coupled nonlinearly with the CUSP double-well system. The standard Hamiltonian (2.15) is furnished with potential

$$\mathcal{V}(q_1, q_2) = \left(q_1^2 - 1\right)^{\kappa} - 1 + Aq_1 + \left(Bq_1 + Cq_1^2 + D\right) q_2^2, \qquad (2.29)$$

where $\lambda = (A, B, C, D)$ are external tunnable parameters and $\kappa = 2, 4$. The model was originally introduced for $\kappa = 4$, $A = B = D = 0$, $C = 1$ only, to describe semiclassically the quantum tunnelling in chaotic potentials [87].

The size parameter of the Creagh-Whelan model is given by the same formula as for the CUSP, see (2.27). The critical triangle connected with the first-order QPT is entirely governed by the control parameter A and is also the same as for the CUSP system, provided $\kappa = 2$ (compare the red dashed lines in Figures 2.2 and 2.4). The Creagh-Whelan model in the parametrisation (2.29) is not capable of simulating a second-order QPT.

As for the rest of the parameters in the Creagh-Whelan model, they do not affect the critical behaviour. Parameter B governs the $A \leftrightarrow -A$ asymmetry of the system, parameter C induces higher localization along the q_2 axis, and D localises the system along the q_1 axis.

The key difference between the CUSP and Creagh-Whelan model is the *nonintegrability*, thus chaoticity, of the latter one.[9] The amount of chaos quantified by the classical fraction of regularity f_{reg} is shown in Figure 2.4 by the shades of green; the more intense the colour, the lower f_{reg} and the higher the fraction of the phase-space energy hypersurface filled by chaotic trajectories. Note that despite there appeared some hints that there could be a tight connection between the ESQPT and a regularity-chaos transition in the dynamics, this hypothesis has been disproved [30, 31].

Another important point studied in the Creagh-Whelan model is the approximate separation of individual degrees of freedom, manifesting itself as multiple replicas of the "CUSP-like critical triangles" with increasing excitation energy, see Figure 2.4. These replicas induce oscillations observable in appropriately smoothed finite-size level density. This effect, always present in highly detuned separable integrable systems, *i.e.* systems with a significantly different frequency in each of the degrees of

---

[9]More on chaos is given in Chapter 3, where the fraction of regularity f_{reg} is properly defined.
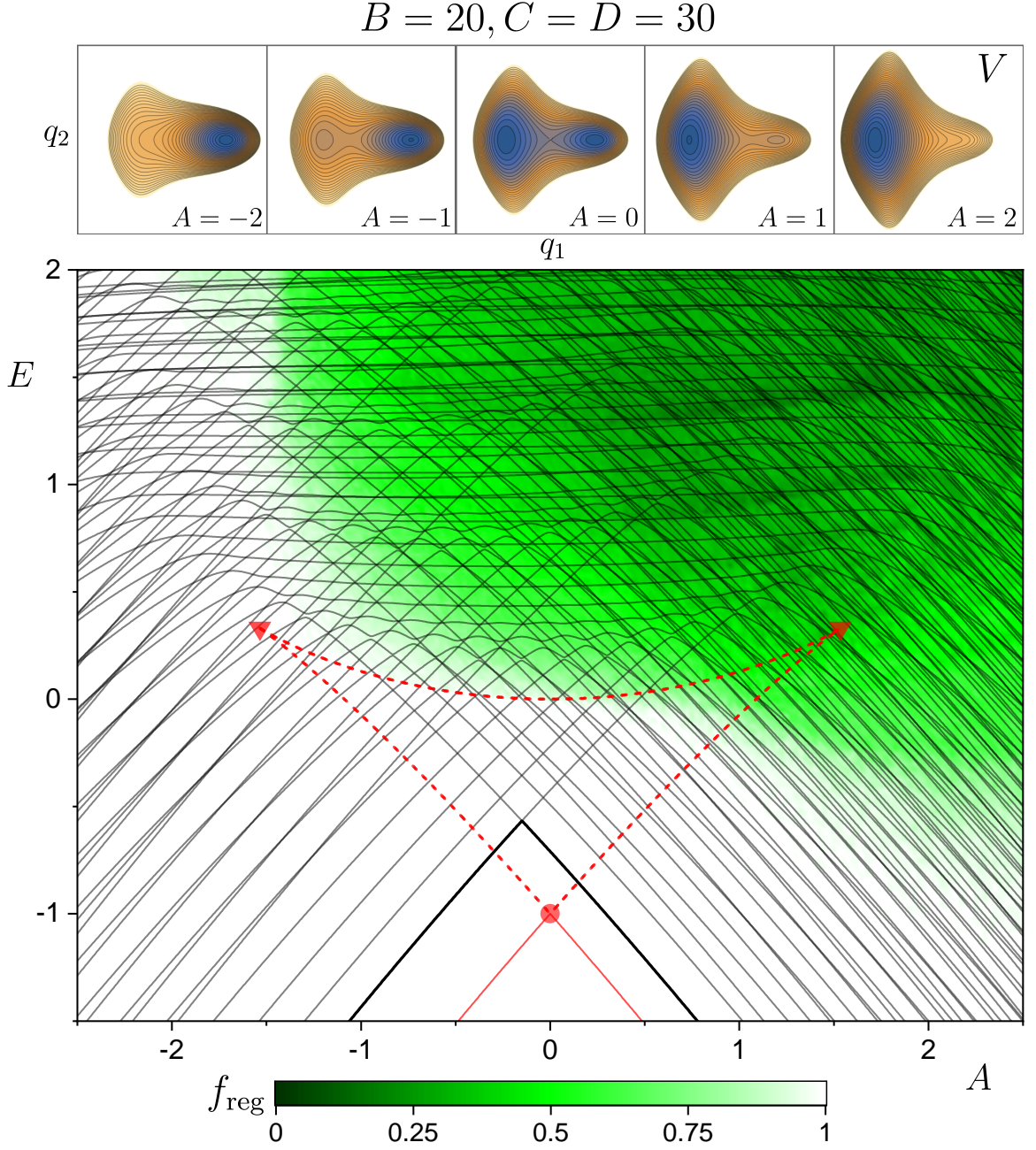
Figure 2.4: **Bottom panel:** Level dynamics $E_n(\lambda)$ for the Creagh-Whelan system (2.29) with $B = 20, C = D = 30$ and control parameter $\lambda \equiv A$. The ground state is highlighted by the thicker line. The first-order QPT is shown by the red bullet. Note that there are no real crossings of energy levels due to the nonseparability of the Hamiltonian; all the apparent crossings are avoided, including the crossings between various excited critical triangles. Positions of all the stationary points of the classical Hamiltonian function are indicated by the red dashed curves. The classical fraction of regularity f_{reg} is shown in shades of green. **Top panels:** Classical potential for five particular values of the control parameter A (blue colour of the density plot corresponds to lower values of the potential). System size is $\mathcal{N} = 12.5$. The

freedom, is rather persistent even when the separability is broken. For more details on the approximate separability see Appendix B. Note also that an ultimate illustration of the model properties is given by a vast amount of numerical results for immense combinations of the control parameters in the author's website [88].

2.2.3 Lipkin-Meshkov-Glick model

The Lipkin-Meshkov-Glick model [89–91], often simply called the Lipkin model, is an algebraic model based on the dynamical u(2) algebra. It was originally introduced as a system of N fermions sitting on two energy levels. Still, it can also describe a bosonic system of two interacting boson excitations or a fully connected set of N interacting two-level subsystems (spins, two-level atoms, etc.), all coupled to the maximum value of the total angular momentum $j = N/2$ [40, 49].

In the boson formalism, the Hamiltonian is constructed from four operators $\hat{\mathfrak{G}}_{kl} \equiv \hat{b}_k^\dagger \hat{b}_l$, $k, l = 0, 1$ that are bilinear products of two independent boson creation and annihilation operators satisfying bosonic commutation relations

$$\left[\hat{b}_j^\dagger, \hat{b}_k\right] = \delta_{jk}, \tag{2.30a}$$

$$\left[\hat{b}_j^\dagger, \hat{b}_k^\dagger\right] = 0, \tag{2.30b}$$

$$\left[\hat{b}_j, \hat{b}_k\right] = 0. \tag{2.30c}$$

The operators $\hat{\mathfrak{G}}_{kl}$ form the u(2) algebra and generate the corresponding U(2) group [92].

The Hamiltonian with one-body terms (describing, for example, an interaction with an external field) and two-body terms (modelling the interaction between the individual excitation in the system) reads

$$\hat{H} = \sum_{kl} c_{kl} \hat{b}_k^\dagger \hat{b}_l + \frac{1}{N-1} \sum_{klps} d_{klps} \hat{b}_k^\dagger \hat{b}_l^\dagger \hat{b}_p \hat{b}_s, \tag{2.31}$$

where c_{kl} and d_{klps} are free parameters; note that they are not completely independent due to the necessary hermiticity condition. The Hamiltonian commutes with the operator

$$\hat{N} = \sum_k \hat{b}_k^\dagger \hat{b}_k, \tag{2.32}$$

of the total number of both types of boson excitations $k = 0, 1$. This helps the theoretical and numerical treatment of the model, as one can fix N (the eigenvalue of $\hat{N}$) and relate it with the size parameter of the system,

$$\mathcal{N} = N. \tag{2.33}$$

The model has thus just $f = 1$ degree of freedom.[10]

---

[10]Another possible interpretation is that the Lipkin model has $f = 2$ degrees of freedom since there are two independent boson excitations. Still, thanks to conserving $\hat{N}$, one can restrict the analysis to one particular subspace of the energy spectrum—a particular representation of the U(2) group.

It is often more convenient to treat this model in the angular momentum formalism. Both the angular momentum formalism and the boson formalism can be related via the Jordan-Schwinger mapping

$$\hat{J}_1 = \frac{1}{2}\left(\hat{b}_1^\dagger \hat{b}_0 + \hat{b}_0^\dagger \hat{b}_1\right), \tag{2.34a}$$

$$\hat{J}_2 = \frac{i}{2}\left(\hat{b}_1^\dagger \hat{b}_0 - \hat{b}_0^\dagger \hat{b}_1\right), \tag{2.34b}$$

$$\hat{J}_3 = \frac{1}{2}\left(\hat{b}_0^\dagger \hat{b}_0 - \hat{b}_1^\dagger \hat{b}_1\right), \tag{2.34c}$$

where $\hat{J}_k, k = 1, 2, 3$ are Hermitian generators of the SU(2) group that satisfy the standard commutation relations for the angular momentum,

$$\left[\hat{J}_k, \hat{J}_l\right] = i\epsilon_{klm}\hat{J}_m. \tag{2.35}$$

The corresponding Hilbert space is spanned over $2j + 1 = N + 1$ states $|j, m\rangle$, $m = -j, \ldots, j$ that are eigenstates of

$$\hat{J}_3 |j, m\rangle = m |j, m\rangle, \tag{2.36a}$$

$$\hat{J}^2 |j, m\rangle = j(j + 1) |j, m\rangle. \tag{2.36b}$$

A particular version of the general Lipkin Hamiltonian (2.31) is the so-called $Q - Q$ *consistent Hamiltonian*, inspired by more sophisticated nuclear algebraic Hamiltonians [93]. It reads

$$\hat{H} = \mathcal{E}\left\{(1 - \lambda)\left(\hat{J}_3 + \frac{N}{2}\right) - \frac{\lambda}{N}\left[2\hat{J}_1 + \chi\left(\hat{J}_3 + \frac{N}{2}\right)\right]^2\right\}, \tag{2.37}$$

where $\mathcal{E}$ is an energy scale, in the theoretical studies usually taken as $\mathcal{E} \equiv 1$ or $\mathcal{E} \equiv 1/N$, and $\lambda \in [0, 1]$ and χ are tunable parameters.[11] When $\chi = 0$, the model can be considered as an infinite-range-interaction limit of a spin chain in a magnetic field,

$$\hat{H} = A\sum_{n=1}^{N}\frac{\hat{\sigma}_3^{(n)}}{2} - \frac{B}{N}\sum_{n<m}\frac{1}{|m - n|^\gamma}\frac{\hat{\sigma}_1^{(n)}}{2}\frac{\hat{\sigma}_1^{(m)}}{2}, \tag{2.38}$$

where $\hat{\sigma}_k^{(n)}$, $k = 1, 2, 3$ are the Pauli matrices corresponding to the spin at the n-th site, A quantifies the interaction of the spins with the external field in the z direction, B is the strength of a two-body interaction between the individual spins, and γ is the range of the interaction: the limit $\gamma \to \infty$ corresponds to the 1D Ising model with nearest-neighbour interaction [94], whereas $\gamma \to 0$ leads to the Lipkin model if one identifies

$$\hat{J}_k = \frac{1}{2}\sum_{n=1}^{N}\hat{\sigma}_k^{(n)}, \quad k = 1, 2, 3. \tag{2.39}$$

---

[11]Note that this Hamiltonian depends *quadratically* on the control parameter χ, so one has to be careful when studying its properties when χ is varied since some part of the theory has been developed under the linearity condition (2.3).

The class of systems with an infinite-range interaction is often called *fully-connected* systems. Note that the dimensionality of the Hilbert space of the fully-connected Lipkin model[12] grows linearly with the size of the system,

$$\dim \mathcal{H}_{\text{Lipkin}} = N + 1, \tag{2.40}$$

in contrast to the exponential dependence of the size in the Ising model

$$\dim \mathcal{H}_{\text{Ising}} = 2^N. \tag{2.41}$$

Therefore, one can reach much bigger effective sizes in the collective dynamics of the Lipkin model than in the Ising model with a local interaction.

The most general Hamiltonian with up to two-body interactions was analysed in [95]. The Lipkin model in a slightly different parametrisation is employed in papers [53, 56].

The classical limit of the Lipkin model (and of any boson models based on a higher $u(n)$ algebra) is achieved by introducing the canonically conjugated coordinates and momenta, $\{\hat{q}_j, \hat{p}_j\}$, $j = 0, 1$ ($j = 0, 1, \ldots, n-1$ for a $u(n)$ model),

$$\hat{b}_j = \sqrt{\frac{N}{2}} \left(\hat{q}_j - i\hat{p}_j \right), \tag{2.42}$$

satisfying the commutation relations

$$\left[\hat{q}_j, \hat{p}_k \right] = \frac{i}{N} \delta_{jk}. \tag{2.43}$$

Hence, the reciprocal value of the system size N can be identified with an effective Planck constant of the system,

$$\hbar_{\text{eff}} \sim \frac{1}{N}, \tag{2.44}$$

and the infinite-size limit $\mathcal{N} = N \to \infty$ coincides with the classical limit $\hbar \to 0$. The next step is to use the conservation of the number of excitations N to eliminate boson $\hat{b}_0$ by a procedure generalising the Holstein-Primakoff transformation [43, 96]. It leads to an effective mapping

$$\hat{b}_0^\dagger, \hat{b}_0 \xmapsto{N\to\infty} \sqrt{2 - (p^2 + q^2)}, \tag{2.45}$$

where the indices are omitted for simplicity, $p \equiv p_1$, $q \equiv q_1$. In the infinite-size limit the operators $\hat{p}_1, \hat{q}_1$ commute, see (2.43), and they can be replaced by continuous variables.

In terms of the quasispin operators $\hat{J}_k$, the mapping is

$$\hat{J}_1 \mapsto \frac{N}{2} q \sqrt{2 - (p^2 + q^2)}, \hat{J}_2 \mapsto \frac{N}{2} p \sqrt{2 - (p^2 + q^2)}, \hat{J}_3 \mapsto \frac{N}{2} \left(p^2 + q^2 - 1 \right), \tag{2.46a}$$

---

[12]One has to restrict oneself to the fully symmetric representation of the U(2) group corresponding to $j = N/2$. This condition must be imposed by hand on the Hamiltonian formulated in terms of the operators $\hat{J}_k$, but it appears naturally if the boson operators are used due to the commutation relation (2.30).

so that the classical limit of the Lipkin Hamiltonian (2.37) reads

$$H(p,q) = \frac{1-\lambda}{2}\left(p^2 + q^2\right) - \lambda\left[q\sqrt{2-(p^2+q^2)} + \frac{\chi}{2}\left(p^2+q^2\right)\right]^2 \qquad (2.47)$$

under the scaling $\mathcal{E} = 1/N$. This way of performing the classical limit leaves us with a compact phase space with the shape of a circle with radius 2,

$$p^2 + q^2 \leq 2. \qquad (2.48)$$

The compactness of the phase space is a consequence of the finiteness of the quantum Hilbert space $\mathcal{H}_{\text{Lipkin}}$. Note, however, that the proper topology of the space is more complicated than a simple circle and is a subject of a current investigation [97].
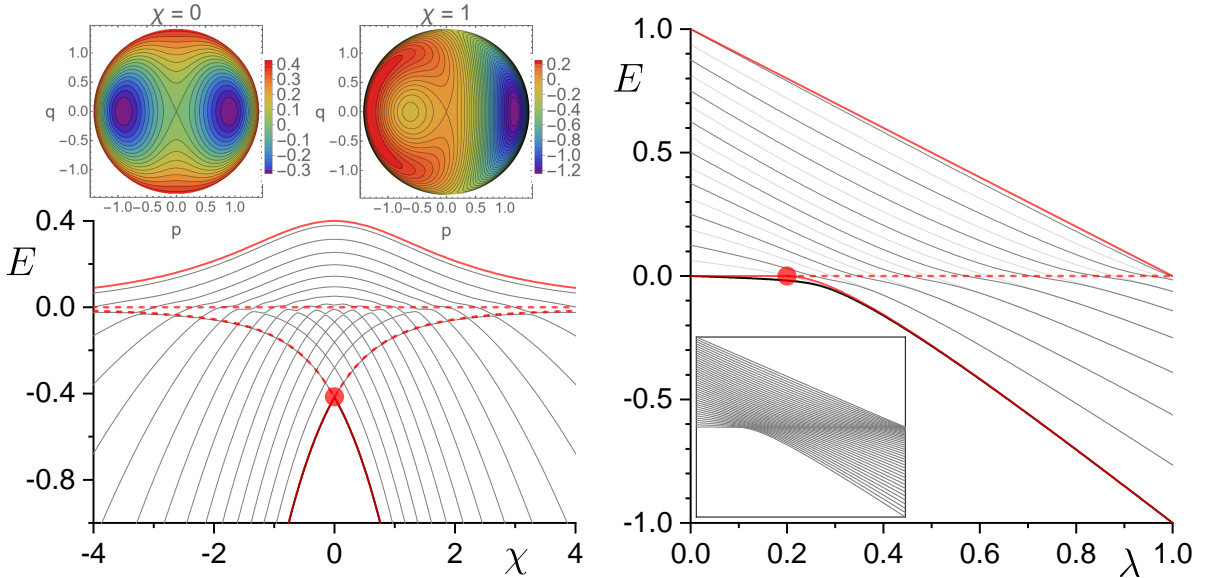

Figure 2.5: Level dynamics $E_n(\lambda)$ of the the Lipkin u(2) model (2.37) with $\mathcal{E} = 1/N$ scaling and system size $N = 16$. **Left panel:** First-order QPT (shown by the red bullet) for fixed $\lambda = 3/5$ and χ varied are shown in the main panel, whereas the equienergy contours of the system's classical limit (2.47) for two values of χ are given in the two top contour plots. **Right panel:** Second-order QPT (shown by the red bullet) for fixed $\chi = 0$ and λ varied. Levels with even (odd) parity are plotted by the black (grey) lines. The red curves show the positions of the stationary points of the classical limit; the solid curves correspond to the global maximum and minimum, and the dashed curves indicate the positions of the local extremes, where also ESQPTs are situated. The inset demonstrates the scaling with system size, $N_{\text{inset}} = 40$ and only even states are shown.

The Lipkin model describes both first- and second-order QPTs and related ESQPTs, as shown in Figure 2.5. The left panel of the figure displays the first-order QPT, which appears at $\chi = 0$ if $\lambda > 1/5$ (in this example, $\lambda = 3/5$ is chosen). The solid red curves correspond to the minimum and maximum of the Hamiltonian. The dashed red curves indicate the stationary points of the classical Hamiltonian, leading the ESQPTs in the infinite-size limit. Note that the spinodal and antispinodal points are at $\chi \to \pm\infty$, in contrast to the CUSP system shown in Figure 2.2. The upper edge of the critical

ESQPT "triangle" is at $E = 0$ and corresponds to the nondegenerate stationary point $(p, q) = (0, 0)$ with index $r = 1$, exhibiting a logarithmic divergence in the smooth level density. The other stationary points are also nondegenerate with $r = 0$ and induce an upward jump in $\bar{\rho}(E)$. Their positions and corresponding energies must be calculated numerically. The classical Hamiltonian (2.47) is shown in the upper subpanels for two values of parameter χ. Note that the phase space is indeed limited to a circle by the condition (2.48).

The right panel of Figure 2.5 shows the second-order QPT, which is obtained for fixed $\chi = 0$ and varying $\lambda \in [0, 1]$. The QPT is occurs for $\lambda_c = 1/5$. The ground state in the infinite-size limit is at $(p, q) = (0, 0)$ and $E_{\text{gs}} = 0$ in the normal phase, $\lambda < \lambda_c$, and decreases with λ as

$$E_{\text{gs}} = -\frac{1}{4}\left(\frac{1}{\lambda} - \frac{1}{\lambda_c}\right)^2 \tag{2.49}$$

in the deformed phase, sitting at $(p, q) = (0, -1/2\sqrt{5 - 1/\lambda})$. The highest-excited state approaches energy $E_{\text{max}} = 1 - \lambda$ in $N \to \infty$ limit. The ESQPT is present in the deformed phase and is connected with the stationary point at $(p, q) = (0, 0)$ of the classical Hamiltonian (2.47), which has index $r = 1$. The inset demonstrates the level bunching at the ESQPT, which becomes visible when the system size is increased.

Note that the level dynamics and the phase structure of the Lipkin model are very similar to those of the CUSP system, *cf.* Figures 2.2 and 2.3, even though the Hilbert space of the Lipkin model is finite, whereas the CUSP's Hilbert space is infinite.

2.2.4 Molecular vibron model

Another model from the class of boson-interacting systems is based on the u(3) *dynamical algebra*. It has been introduced to describe the bending modes of linear polyatomic molecules [98, 99] and since then, it has served both to fit the spectra of simple molecules such as H_2O, D_2O, H_2S, HCN and others [100] and as a toy model to test purely theoretical concepts including the quantum critical phenomena [101, 102]. Recently, the model has also been applied to study the three-state spinor Bose-Einstein condensates [103, 104], experimentally realised by a condensate of cold rubidium atoms [105]. The main advantages of the u(3) vibron model are (i) the finiteness of its Hilbert space (similarly to the Lipkin model), (ii) the existence of the classical limit, and (iii) nonintegrability and the possibility of tuning its chaoticity by varying its parameters. Therefore, it is a suitable model to study the ESQPTs, quantum chaos and the relation of these two concepts.

The u(3) algebra contains *nine* operators $\hat{\mathfrak{G}}_{kl} = \hat{\mathsf{b}}_k^\dagger \hat{\mathsf{b}}_l$, $j, k = 0, 1, 2$ that generate corresponding U(3) symmetry group. The individual boson operators are often called the *scalar boson operator* $\hat{\mathsf{s}} \equiv \hat{\mathsf{b}}_0$ and the *circular boson operators* $\hat{\tau}_\pm \equiv \left(\hat{\mathsf{b}}_1 \pm i\hat{\mathsf{b}}_2\right)/\sqrt{2}$ [99]. Similarly to the Lipkin model, the Hamiltonian (and any other operator constructed from the generators $\hat{\mathfrak{G}}_{kl}$) commutes with the operator of the total number of boson excitations

$$\hat{\mathsf{N}} = \hat{\mathsf{s}}^\dagger\hat{\mathsf{s}} + \hat{\tau}_+^\dagger\hat{\tau}_+ + \hat{\tau}_-^\dagger\hat{\tau}_-. \tag{2.50}$$

The eigenvalue N of $\hat{N}$ specifies the dimensionality of the Hilbert space,

$$\dim \mathcal{H}_{\text{vibron}} = \frac{1}{2}(N+1)(N+2). \tag{2.51}$$

Instead of constructing the Hamiltonian directly from the generators $\tilde{\mathfrak{G}}_{kl}$, it is more convenient to use the independent Camisir operators of all the subgroups of the u(3) dynamical algebra. At the end of the subgroup chains is the *symmetry algebra* reflecting the physical symmetry of the system; the u(3) model often, but not always, conserves the o(2) symmetry.[13] There are three algebra chains in the u(3) model,

$$\text{I} : \text{u}(3) \supset \text{u}(2) \supset \text{o}(2), \tag{2.52a}$$

$$\text{II} : \text{u}(3) \supset \text{o}(3) \supset \text{o}(2), \tag{2.52b}$$

$$\overline{\text{II}} : \text{u}(3) \supset \overline{\text{o}}(3) \supset \text{o}(2). \tag{2.52c}$$

The chains II and $\overline{\text{II}}$ are equivalent, related via a unitary transformation [107].

Similarly to the $Q - Q$ consistent Lipkin model (2.37) we shall consider a Hamiltonian constructed only from two Casimir operators,

$$\hat{H}_0 = \mathcal{E}\left\{(1-\lambda)\,\hat{C}_1[\text{u}(2)] - \frac{\lambda}{N+1}\hat{C}_2[\text{o}(3)]\right\}, \tag{2.53}$$

where

$$\hat{C}_1[\text{u}(2)] = \hat{n}_\tau = \hat{\tau}_+^\dagger \hat{\tau}_+ + \hat{\tau}_-^\dagger \hat{\tau}_-, \tag{2.54a}$$

$$\hat{C}_2[\text{o}(3)] = \hat{\mathbf{D}}^2 = \frac{1}{2}\left(\hat{D}_+\hat{D}_- + \hat{D}_-\hat{D}_+\right) + \hat{l}^2, \tag{2.54b}$$

$$\hat{D}_\pm = \pm\sqrt{2}\left(\hat{\tau}_\pm^\dagger \hat{s} - \hat{s}^\dagger \hat{\tau}_\mp\right), \tag{2.54c}$$

$$\hat{l} = \hat{\tau}_+^\dagger \hat{\tau}_+ - \hat{\tau}_-^\dagger \hat{\tau}_-, \tag{2.54d}$$

are the linear Casimir operator of the u(2) algebra and quadratic Casimir operator of the o(3) algebra, respectively, and $\mathcal{E}$ is an energy scale. The Hamiltonian is in the form (2.4), covering naturally the transition between the u(2) phase (usually called the *symmetric phase*) for $\lambda = 0$ and the o(3) phase (the *deformed phase* or *displaced phase*) for $\lambda = 1$. The quantum phase transition occurs at $\lambda = 1/5$ in the infinite-size limit [101]. The normalising factor $N+1$ in the denominator of the second term, instead of $N-1$ of the general two-body Hamiltonian (2.31) or instead of N in the Lipkin model (2.37), is used to fit the o(3) spectrum into the interval $[0, 1]$.

The system described by the Hamiltonian $\hat{H}_0$ has $f = 2$ degrees of freedom and is integrable; the set of independent integrals of motion consists of the energy and the axial angular momentum $\hat{l}^2$ given by the o(2) Casimir operator. The integrability can be broken by an additional term violating the o(2) symmetry,

$$\hat{H} = \hat{H}_0 - \epsilon D_x, \tag{2.55}$$

---

[13]Models based on higher algebras, such as the u(4) vibron model [106] or the u(6) interacting boson model [93], are invariant with respect to the space rotations reflected in the o(3) algebra.

where $\hat{D}_x = \left(\hat{D}_+ + \hat{D}_-\right)/2$ is the dipole operator. $\hat{H}$ still has a discrete Z_2 symmetry, which must be adequately treated when studying quantum chaos, see Section 3.

The classical limit can be performed by following the same steps as in the Lipkin model. The $\hat{s}$ boson is eliminated via the generalised Holstein-Primakoff transformation, and two pairs of conjugate coordinates and momenta connected with the circular bosons $\hat{\tau}_{1,2}$ are introduced. Then, the limit $N \to \infty$ leads to the Hamiltonian

$$H(p_1, p_2, q_1, q_2) = (1 - \lambda)\frac{s^2}{2} - \lambda \left[\left(p_1^2 + p_2^2\right)\left(2 - s^2\right) + (p_1 q_2 - q_1 p_2)^2\right] - \epsilon p_2 \sqrt{2 - s^2}, \tag{2.56}$$

where

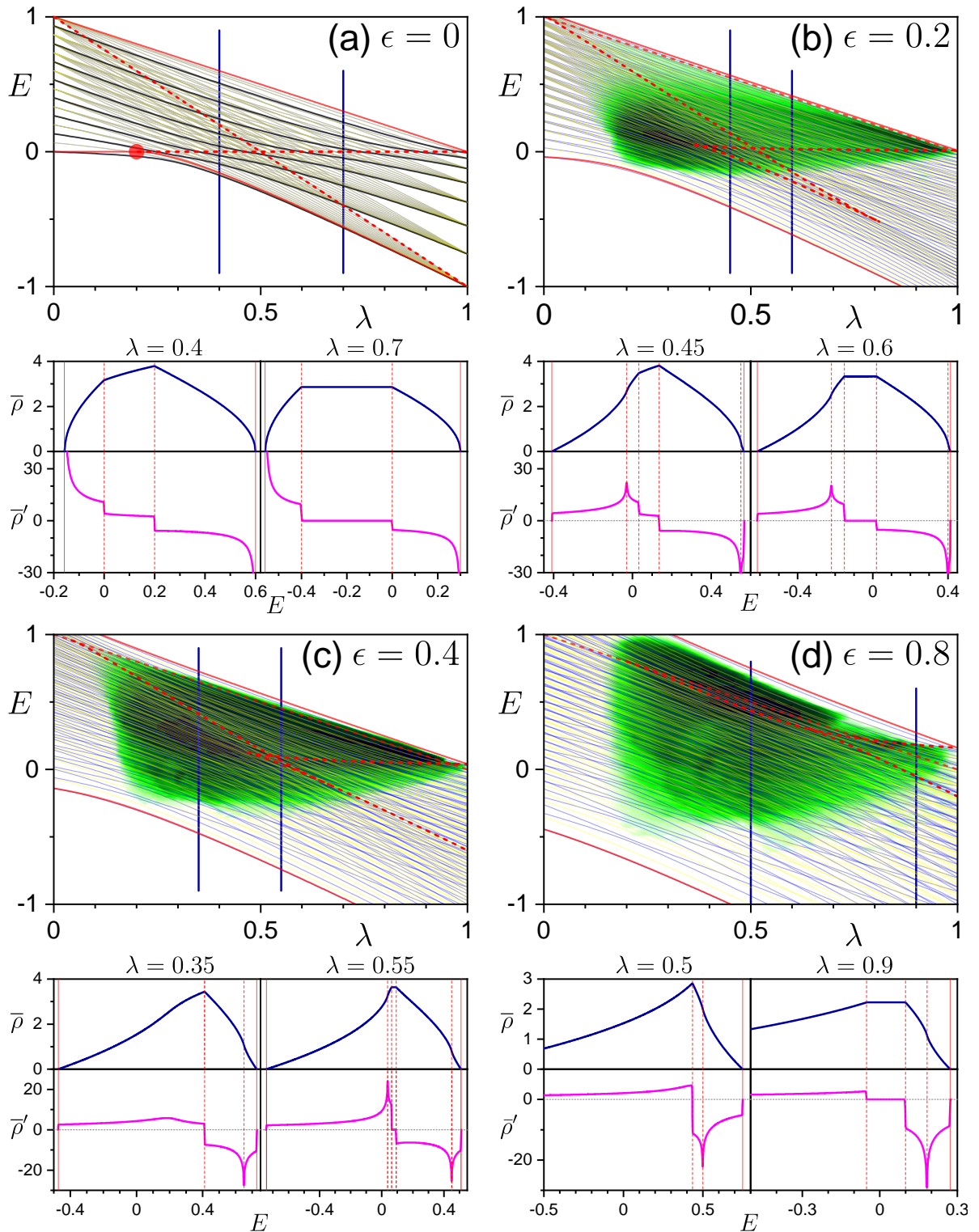$$s^2 \equiv p_1^2 + p_2^2 + q_1^2 + q_2^2 \leq 2. \tag{2.57}$$

The level dynamics and level densities for various values of the nonintegrability parameter ϵ are displayed in Figure 2.6. Panel (a) shows the integrable, hence nonchaotic case $\epsilon = 0$, with the second-order QPT at $\lambda = \lambda_c$. The o(2) symmetry is conserved, so there exists an additional integral of motion given by the Casimir operator of the o(2) algebra $\hat{l}^2$,

$$\left[\hat{H}, \hat{l}^2\right] = 0. \tag{2.58}$$

If restricted to a subspace with a particular eigenvalue of this conserved quantity, usually $\hat{l}^2 = 0$, one obtains a system with effectively $f = 1$ degree of freedom highlighted with the thick black lines in Figure 2.6 (a). This subset of the energy levels is very similar to the Lipkin model with the characteristic bunching of eigenstates along the $E = 0$ ESQPT; see the right panel of Figure 2.5. Only the $\hat{l}^2 = 0$ subset of states is often studied in the literature; see, for example, References [101, 102].

If, on the other hand, one takes all states with all available values of $\hat{l}^2$, the ESQPT structure of the system gets richer. First of all, another ESQPT at $E_2 = 1 - 2\lambda$ appears. Secondly, since the full system has $f = 2$ degrees of freedom, the singularities appear in the first derivative of the smooth level density instead of the level density itself; see the group of four panels below the level dynamics in Figure 2.6 (a) where the smooth level density and its derivative are shown for two values of parameter λ; the λ values for the level density are also indicated by the vertical solid blue lines in the level dynamics panel. Thirdly, the ESQPT at $E_1 = 0$ is not of the logarithmic type but has a shape of the downward jump connected with a nondegenerate stationary point with index $r = 2$. The logarithmic divergence still appears at the ground state in the deformed phase $\lambda > \lambda_c$; however, the corresponding stationary point is degenerate. The new ESQPT at E_2 also manifests as a downward jump in $\bar{\rho}'$ and is related to another nondegenerate stationary point with index $r = 2$. Note that the smooth level density is constant between the ESQPTs E_1 and E_2 after they cross each other, *i.e.*, for $\lambda > 1/2$. Similar behaviour—constant level density for a set of parameter values—is also observed in the algebraic u(6) IBM model, see Appendix C.

When the integrability is broken by setting $\epsilon > 0$, the QPT vanishes, but the ESQPT structure remains and even becomes richer. Two other ESQPT lines appear, one separating from the deformed ground state line and one staying at $E_3 = 1 - \lambda$ where originally, for $\epsilon = 0$, the global maximum was, see Figure 2.6 (b). The first new ESQPT manifests as an upward logarithmic divergence in $\bar{\rho}'$ connected with a

Figure 2.6: Level dynamics $E_n(\lambda)$ and the smooth part of the level density $\bar{\rho}(E)$ and its derivative $\bar{\rho}'(E) \equiv \partial\bar{\rho}/\partial E$ for the algebraic u(3) model (2.55). Blue and yellow lines correspond to the independent subsets of levels due to the Z_2 symmetry. The size of the nonintegrable perturbation ϵ is indicated in the panels. For each value of ϵ, two level densities are plotted. The dashed red lines show the position of the ESQPTs. System size is $N = 16$.

nondegenerate stationary point with $r = 1$. The second new ESQPT—a downward logarithmic divergence in the derivative of the smooth level density—comes from a nondegenerate stationary point with $r = 3$. A detailed analysis of the ESQPTs in the u(3) model is a subject of a current study [97].

Besides qualitatively changing the structure of ESQPT borderlines, the noninte-grable perturbation also introduces chaos in the system, which can be observed in panels (b)—(d) of Figure 2.6. Similarly to the Creagh-Whelan model, the chaoticity is measured by the fraction of regularity f_{reg} and displayed by the shades of green in the background of the graphs. The darker the green colour, the more the system is chaotic. More on chaos, its measures in general and an application of the chaos theory to the vibron u(3) model are given in Section 3 and Appendix L.

2.3 Dynamic signatures

So far, we have discussed the static manifestations of the ESQPTs. However, the presence of the ESQPTs has also consequences in the dynamics induced by non-thermal excitations of the system, which can be achieved by temporal change of the control parameters in the Hamiltonian. The driving can be very fast, approximated by a sudden change in the parameter value and called the *quantum quench*, or slow, nearly adiabatic. We shall focus mainly on the quench dynamics.

Let us suppose we have a system prepared in a state $|\psi_i\rangle$, which is an eigenstate (often the ground state) of a parameter-dependent Hamiltonian (2.3) at λ_i, and then we switch the parameter to another value λ_f. Providing $\left[\hat{H}(\lambda_i), \hat{H}(\lambda_f)\right] \neq 0$, the state $|\psi_i\rangle$ is not an eigenstate of $\hat{H}(\lambda_f)$, so that it begins to evolve with time t. The most straightforward quantity to study is the *survival amplitude*, which is an overlap of the evolved state with the initial one,

$$A(t) = \left\langle \psi_i \left| e^{-\frac{i}{\hbar} \hat{H}(\lambda_f) t} \right| \psi_i \right\rangle, \tag{2.59}$$

and the *survival probability*

$$P(t) = |A(t)|^2. \tag{2.60}$$

The survival amplitude is a Fourier transform of the *strength function*

$$W(E) = \sum_j \left| \left\langle E_j(\lambda_f) | \psi_i \right\rangle \right|^2 \delta(E - E_j(\lambda_f)), \tag{2.61}$$

$$A(t) = \int W(E) e^{-\frac{i}{\hbar} E t} \, dE, \tag{2.62}$$

see Reference [49].

The time evolution of $P(t)$ is rather complicated and can be divided into several regimes [41]: an initial Gaussian decay often followed by an almost periodic series of revivals with algebraically diminishing amplitudes, into an asymptotic regime after the *Heisenberg time* t_H characterised by stationary oscillations with no further qualitative change.

The ESQPTs can affect each of the evolution stages and can have either a stabilising or a destabilising effect based on the particular quench. The effect can be understood by projecting the eigenstates into some kind of wave packets and using semiclassical description, for example by employing the Wigner quasiprobability distribution [108, 109] and its semiclassical approximation called the *truncated Wigner approximation* [110]. The evolution of the initial wave packet is strongly influenced by the stationary points of the classical Hamiltonian $H(\lambda; \boldsymbol{x})$. If a stationary point of the final Hamiltonian is situated exactly where the initial-state wave packet sits at time $t = 0$, the stationary point has a strong stabilising effect. It prevents a part of the packet from leaving the stationary point, so the decay observed in the survival probability is slower and $P(t)$ never reaches values close to zero before the saturation is achieved. If, on the other hand, the after-quench wave packet sits at the energy of the ESQPT stationary point, but the stationary point is located at a different position in the phase space $\boldsymbol{x}$, there is an abnormal gap between $t = 0$ and the first revival, the revivals are suppressed and the transition to the asymptotic regime is faster.

The effect of ESQPTs on various post-quench dynamics has been demonstrated in the Dicke model and its integrable version called the Tavis-Cummings model [41, 50]. It has also been shown that by increasing the quench distance in the parameter λ we can reach a different ESQPT connected with a stationary point of even stabler dynamics so that longer quenches can surprisingly lead to higher survival probability [52].

Note that the survival probability is a key quantity for the Dynamical Quantum Phase Transitions (DQPTs), which occurs when the $P(t) \rightarrow 0$ for $t > 0$ and $\mathcal{N} \rightarrow \infty$. A possible connection between the ESQPTs and DQPTs has been analysed using $P(t)$ extended to complex times [54] and is a subject of current research.

Non-quench driving protocols in systems with ESPQTs are introduced and discussed in review [49].

2.4 Thermodynamic consequences

Due to the existence of the straightforward between the quantum level density, shown to be strongly affected by the ESQPTs, and statistical mechanics, one can expect that a system with ESQPTs will have, to some extent, anomalous thermodynamics. The prominent thermodynamical quantity is the canonical heat capacity

$$C(\beta) = \beta^2 \frac{\partial^2 \ln Z}{\partial \beta^2}, \qquad (2.63)$$

where β is the inverse temperature and

$$Z(\beta) = \operatorname{Tr} e^{-\beta \hat{H}} = \int \rho(E) e^{-\beta E} dE \qquad (2.64)$$

is the canonical partition function, which can be, due to the Thomas-Fermi formula (2.9) semiclassically represented as

$$Z(\beta) = \frac{1}{2\pi\hbar}^f \int e^{-\beta H(\boldsymbol{x})} d\boldsymbol{x}. \qquad (2.65)$$

On the other hand, the microcanonical heat capacity is built on the microcanonical inverse temperature

$$\beta_{\mathrm{m}}(E) = \frac{\partial \ln \rho}{\partial E}. \tag{2.66}$$

This equation, for a given value $\beta_{\mathrm{m}}(E) = \beta$, represents a condition for a vanishing derivative of the canonical thermal energy distribution

$$w_\beta(E) = \frac{\mathrm{e}^{-\beta E}}{Z(\beta)} \rho(E). \tag{2.67}$$

This distribution typically has a single maximum, hence the equation (2.66) provides a unique solution $E(\beta)$ and leads to the microcanonical heat capacity

$$c(\beta) = -\beta^2 \frac{\partial E(\beta)}{\partial \beta} = -\beta^2 \left[\frac{\partial^2 \ln \rho}{\partial E^2} \right]^{-1}_{E=E(\beta)}. \tag{2.68}$$

Canonical (2.63) and microcanonical (2.68) heat capacities are similar, but in the canonical one, there stands the average thermal energy $\langle E \rangle_\beta$, whereas in the microcanonical one the most probable energy $E(\beta)$. In the standard thermodynamics, both $\langle E \rangle_\beta / N$ and $E(\beta)/N$ converge to the same value and the heat capacities $C(\beta)$ and $c(\beta)$ coincide in the infinite-size (thermodynamic) limit $N \to \infty$, $f \to \infty$ [111].

However, a question arises: What happens in the case of collective dynamics when the limit is performed in N only, but f remains fixed (and small)? And, on top of that, What if the system counts with ESQPTs? It turns out that the microcanonical thermodynamics cannot be properly defined if $f \leq 3$ due to the second derivative in (2.68) because a generic ESQPT connected with a nondegenerate stationary point has a singularity in $\partial^2 \rho(E)/\partial E^2$, recall formula (2.19). If the number of the collective degrees of freedom f is higher, $c(\beta)$ becomes smoother and smoother and approaches the canonical heat capacity $C(\beta)$, but there are still significant differences between the two, even for a rather high $f \sim 10$. The ESQPTs induce non-monotonous behaviour with temperature in both heat capacities. Illustrative figures and a more detailed discussion are presented in Appendix E.

It has just been shown that The ESQPTs strongly affect microcanonical thermodynamics, but what about a possible connection between the ESQPTs and the Thermal Phase Transitions (TPTs)? Although there is a relation between these two types of criticality [37, 112, 113], they represent distinct phenomena applicable in different contexts.

Chapter 3

Classical and Quantum Chaos

> Quantum's chaos dances, defying all bounds,
> Uncertainty's frenzy, out-of-time-order resounds,
> Dimensions entangle, their order ablaze,
> Chaos and entanglement, in quantum's cosmic maze.
>
> ——————————————————————————
> ChatGPT, chaotic single-verse poem on quantum chaos

This chapter introduces the essential theoretical background of classical and quantum chaos in physics. Since the topic of chaos in physics and the classical-quantum correspondence was a subject of the author's PhD thesis [114], whose main results were published in two papers [10, 11], the focus here will be mainly on recently developed ideas, which are related to the Out-of-Time-Ordered Correlator (OTOC)—an expectation value of a squared commutator of two quantum observables taken at different times—and its short-time and long-time behaviour. Both of them can serve as quantum chaos indicators, but they are associated with different classical concepts: the short-time evolution is connected with the classical Lyapunov exponent measuring local stability, whereas the OTOC asymptotic value quantifies the overall chaoticity and its classical counterpart would be the relative measure of the chaotic domain in the classical phase space.

The theoretical results will be numerically demonstrated mainly in the vibron u(3) model introduced in Section 2.2.4, and partly also in the nonintegrable Creagh-Whelan model introduced in Section 2.2.2. We shall take advantage of the existence of the classical limit in both models and compare the quantum results with classical measures of chaos.

This chapter begins with a brief introduction to classical and quantum chaos (Sections 3.1 and 3.2), but the emphasis will be laid on the OTOCs (Section 3.3) and a short discussion on the connection between the ESQPTs and chaos (Section 3.4). If the reader wants to learn more about chaos theory, plenty of excellent monographs are available on the market [77, 79, 115, 116].

3.1 Classical chaos

Before we dive into the area of chaos in quantum mechanics, let us summarise the basic concepts of a much more firmly and rigorously established discipline of classical chaos.

Classical mechanics is deterministic: the future (and also the past) of a closed macroscopic system is given by a solution of deterministic differential equations of motion, either the Hamilton equations in nonrelativistic mechanics or the Einstein field equations in general relativity. This means that, in principle, it is possible to calculate the exact state $x(t)$ of the system at any time t, provided we know the exact positions q_i and canonically conjugated momenta $p_i, i = 1, \dots, f$ of all its f constituents at any other time t_0; f is the number of degrees of freedom and

$$x \equiv \left(q_1, \dots, q_f, p_1 \dots, p_f \right) \tag{3.1}$$

specifies a point in the phase space. However, in practice, this task turns out to be unfeasible. The devil working against our god-like capabilities is hidden in the word "exact". In the real world, there is always a finite precision of every measurement, and, on top of that, the numerical differential-equation solvers offer only limited accuracy. All errors caused by the imprecision of our methods and measurements grow, as a rule, exponentially with time, which prevents us from making predictions for long into the future.

3.1.1 Lyapunov exponent

The prerequisites for the presence of classical chaos in the system are three [79]:

1. *Topological transitivity (mixing)*, which says that each trajectory in the phase space passes, at some time, through an arbitrary open neighbourhood of a given point.

2. *A dense set of periodic orbits*, which means that an open neighbourhood of each point x in the phase space is visited by a periodic trajectory, *i.e.,* a trajectory satisfying $x_p(t) = x_p(t_0), t \neq t_0$.

3. *The sensitivity to initial conditions*, which states that any, however tiny, deviation δx from the initial vector $x_0 \equiv x(t_0)$ grows so fast that in a relatively short time, the deviation exceeeds the characteristic dimensions of the phase space. More specifically, the divergence is exponential,

$$\delta x(t) \sim \delta x_0 \, e^{\lambda_{cl}(t-t_0)}, \tag{3.2}$$

and the divergence rate is quantified by the *Lyapunov exponent* λ_{cl}, rigorously defined as

$$\lambda_{cl}(x) = \lim_{t \to \infty} \lim_{|\delta x_0| \to 0} \frac{1}{t} \log \frac{|\delta x(t)|}{|\delta x_0|}, \tag{3.3}$$

where $|\bullet|$ is a norm in the phase space. The inverse value of the Lyapunov exponent, the *Lyapunov time*

$$t_L \equiv \frac{1}{\lambda_{cl}}, \tag{3.4}$$

which estimates the time (or the time order) up to which the solution of the equations of motion makes sense.[1,2]

It is the sensitivity to the initial conditions quantified by the Lyapunov exponent that has become the prominent signature of classical chaos and has been poetically dubbed *the butterfly effect* [120], reflecting the fact that some minor perturbation as tiny as a flap of butterfly wings can, at later times, have a major effect and produce extreme conditions, such as a tornado.

The stability of a trajectory is a *local property*, meaning that it can vary with the initial conditions, even if their energies are the same. The energy hypersurface of the phase space is covered, in general, by a chaotic sea of exponentially unstable trajectories (an infinite countable subset of them are periodic as a consequence of point 2 given above), from which islands of regular (stable) dynamics rise.[3] The neighbouring regular trajectories diverge at most polynomially and their Lyapunov exponent vanishes ($\lambda_{cl} = 0$). Due to topological reasons, in compact systems with $f \geq 3$ degrees of freedom and no additional constant of motion besides the energy, there is only one connected chaotic "ocean" in the phase space in which all the trajectories have the same Lyapunov exponent [124]. Note that the coastal region of the regular islands can have a fractal structure with intermittently stable and unstable dynamics (called the stickiness effect [125]), which can result in the nonexistence of the limit (3.3).[4] For numerical studies, however, it is not a big obstacle because due to the finite precision and due to the time cutoff t_{max} in which the Lyapunov exponent (3.3) is computed, the trajectory will always be classified as either regular or chaotic based on an arbitrary suitable numerical threshold, and the calculated value of the exponent will always be determined with some statistical error.

3.1.2 Fraction of regularity

Apart from the Lyapunov exponent λ_{cl}, which describes a local property of the phase space, one can study the chaoticity of the whole energy hypersurface Σ_E of the phase space (*global property*). If $\Gamma_{reg}(E)$ is the volume of all the regular regions in Σ_E, *i.e.*, regions with $\lambda_{cl} = 0$, and

$$\Gamma(E) = \int d^{2f}\boldsymbol{x}\,\delta(E - H(\boldsymbol{x})) \tag{3.5}$$

is the entire volume of Σ_E, then the *fraction of regularity* [10]

$$f_{reg}(E) = \frac{\Gamma_{reg}(E)}{\Gamma(E)} \in [0, 1], \tag{3.6}$$

reflects the overall chaoticity of the system with energy E, ranging from $f_{reg} = 0$ for a completely chaotic case to $f_{reg} = 1$ for energies with fully stable dynamics.

---

[1]This statement follows from the fact that we never know the initial state with a precision higher than several digits.

[2]As an example, the upper limit for the Lyapunov time of the Solar system has been numerically determined as $t_L \approx 2\,Myr$ [117–119].

[3]The exact topology is given by the Kolmogorov-Arnol'd-Moser (KAM) theorem [121–123].

[4]Although a completely different effect, natural coastlines also have a fractal structure and even led to the definition of the notion fractal [126] and is still a subject of active research [127].

The fraction of regularity generally depends on the energy. A system is usually regular close to its ground state because a global minimum of a generic Hamiltonian with f degrees of freedom can be expanded into a quadratic form of $2f$ independent (separable) harmonic oscillators (recall the Morse lemma in Section 2.1). When the energy increases and the system gets further from the domain of validity of the harmonic approximation, nonlinear coupling between individual degrees of freedom causes the regularity to be broken. However, the decrease of regularity may not be final: in asymptotically bound systems whose Hamiltonians satisfy the condition

$$\lim_{x_j \to \pm\infty} H(\boldsymbol{x}) \to \infty \quad \forall j = 1, \ldots, 2f \tag{3.7}$$

there can exist a term in the Hamiltonian that becomes dominant at high energies, and that leads again to regular dynamics [10].

3.1.3 Classical integrability

Even though a generic system is chaotic, there are exceptions with fully regular dynamics called *integrable systems*. These systems have enough functionally independent integrals of motions $I_j(\boldsymbol{x})$ that are functions of phase space coordinates and remain constant along a trajectory $\boldsymbol{x}(t)$. Their Poisson brackets with the Hamiltonian $H(\boldsymbol{x})$ vanish, as well as their mutual Poisson brackets,

$$\{I_j, H\} = 0, \tag{3.8a}$$

$$\{I_j, I_k\} = 0; \tag{3.8b}$$

it is said that the integrals of motion are in involution. If there are f integrals of motion in involution (the Hamiltonian can be one of them), then the system is integrable. It can be canonically transformed[5] into the *action-angle coordinates* (J_j, θ_j), $j = 1, \ldots, f$, in which the Hamiltonian depends solely on the actions, $H = H(J_1, \ldots, J_f)$. The corresponding Hamilton equations and motion are trivial, as well as their solution

$$\theta_j(t) = \omega_j(t) + \theta_j(0), \tag{3.9a}$$

$$J_j(t) = J_j(0), \tag{3.9b}$$

where

$$\omega_j(t) \equiv \frac{\partial H}{\partial J_j} \tag{3.10}$$

are f frequencies associated with the motion in individual degrees of freedom. Therefore, the motion occurs on a manifold with the topology on an f-torus, it is solvable and stable.

The integrals of motion are always connected with an additional symmetry of the system. Note that there can be even more integrals of motion than the number of degrees of freedom. Such systems are called *superintegrable* [129].

---

[5]Note that there can be situations where the transformation does not exist related to the phenomenon called *monodromy* [128].

3.2 Quantum chaos

The notion of quantum chaos was initially related to particular correlations in the energy spectrum [77]. It was conjectured [130] that bound systems whose classical counterparts are regular have uncorrelated quantum energies, whereas subsets of eigenenergies of quantised fully chaotic classical systems have correlations described by spectra of the Gaussian random matrices [131]; the states in each subset must have the same values of additional conserved quantities, such as the angular momentum or parity. The correlations manifest as the repulsion of quantum levels (if one studies the nearest-neighbour correlations [130]), the spectral rigidity (in the long-range correlations [132]), antipersistence (in $1/f$ studies of time series constructed from the quantum spectrum [133]), or a particular distribution of the eigenstates components [134]. The presence of spectral correlations has even served as a (somewhat controversial) definition of quantum chaos [135] useful especially in situations when the quantum system does not have a classical counterpart.

3.2.1 Quantum integrability

In accord with the classical integrability, a quantum system with f degrees of freedom is called integrable when there exist f independent operators $\hat{I}_J$ including the Hamiltonian $\hat{H}$ that satisfy

$$\left[\hat{I}_j, \hat{H}\right] = 0, \tag{3.11a}$$

$$\left[\hat{I}_j, \hat{I}_k\right] = 0. \tag{3.11b}$$

Operators $\left\{\hat{I}_1, \ldots, \hat{I}_f\right\}$ form a complete set of commuting operators and the basis of the corresponding Hilbert space $\mathcal{H}$ can be formed from mutual eigenstates $\left|n_1, \ldots, n_f\right\rangle$ of all these operators,

$$\hat{I}_j \left|n_1, \ldots, n_f\right\rangle = n_f \left|n_1, \ldots, n_f\right\rangle, \tag{3.12}$$

where n_j is an eigenvalue of $\hat{I}_j$. Therefore, there is no correlation between states belonging to different eigenvalues of any of the constant of motion $\hat{I}_j$. On the other hand, if there are not enough integrals of motion, the Hamiltonian consists of blocks that must be diagonalised, and the diagonalisation induces eigenlevel correlations.

Let us remark that the definition of quantum integrability, in contrast to the definition of integrability in classical mechanics, is not flawless. The functional independence of the constants of motion is meaningless in quantum mechanics, which makes it impossible to separate quantum systems into two disjoint sets with different properties (integrable and non-integrable) and to define chaos in quantum mechanics axiomatically [136]. Indeed, there are examples of systems that are classically integrable, but chaotic in quantum mechanics, and vice versa [137, 138].

3.2.2 Spectral correlations

The field of quantum chaos started developing with the work of Eugene Wigner in the 1950s. He noticed a lack of close nuclear resonances in the high-lying part of

measured spectra and he dared to explain it not as a consequence of an imperfection in the measuring techniques, but by an application of the Random Matrix Theory (RMT) [139–141]. He formulated a hypothesis today known as the *Wigner surmise*:

> Suppose we have a complicated and complex system with an (often high) unknown number of degrees of freedom (such as a highly excited atomic nucleus and we do not know anything about the interaction among the constituents. The only thing we know about the Hamiltonian is the symmetry it satisfies (rotational invariance, time-reversal invariance etc.). Then a sequence of consecutive energy levels with the same spin and parity will have the same statistical properties as the spectrum of a random matrix whose elements are independent numbers taken from the Gaussian normal distribution. Levels of different spin and parity are not correlated.

He also derived the probability distribution of the distances between adjacent eigenlevels $s_j = E_{j+1} - E_j$, called the Nearest-Neighbour Spacing Distribution (NNSD),

$$p_W(s) = \frac{\pi}{2} s \, e^{-\frac{\pi}{4} s^2} . \tag{3.13}$$

The spectrum is normalised in such a way that the mean level spacing is one,

$$\langle s \rangle = \int s p_W(s) \mathrm{d}s = 1. \tag{3.14}$$

The transformation that achieves such normalisation by removing the smooth part of the level density $\bar{\rho}$, keeping just the oscillating part $\tilde{\rho}$ (see also Section 2.1.1), is called the *unfolding* [131].

The Wigner distribution (3.13) predicts zero probability of finding very close levels with $s \approx 0$, in contrast with the distribution of uncorrelated independent energies given by the Poisson formula

$$p_P(s) = e^{-s} . \tag{3.15}$$

This was in accord with the observed level repulsion between the nuclear resonances.

Finally, the connection between the spectral correlations and chaos was established in the already mentioned *Bohigas-Giannoni-Schmit conjecture* [130]:

> All quantum systems whose classical analogues are chaotic exhibit the same spectral fluctuation properties as predicted by the theory of random matrices. On the contrary, quantum systems with stable classical analogues (not necessarily integrable) have uncorrelated energy levels.

Note that the unfolding procedure is delicate and, to a great extent, arbitrary, usually based on a polynomial fitting. Performed carelessly can lead to erroneous conclusions [142]. Therefore, there has been a lot of effort to improve the unfolding and get rid of the arbitrariness, see for instance [18, 143]. There have also been proposed spectral correlations that do not require unfolded spectrum, for instance, the one based on the ratio of consecutive level spacings [144, 145].

3.2.3 Out-of-time-ordered correlators

One of the disadvantages of the spectral statistics as quantum chaos indicators is their need for a large and complete set of consecutive states with no gaps or spurious intruders. The appropriate train of states can be obtained as a result of extensive calculations based on theoretical models but is seldom available experimentally. Therefore, the attention has turned elsewhere. One of the quantities that have received a lot of attention recently is the OTOC, which is a four-point correlation function of two quantum operators $\hat{V}, \hat{W}$ taken at different times, most often taken in the form of an expectation value of the operators' commutator

$$C(t) = \left\langle \left[\hat{V}(t), \hat{W}(0) \right]^2 \right\rangle, \tag{3.16}$$

where

$$\hat{V}(t) = e^{\frac{i}{\hbar}\hat{H}t} \, \hat{V} \, e^{-\frac{i}{\hbar}\hat{H}t} \tag{3.17}$$

is the Heisenberg picture of operator $\hat{V}$ at time t and $\langle \bullet \rangle$ can be a thermal average in the canonical ensemble at a finite [146, 147] or infinite [148] inverse temperature β, an expectation value in a particular superposition of quantum states, such as a coherent state [73], or an expectation value in energy eigenstates $|E_n\rangle$,

$$C_n(t) = \left\langle E_n \left| \left[\hat{V}(t), \hat{W}(0) \right]^2 \right| E_n \right\rangle. \tag{3.18}$$

We shall employ the last option, usually called the *microcanonical OTOC* in the literature [47, 149].

Since its introduction as a semiclassical tool to study superconductivity [150], it has proved to be a robust tool in various areas of physics, ranging from black-hole physics and the AdS/CFT duality [146, 151] through the spread of quantum information and information scrambling [152, 153] to many-body physics [154–156] and quantum circuits [157]. The many-body properties can hint emergence of thermal physics [158, 159]. The common denominator of all these works is a relation to chaos, stability and exponential divergence. In quantum systems with the classical limit, the short-time OTOC evolution is related to the exponential spreading of neighbouring classical trajectories

$$C(t) \propto e^{2\lambda_{\mathrm{q}}t} \tag{3.19}$$

and the rate λ_{q} is often dubbed the *quantum Lyapunov exponent* [160]. The OTOCs have also been related to spectral statistics via a special operator called Lyapunovian [161].

The long-time behaviour, on the other hand, is captured in the mean value and variance,

$$\bar{C}_n = \lim_{T\to\infty} \frac{1}{T} \int_0^T C_n(t)\mathrm{d}t, \tag{3.20a}$$

$$\sigma_n^2 = \lim_{T\to\infty} \frac{1}{T} \int_0^T C_n^2(t)\mathrm{d}t - \bar{C}_n^2, \tag{3.20b}$$

and by higher moments of $C_n(t)$ in general. It will be shown that crucial is the ratio of the asymptotic mean value and the square root of the variance,

$$\nu_n \equiv \frac{\sigma_n}{\bar{C}_n}, \tag{3.21}$$

called *wiggliness* for simplicity.

3.3 Classical-quantum correspondence

The classical fraction of regularity f_{reg} in nonintegrable models have already been shown in Section 2.2, recall Figures 2.4 (Creagh-Whelan model) and 2.6 (algebraic u(3) vibron model). We shall focus here on the latter model described by Hamiltonian (2.55) and compare classical and quantum chaos quantities, namely the classical and quantum Lyapunov exponents and the f_{reg} with the wiggliness ν.

The u(3) model is integrable for $\epsilon = 0$; the additional integral of motion to the Hamiltonian itself is the o(2) Casimir operator reflecting the conservation of the angular momentum around one axis.[6] When ϵ grows, the unstable dynamics appears firstly near $\lambda = 1/5$ where the second-order QPT in the integrable regime sits, and along and above the ESQPT line $E = 0$.[7] The system is the most chaotic at around $\epsilon \approx 0.5$. Higher values of ϵ do not increase chaoticity anymore; the reason is that the system turns, after a proper rescaling, into integrable in the limit $\epsilon \to \infty$.

The classical chaos of the u(3) model is demonstrated in detail in Figure 3.1 for a nonintegrable configuration with $\epsilon = 0.4$. The left panel shows the fraction of regularity (3.6) encoded in colours; the white colour corresponds to fully regular dynamics, whereas the black colour indicates regions with phase space covered with unstable trajectories only. The right panel shows the classical Lyapunov exponent (3.3), which ranges, for the selected values of the model parameters, from $\lambda_{\text{cl}} = 0$ to $\lambda_{\text{cl}} \approx 0.2$.

The system is regular both near the minimum energy and the maximum energy of the system, in accord with the general discussion given in Section 3.1, and the chaotic region is roughly demarcated by lines $\lambda \gtrsim 0.2$ and $0 \lesssim E \lesssim 1 - \lambda$. A useful visual tool for classical chaos in systems with $f = 2$ degrees of freedom is the *Poincaré sections*, obtained by cutting the classical phase space by a plane and showing each passage of a trajectory as a point with coordinates given by two independent coordinates of the original phase space; for the Poincaré sections in Figure 3.1 plane $q_1 = 0$ and coordinates (q_2, p_2) are selected. Since trajectories do not cross in the phase space, each point of the Poincaré section corresponds to an individual trajectory provided the equienergy hypersurfaces do not have too complicated topology..[8] This allows us to visually distinguish regular regions from chaotic ones: individual trajectories in regular regions display as lines or even isolated points (if the trajectory is periodic) because they are localised to the remaining unbroken tori, whereas a chaotic trajectory covers a surface in the Poincaré section, see black regular regions versus wine chaotic

---

[6]The model is also integrable for any ϵ and for $\lambda = 0, 1$, see Appendix [57].

[7]This behaviour is common to other models with QPTs, *cf.* the chaos analysis in the Dicke model [37] and Appendices H and [162].

[8]A complicated topology is not a huge obstacle in $f = 2$ systems—one can select a subset of trajectory-section crossings that will determine phase space trajectories uniquely [163].
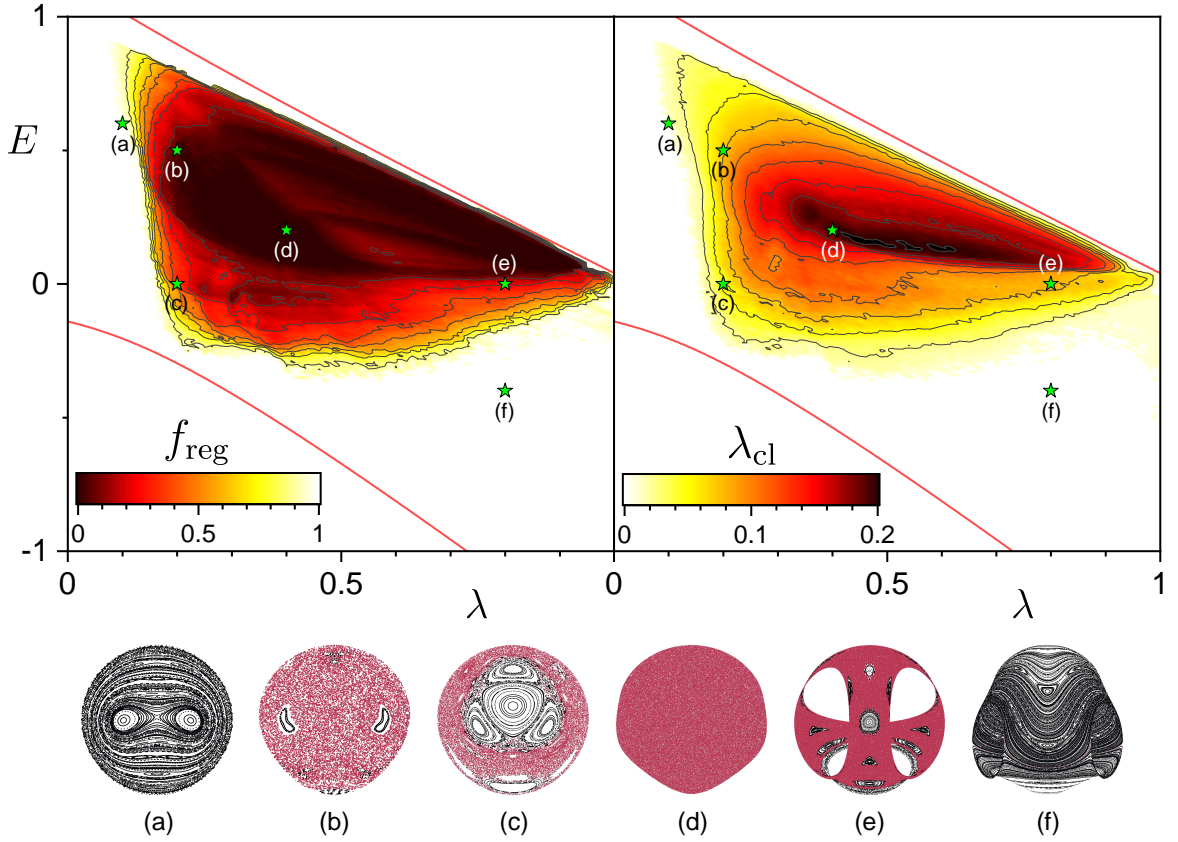
Figure 3.1: Classical fraction of regularity f_{reg} (top left panel) and classical Lyapunov exponent λ_{cl} (top right panel) for the algebraic u(3) model for $\epsilon = 0.4$ calculated for the Hamiltonian (2.56) on the mesh 100×220 points in the $\lambda \times E$ plane. The bottom panels show selected Poincaré sections by plane $q_1 = 0$ at (λ, E) values indicated by green stars in the main panels; stable and chaotic trajectories are represented by black and wine colours, respectively.

regions in the Figure. The phase space topology of the vibron model is intricate with holes, which is evident in Figure 3.1 (e).

A final remark to the classical chaos is related to the fact that as observed, the fraction of regularity is not correlated with the value of the Lyapunov exponent (besides the trivial fact that a nonzero value of λ_{cl} induces $f_{\text{reg}} < 1$). This demonstrates that each of the quantities is related to a different property: the Lyapunov exponent gives the rate of divergence of neighbouring trajectories, whereas f_{reg} measures the chaotic part of the phase space no matter how big the Lyapunov exponent is.

Let us turn now to the quantum calculation. As mentioned above, the time dependence of the OTOCs can be divided into short-time and long-time regimes, which can be limited by the Ehrenfest time

$$t_{\text{E}} \propto \mathcal{N}^{\alpha} \tag{3.22a}$$

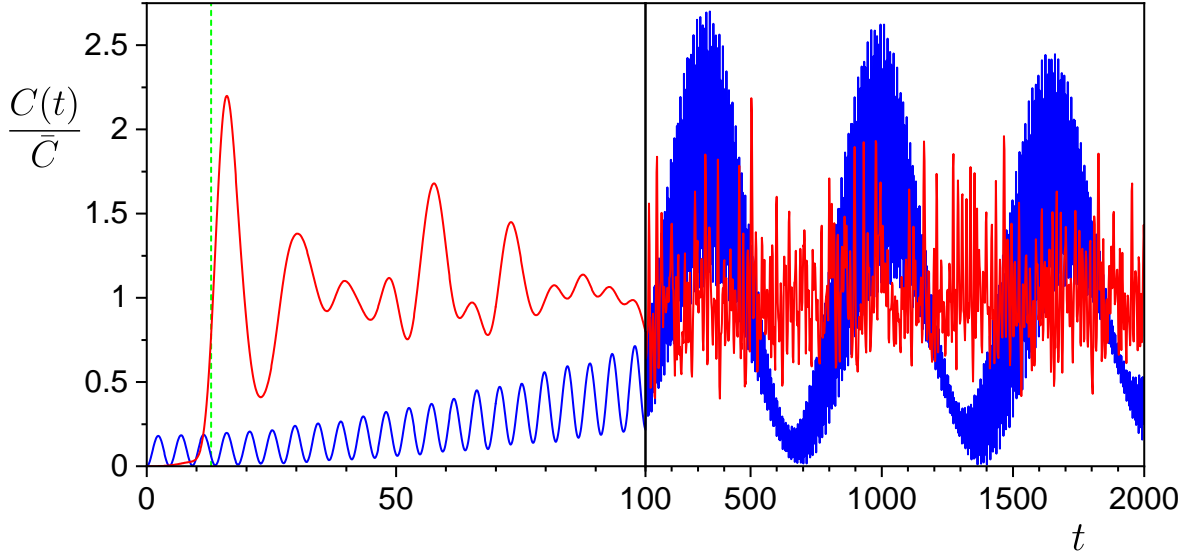for integrable systems, where $\alpha > 0$ is a characteristic exponent and depends on the

Figure 3.2: Short-time and long-time OTOC evolution for the choice $\hat{V} = \hat{W} = \hat{I}$ of OTOC operators in the vibron u(3) model with $\lambda = 0.4$ and $\epsilon = 0.4$ and system size $N = 50$. Two states are shown: a regular state $n = 7$ (blue curve) and a chaotic state $n = 621$ (red curve). For better comparison, the OTOCs are normalised by their mean value $\bar{C}(E_5 = 0.48) \approx 4 \cdot 10^3$, $\bar{C}(E_{621} = 0.21) \approx 6 \cdot 10^5$. The vertical dashed green line indicates the estimated Ehrenfest time $\tilde{t}$ for the chaotic state.

specific class of the system, and

$$t_{\mathrm{E}} \propto \frac{1}{\lambda_{\mathrm{cl}}} \ln \mathcal{N} \tag{3.22b}$$

for chaotic systems; $\mathcal{N}$ is the size parameter. Its meaning can be understood in the following way: Imagine a localised quantum wave packet, for instance, a coherent state, at time $t = 0$. Then the Ehrenfest theorem predicts that the expectation values of quantum operators for such a localised state correspond to the classical dynamics. However, quantum dynamics makes the packet spread and at a moment given by the t_E, its characteristic size reaches the characteristic size of the whole system and the Ehrenfest theorem ceases to be applicable. If the system is chaotic, the wave-packet spreading is exponential, hence the qualitative difference between $t_{\mathrm{E}}(\mathcal{N})$ for regular and chaotic systems. An example of the OTOC time evolutions for a state from a low-lying regular energy domain (blue curve) and an excited state from the middle chaotic part of the spectrum (red curve) of the vibron u(3) model are shown in Figure 3.2. Both curves are normalised to asymptotically oscillate around 1. The regular OTOC has a regular quasiperiodic shape (its Fourier transform has only a few significant frequencies) with strong "recurrences" in which $C(t)$ falls back almost to its initial value $C(0) = 0$. On the other hand, the chaotic OTOC quickly explodes following the exponential law (3.19) and erratically oscillates in the asymptotic times (its Fourier transform would resemble the white noise); the oscillations, however, have a smaller variance than in the case of the regular OTOC.

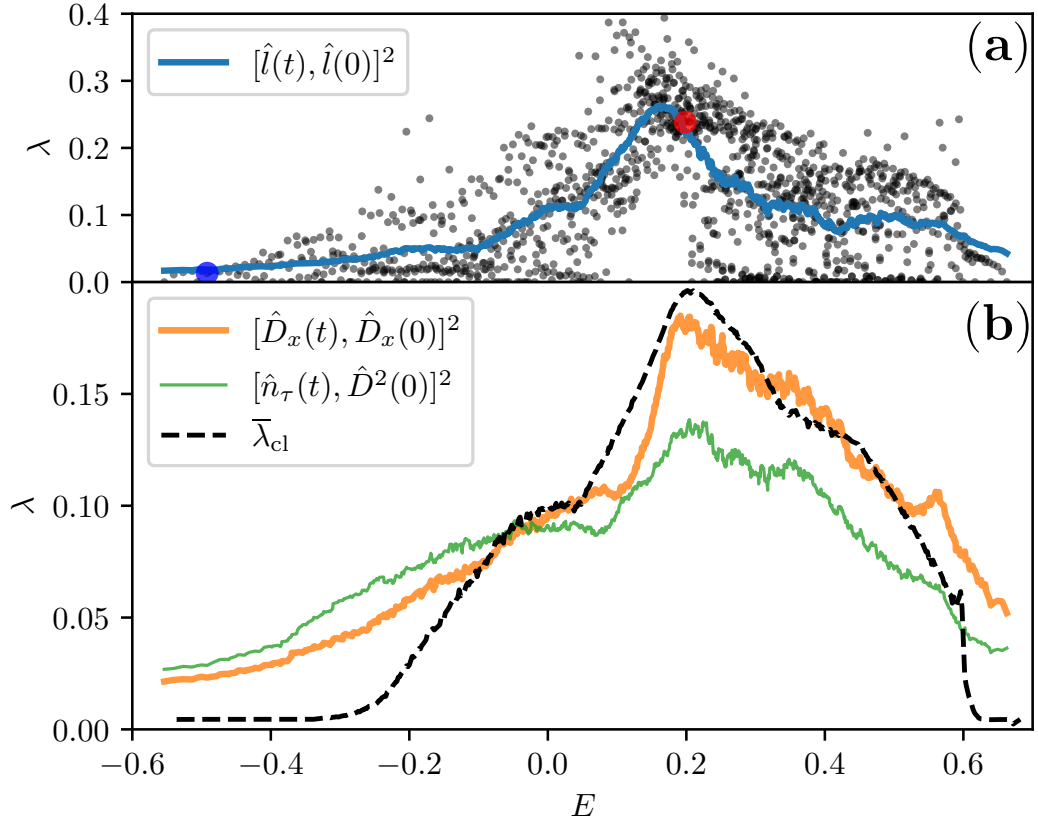The quantum Lyapunov exponent calculated from the short-time OTOC behaviour

Figure 3.3: Classical and quantum Lyapunov exponents $\lambda_{\mathrm{cl}}, \lambda_{\mathrm{q}}$ for the microcanonical OTOC in the vibron u(3) model (2.55) with $\lambda = 0.4$ and $\epsilon = 0.4$ and system size $\mathcal{N} \equiv N = 50$. Various choices of OTOC operators are indicated in the legend. (a) Dots correspond to $\lambda_{\mathrm{q},j}$ for individual eigenstates $|E_j\rangle$ fitted from (3.19) up to the estimated Ehrenfest time; the solid lines are smoothed values by a moving average over several neighbouring OTOC values C_j. Note that for the sake of visual clarity, error bars are not shown. The states shown in Figure 3.2 are highlighted by the same colours. (b) Smoothed values of the wiggliness for two other choices of the OTOC operators, and comparison with the classical Lyapunov exponent. *Adapted from* [57].

for the vibron model in a chaotic regime and various choices of the OTOC operators $\hat{V}, \hat{W}$ is shown in Figure 3.3 (beware the collision in notation; the vertical axes in the figure display the Lyapunov exponents $\lambda_{\mathrm{cl}}, \lambda_{\mathrm{q}}$, not the model's control parameter λ). Panel (a) shows by the black dots the quantum Lyapunov exponent fitted from (3.19) for each quantum state and OTOC with $\hat{V} = \hat{W} = \hat{l}$,

$$C_n(t) = -\left\langle E_n \left| \left[\hat{l}(t), \hat{l}(0) \right]^2 \right| E_n \right\rangle, \tag{3.23}$$

where $\hat{l}$ is the o(2) Casimir operator (2.54); the fit is up to the approximate Ehrenfest time estimated as the time when the OTOC for the first time reaches the value. The Ehrenfest time for each state is estimated from the asymptotic OTOC values as the smallest time $\tilde{t}$ satisfying

$$C_n(\tilde{t}_n) = \bar{C}_n - \sigma_n, \tag{3.24}$$

see also the vertical dashed green line in Figure 3.2; more details on estimating the Ehrenfest time are given in Appendix L. The regular and chaotic states from Figure 3.2 are highlighted by the same colours, and the values of their quantum Lyapunov exponent reflect their stability.
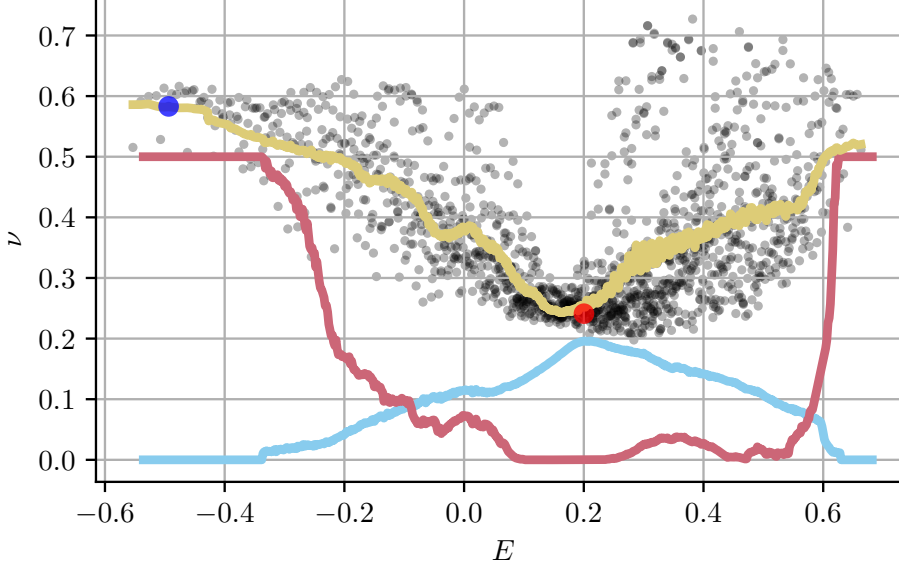

Figure 3.4: The asymptotic relative oscillations (wiggliness) for OTOC operators $\hat{V} = \hat{W} = \hat{I}$ of the u(3) algebraic model (2.55) with $\epsilon = 0.4$, $\xi = 0.4$ and $N = 50$. The dots denote the individual wiggliness values ν_n and the thick yellow lines the smoothed values $\bar{\nu}(E)$ by the moving window average. The smooth value compares to the classical fraction of regularity f_{reg}, shown by the solid red line. The blue and red points indicate the states shown in Figure 3.2.

The numerical quantum Lyapunov exponent $\lambda_{q,n}$ differs from state to state, since some of them capture more of the remnants of regularity in the system while the behaviour of others is dominated by the presence of chaos. However, after performing a simple smoothing procedure by a moving average over $\lambda_{q,n}$ of several neighbouring eigenstates $|E_n\rangle$, the resulting curves $\bar{\lambda}_q(E)$ for various choices of the OTOC operators can be compared, within the error margins of about $\Delta\lambda_q \approx 0.05$, with the classical λ_{cl}, see panel (b). This correspondence is confirmed in several other systems, see also Appendix H, where the Dicke model of atom-field interaction is employed and the OTOC operators correspond to the field-oscillator operators of coordinate and momentum. The short-time OTOC behaviour thus, indeed, testifies to the local stability of the system quantified by an average Lyapunov exponent.

A specific counterexample to this correspondence is related to the existence of isolated points of unstable equilibrium in the system. These points of measure zero in the whole phase space do not affect the classical dynamics. In the quantum case, on the other hand, due to the uncertainty relations, there is a subset of quantum states that can feel their presence and behave accordingly with an initial exponentially fast OTOC evolution inducing high quantum Lyapunov exponent, even in integrable systems, such as the Lipkin model. This behaviour is demonstrated and thoroughly

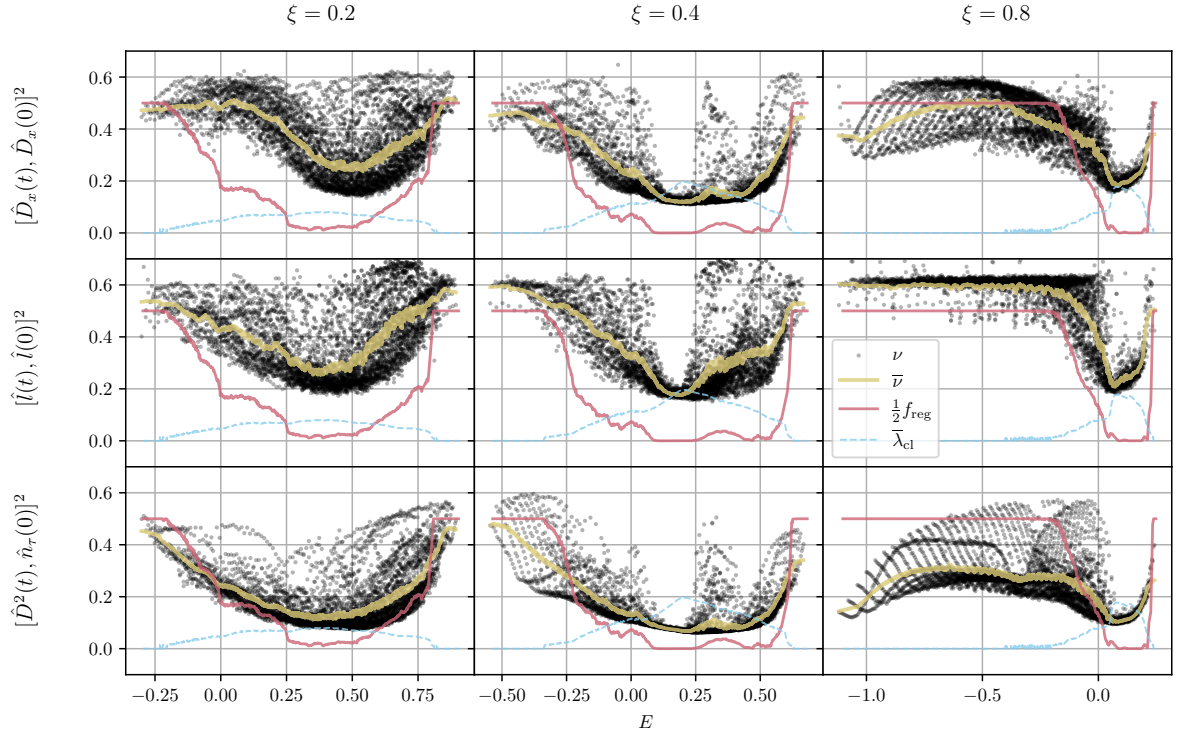discussed in Appendix I, as well as in References [73, 164]

Figure 3.5: The asymptotic relative oscillations (wiggliness) for three different choices of the OTOC operators (arranged in rows) and three different regimes of the u(3) algebraic model (2.55) with $\epsilon = 0.4$ and $\xi = \{0.2, 0.4, 0.8\}$ (arranged in columns). The dots denote the individual wiggliness values ν_n and the thick yellow lines the smoothed values $\bar{\nu}(E)$ by the moving window average. The smooth value compares to the classical fraction of regularity f_{reg}, shown by the solid red line. *Adapted from* [57].

Since the neighbouring points in the classical chaotic dynamics diverge exponentially, the Ehrenfest time is relatively small, especially for modestly big systems available experimentally, and may not be long enough to distinguish the stable dynamics from the chaotic dynamics with certainty. That is where the long-time relative OTOC oscillations, quantified by the wiggliness ν, come into play. Figures 3.4 and 3.5 show the wiggliness for several model configurations and choices of the OTOC operators and for two different sizes N. The smooth wiggliness $\bar{\nu}(E)$ is qualitatively comparable with the classical fraction of regularity f_{reg}; the most prominent example is given in the middle column of Figure 3.5, where the $f_{\text{reg}}(E)$ evolution has the most untrivial behaviour with several local extremes, all of them captured by $\bar{\nu}(E)$ for all distinct choices of the OTOC operators. Higher values of N bring better energy resolution.

In conclusion, the wiggliness (or, more precisely, its smoothed value) testifies to the overall chaoticity of the quantum system and can serve as a chaos indicator, especially in small systems and systems with large Lyapunov exponent.

Note that $\nu_n \to 0$ for chaotic states follows an algebraic power law,

$$\nu_n \propto N^{\alpha} \tag{3.25}$$

as can be observed by comparing Figures 3.4 and 3.5, whereas it remains constant for states from the regular part of the quantum spectrum. The rate α can be also considered a chaos measure. This scaling and other subtleties of the wiggliness as a tool for quantifying quantum chaoticity are exposed in detail in Appendix L.

3.4 Relation to the ESQPTs

It was hinted [165] that an ESQPT existence, especially the one connected with a stationary point of a saddle type (for instance, index $r = 1$ in systems with $f = 2$), could induce chaos in the system. The reasoning was based on the fact that the stationary points of the Hamiltonian with $r > 0$ are usually points of unstable equilibria, hence unstable dynamics and that the equicontours of the Hamiltonian are often convex (focusing) below the stationary point and concave (dispersing) above.[9]

Even though this conjecture works in many systems, it has been disproved in general by finding several counterexamples, usually in systems where the chaos breaks out well below the unstable stationary point, see the fraction of regularity in the Creagh-Whelan model in Figure 2.4 or in the algebraic u(3) vibron model in Figure 2.6.

Other aspects come into play, such as integrability (though the unstable points induce chaotic properties in the quantum dynamics even in integrable systems, see Appendix I), or the fact that not all stationary points with $r > 0$ are dynamically unstable, especially in algebraic systems with intricate Hamiltonians. A simple illustrative example is the strongly detuned Rabi model, which has effectively $f = 1$ degree of freedom. It contains a stationary point that evolves with increasing strength of interaction from a (global) minimum with $r = 0$ to an $r = 1$ saddle point with unstable quantum dynamics to $r = 2$ maximum, which, surprisingly, exhibits stabilised dynamics. Note, however, that the stability we are talking about is related to individual points affecting individual classical trajectories, not the global dynamics.

To conclude this short section, so far, there is no theoretical connection between the ESQPTs and the chaoticity of the system.

---

[9]A connection between (i) the shape of equipotential contours, (ii) the curvature of the geometric embedding of the Hamiltonian motion and (iii) classical chaos was analysed in papers [31, 32].

Chapter 4

Complex and non-Hermitian extensions

Non-Hermitian notions negotiate notable nebulousness, nurturing novel narratives. Nonsensically non-normal, non-conservative, and non-unitary, they necessitate navigating numerous non-realms.

ChatGPT, A short explanation of non-Hermiticity with all words starting with the letter n.

So far, we have considered systems that are described by a Hermitian Hamiltonian $\hat{H}(\lambda)$ whose control parameters $\lambda = \left(\lambda_1, \ldots, \lambda_{N_p}\right)$ are real (2.1). We have seen that the individual energy levels tangle nontrivially with the change of λ, recall Figures 2.2—2.6. If we assume there is no symmetry in the system, *i.e.,* there is no operator commuting with $\hat{H}(\lambda)$, then there are almost no real energy level crossings in the system due to the *no-crossing theorem* [166]; it is said that the crossings are *avoided*. However, true eigenlevel degeneracies $E_n = E_m, n \neq m$ called *exceptional points* (EPs) appear when the control parameters are extended into the complex plane,

$$\lambda \mapsto \Lambda = \lambda + i\mu, \tag{4.1}$$

leading to a non-Hermitian Hamiltonian [167]. An EP generally represents the square-root type of branch point and connects two Riemann sheets belonging to a pair of complex eigenvalues E_n, E_m.

For simplicity, let us focus on one-parameter finite systems described by the Hamiltonian

$$\hat{H}(\Lambda) = \hat{H}_0 + \Lambda\hat{V}, \quad \Lambda \in \mathbb{C}, \tag{4.2}$$

that lives in the Hilbert space $\mathcal{H}$ of dimension $\dim \mathcal{H} = \mathcal{N}$. We shall denote the EPs positions as $\Lambda_j^{(\text{EP})}, j = 1, \ldots, N_{\text{EP}}$, where

$$N_{\text{EP}} = 2\mathcal{N}(\mathcal{N} - 1) \tag{4.3}$$

is the total number of EPs. The EPs come in complex conjugate pairs, $\Lambda_j^{(\text{EP})} = \overline{\Lambda}_{N_{\text{EP}}-j}^{(\text{EP})}$ [168].

A natural question arises, What is the use of a complex extension? Is it not just a smug mathematical game? The answer is *no*. As will be demonstrated in this

chapter, in the "real" world, we can observe imprints of events and phenomena that are firmly placed in the complex extension, in the same way as the prisoners in Plato's cave observe just shadows cast by the true reality [169]. Hence, moving complex, although often difficult and painful, can help us free ourselves from the cave illusion and understand the source of our observations in a more profound way [170].

We shall present three different research areas where the complex extension of the standard mechanics can be used: an analysis of the properties of the EPs when the system undergoes a QPT (Section 4.1), a study of the behaviour of the spectrum when a closed subsystem is coupled to a continuum (Section 4.2) and an application of the complex-extended level density to study quantum tunnelling through multibarrier one-dimensional potentials (Section 4.3). In addition, we have recently published a mathematical paper that derives the equations of motion for the exceptional points in multiparametric systems [55], and another paper in which we extend the survival amplitude of a quenched quantum system into the complex domain, compare it with the complexified partition function and analyse the distribution of its zeros in a system with ESQPTs and another critical concept called a Dynamical Quantum Phase Transition (DQPT) [54].

Note that there are other ways to use complex extensions in quantum mechanics. One of the important areas of research that should not be omitted to mention is the parity-time-symmetric (*PT*-symmetric) extension of the quantum mechanics [171, 172]. As a curiosity, the CUSP system introduced in Section 2.2.1 also received a PT-symmetric extension [173].

4.1 Quantum phase transitions and exceptional points

It was mentioned in Chapter 2 that one of the essential features of the QPTs is the closing gap between the ground-state energy and the first excited-state energy. Since the width of the gap

$$g = E_1 - E_{\text{gs}} \tag{4.4}$$

is known to be connected with the imaginary components of the energy at a corresponding EP, the non-Hermitian extension and the distribution of EPs offer valuable tools for studying the QPTs [174–176] and ESQPTs [177]. Another piece of theory that can be exploited is the analogy between the Yang-Lee zeros of the partition function $Z(\beta)$ at thermal phase transitions [178, 179] and the EPs, which says that the zeros of $Z(B)$ for complex inverse temperature $B = \beta + i\zeta$ accumulate near the real critical inverse temperature β_c and the rate of accumulation determines the order of the thermal phase transition [180–182]. A similar conclusion can be made for the QPTs at zero temperature if, instead of zeros of $Z(B)$, one considers the EPs distribution of $\hat{H}(\Lambda)$ and its behaviour with increasing system size [35, 183].

A detailed study of this analogy in the Lipkin model (2.37) reveals that, indeed, the EPs tend to converge to the real axis in the vicinity of the QPT if the system size $\mathcal{N} \equiv N$ grows. The EP situated the closest to the real axis, corresponding to the level crossing of the ground state and the first excited state, approaches the real axis exponentially fast for the first-order QPT and algebraically fast for the second-order QPT.
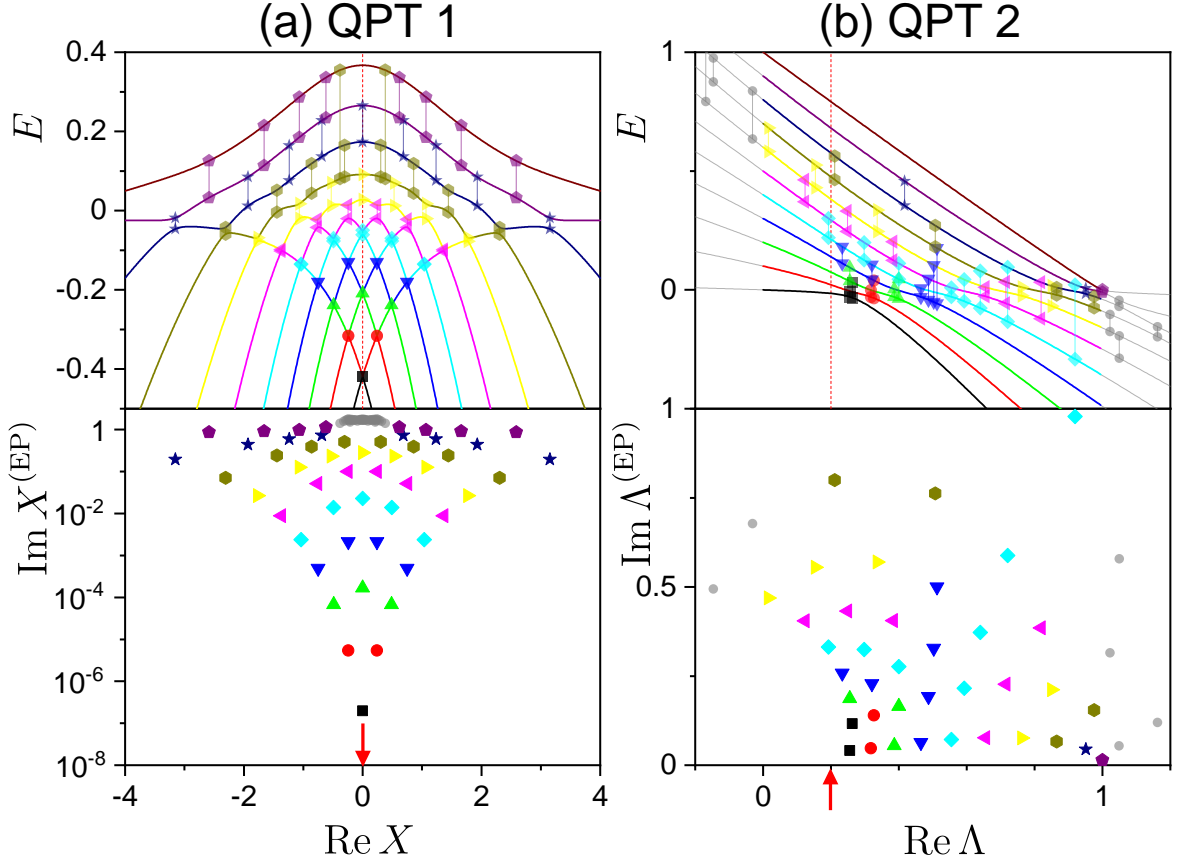
Figure 4.1: Level dynamics (**top panels**; each eigenlevel is displayed by a curve of a different colour) and the positions of the EPs (**bottom panels**) in the non-Hermitian extension of the Lipkin model (2.37) by mapping $\lambda, \chi \in \mathbb{R} \mapsto \Lambda, X \in \mathbb{C}$. Only half of the EPs with $\mathrm{Re}\, X^{(\mathrm{EP})} > 0, \mathrm{Re}\, \Lambda^{(\mathrm{EP})} > 0$ are shown (the second half is obtained by reflecting the displayed EP along the horizontal axis). If the EPs can be associated with the avoided crossings in the level dynamics, they are marked in both top and bottom panels by the same colour (of the lower eigenlevel) and point type; if not, they appear in the bottom panels in light grey. The dashed red lines and the red arrows indicate the value of the corresponding control parameter at which the QPTs in the $\mathcal{N} \to \infty$ limit occur. (a) First-order QPT regime with $\Lambda = 0.6 + 0i$, $N = 10$. (b) Second-order QPT regime with $X = 0 + 0i$ and $N = 20$. Only the even-parity subspace is shown in this configuration. The level dynamics is extended beyond the usual interval $\mathrm{Re}\, \Lambda \in [0, 1]$.

   The EP distribution for the finite-size precursors of both the first- and second-order QPTs is illustrated for relatively small system size N in Figure 4.1. The Lipkin model is complexified by extending $\lambda, \chi \in \mathbb{R} \mapsto \Lambda, X \in \mathbb{C}$. The first-order QPT at $X = 0$ demonstrated in column (a) exhibits a much tighter gap g (see the black and red curves in the top subfigure), reflected by a small imaginary component $\mathrm{Im}\, X_0^{(\mathrm{EP})} \approx 10^{-7}$ of the corresponding EP (black square in the bottom subfigure), even for a chosen small system size. The imaginary component connected with the QPT gap asymptotically scales as

$$\mathrm{Im}\, X_0^{(\mathrm{EP})} \propto N^{-\zeta}\, \mathrm{e}^{-\eta N} \tag{4.5}$$

where, for the Lipkin model, a fit of the constants gives $(\zeta, \eta) \approx (0.52, 1.49)$, see Appendix F.

Note that the gap g is more than one order of magnitude smaller than the gaps between the excited states. Therefore, it turns out that the essence of the first-order QPT can be described solely by the two-level interaction between the ground state and the first excited state, and the rest of the spectrum can be disregarded.

The second-order QPT at $\Lambda = 1/5$ shown in column (b) is, on the other hand, connected with a more complicated "collective" interplay of several exceptional points originating in avoided crossings of a bunch of lowest-lying eigenlevels. The gap g is wider and decreases slower than in the case of the first-order QPT when the system size grows. The corresponding EP has $\operatorname{Im} \Lambda_0^{(\mathrm{EP})} \approx 0.04$ and scales algebraically with the system size,

$$\operatorname{Im} \operatorname{Im} \Lambda_0^{(\mathrm{EP})} \propto N^{-\kappa}, \tag{4.6}$$

where the fitted value of the exponent is $\kappa \approx 0.67$.

Notice that in the lower subfigure, there is another EP very close to the real axis depicted by the filled violet pentagon. This EP is connected with the narrow avoided crossing between the highest level and the second-highest level, which is connected with a QPT-like behaviour of the highest level at $\Lambda = 1$.

The EPs can be associated with avoided crossings between specific levels provided the levels are not far from one another. The algorithm consists of connecting a selected EP by the shortest line with the real axis of the corresponding parameter. Then from the evolution of the real parts of the energy levels, one can determine which energy levels intersect at the selected EP. Since the complex-energy-level sheets are analytical extensions of the real energies, the indices of the levels intersecting at the EP are identical to the indices of their real parts on the real axis [184]. This procedure fails if there is another EP in the vicinity of the line connecting the selected EP and the real axis because this EP mixes and swaps another pair of energy levels (an effect called *EP shadowing*). It is the case of several EPs accumulated near $X \approx 0 + 0.2\mathrm{i}$, shown by grey points in the top-left panel of Figure 4.1.

A detailed theoretical and numerical study of the EPs convergence speed to the real axis for different orders of QPTs is presented in Appendix F. The Appendix also shows what happens when the critical Hamiltonian is randomly perturbed and demonstrates that the presence of criticality leads to qualitatively different distributions of the EPs.

4.2 Non-Hermitian superradiance

A non-Hermitian Hamiltonian can effectively describe an open quantum system in the sense of the Feshbach theory [185, 186]. Let us model such a system with a finite Hamiltonian on an n-dimensional Hilbert space $\mathcal{H}$, describing a bound subsystem with real energies $E_k^{(0)}$ and corresponding orthonormal eigenvectors $\left| E_k^{(0)} \right\rangle$, $k = 1, \ldots, n$, coupled to a continuum via an effective "decay" Hamiltonian $\hat{\mathsf{H}}_\mathrm{d}$, living in a d-dimensional subspace $\mathcal{H}_\mathrm{d} \subset \mathcal{H}$ whose basis is spanned over the states $\left| \phi_j \right\rangle$, $j = 1, \ldots, d$ and have, in general, nonvanishing overlap with all the unperturbed states $\left| E_k^{(0)} \right\rangle$, *i.e.,*

$\left\langle E_k^{(0)} \middle| \phi_j \right\rangle \neq 0 \; \forall k, j$. The full Hamiltonian will read

$$\hat{H}(\Lambda) = \hat{H}_0 + \underbrace{(\epsilon - i\gamma)}_{\Lambda} \sum_{j=1}^{d} |\phi_j\rangle\langle\phi_j|, \tag{4.7}$$

where the complex parameter Λ is the coupling strength between the bound and open subsystems. For simplicity, all the states $|\phi_j\rangle$ have the same decay widths $\gamma = \hbar/(2\tau) \geq 0$, reciprocal to the mean lifetime τ, and energy offset ϵ, which can be set to zero. Under a nonzero value of γ the whole system (4.7) becomes unstable, resulting in complex eigenenergies

$$\mathcal{E}_k(\gamma) = E_k(\gamma) - i\Gamma_k(\gamma), \tag{4.8}$$

whose imaginary parts Γ_k specify the decay widths of the eigenstates of the full Hamiltonian $\hat{H}$.

When one starts opening the system, all the widths Γ_k initially increase linearly with γ due to the perturbation theory. However, at γ values comparable with the spacings between the unperturbed energies, the set of eigenstates of $\hat{H}$ splits into two groups: (i) d eigenstates whose widths keep growing and the growth rate saturates at $\Gamma_k(\gamma) \approx \gamma$ for high γ, and (ii) $n - d$ eigenstates that turn back towards the real axis and become asymptotically stable, $\Gamma_k(\gamma \to \infty) \to 0$. The real parts $E_k(\gamma)$ also changes with γ, but always stays within the range $E_k(\gamma) \in [E_1^{(0)}, E_n^{(0)}]$ of the unperturbed system.

The splitting of energies into fast-decaying ones and long-living ones was for the first time described in the continuum nuclear shell model [187] and later revealed in other many-body models [188]. This phenomenon is related to the so-called Dicke superradiance [189], which is a spontaneous radiation burst emitted from an ensemble of atoms strongly coupled with an electromagnetic field. In our case, the mediating field is substituted by $\hat{H}_d$ and the superradiant burst is related to the very short-living superradiant states. This is why the phenomenon has been called the *non-Hermitian superradiance* (NHSR).

A demonstration of the complex level dynamics and its evolution leading towards the NHSR is given in Figure 4.2, in which the Lipkin Hamiltonian (2.37) at the first-order QPT (panel a) and the second-order QPT (panel b) models the bound system H_0. The basis $|\phi_j\rangle$ for the decay zone of the total Hamiltonian is selected as a subset of d eigenstates of a $n \times n$ random matrix from the Gaussian Orthogonal Ensemble, known to have eigenvectors pointing at completely random directions in the n-dimensional space [131], hence, due to their normalisation, covering uniformly a unit n-dimensional sphere. Each line in the Figure corresponds to one eigenstate of $\hat{H}$ with energy given on the horizontal axis and the decay width on the vertical axis. The colour of the curves encodes the coupling strength γ between the Lipkin system and the open channels.

One observes that initially, for $\gamma \lessgtr 0.01$ (blue colour), all the eigenstates open simultaneously. When the coupling strength reaches the mean level density $\bar{\rho} \approx 0.05$ (dark green colour), the levels begin to curve and tangle. If γ increases further (red colour), d levels decouple and decay, whereas the rest of the states return to the safety of the real axis.
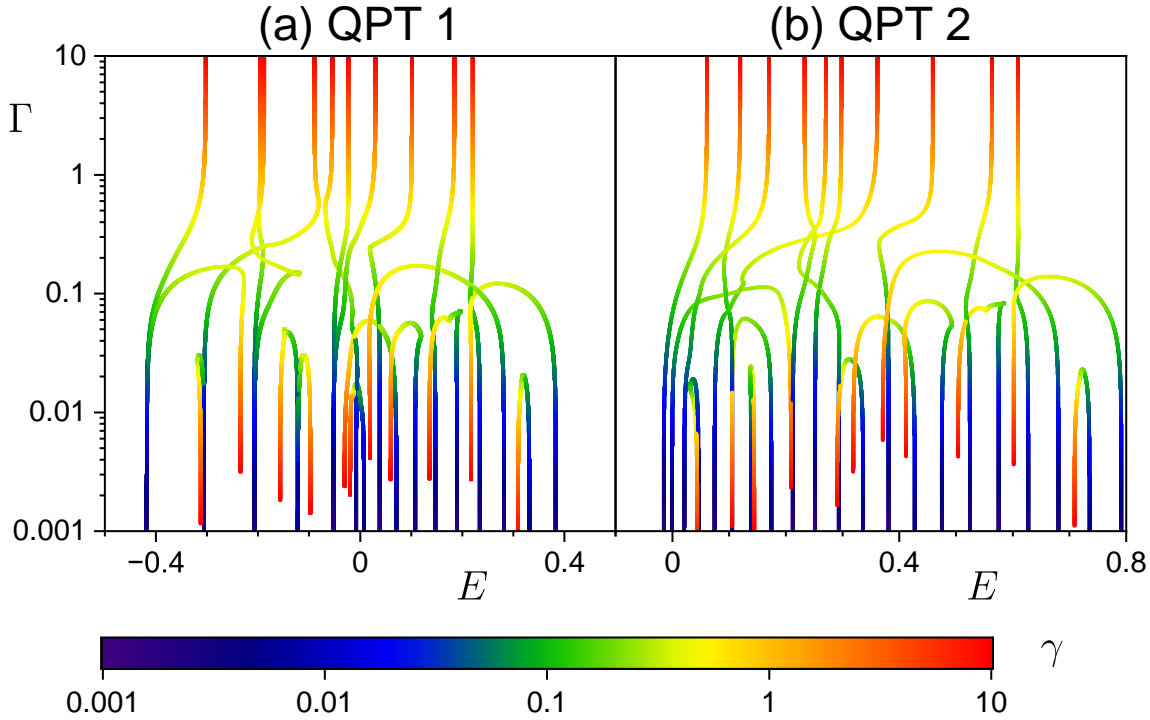
Figure 4.2: Complex level dynamics of Hamiltonian (4.7) with $d = 10$ open channels. The unperturbed Hamiltonian $\hat{H}_0$ is the Lipkin model (2.37) with $n = N = 20$ at (a) the first-order QPT ($\lambda = 0.6, \chi = 0$) and (b) the second-order QPT ($\lambda = 0.2, \chi = 0$). Randomly chosen decay-inducing eigenvectors $\left| \phi_j \right\rangle$, $j = 1, \ldots, 10$ are the same in both cases (a) and (b).

Since the Hamiltonian (4.7) is non-Hermitian and has the form of Equation (4.2), a question arises whether the distribution of EPs in the parameter $\Lambda = \epsilon - i\gamma$ can give insight into the mechanism of the NHSR and distinguish systems with QPTs from noncritical ones. As was discussed earlier in this chapter, the imaginary component of an EP is proportional to the distance of two energy levels at their avoided crossing, and the QPTs are characterised by a tight avoided crossing between the ground state and the first excited state. Therefore, the distribution of the EPs for the NHSR Hamiltonian when its unperturbed part $\hat{H}_0$ undergoes a QPT should be shifted towards the origin, compared to a generic case with noncritical $\hat{H}_0$. An illustration of why it should be so is presented in Figure 4.3, in which the real level dynamics in parameter ϵ and the EPs in Λ are shown both for $\hat{H}_0$ modelling a first-order QPT (panel a) and second-order QPT (panel b). The levels at the first-order QPT bunch together in pairs, so any generic perturbation to the Hamiltonian $\hat{H}_0$ governed by parameter Λ leads to an immediate avoided crossing with $\left| \Lambda^{\text{EP}} \right| \approx 0$. The EPs corresponding to the first three eigenlevel pairs are highlighted in Figure 4.2 (a) by the green squares, which, indeed, lie very close to the origin in the inset. A similar, but more subtle shift in the EPs distribution can be observed for the second-order QPT.

In order to obtain a full account of the distribution of the EPs, we generate many realisations of the decay-inducing subspace $\mathcal{H}_{\text{d}}$. We also perform an ensemble averaging to obtain a bulk evolution of both decayed and stabilised states, which significantly
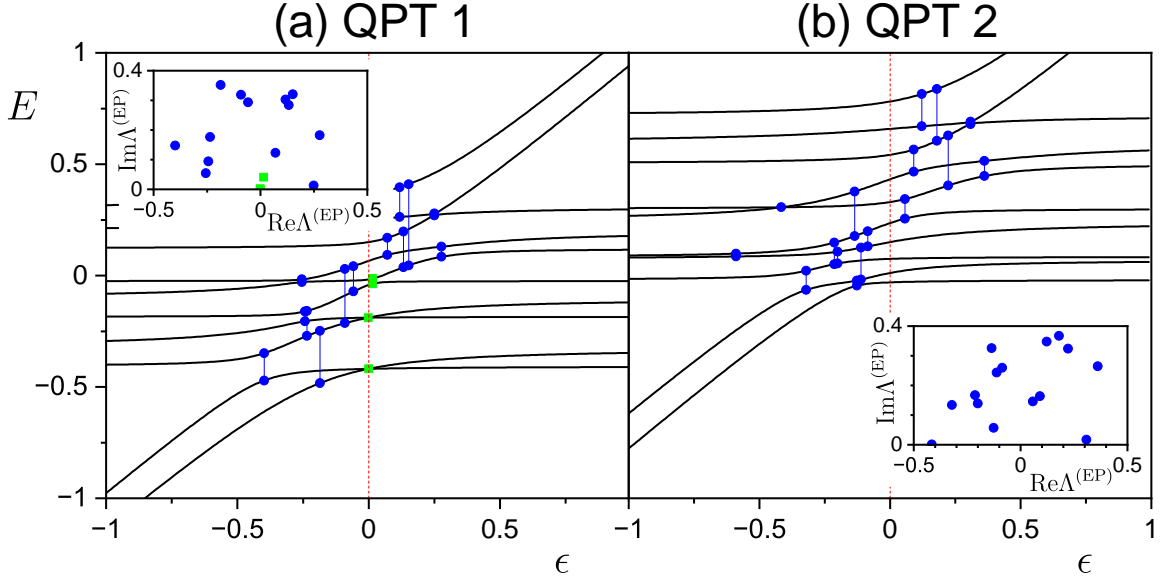
Figure 4.3: Real level dynamics of the NHSR Hamiltonian (4.7) with $d = 2$ open channels (main panels) and exceptional points in parameter Λ (insets). The unperturbed Hamiltonian $\hat{H}_0$ is the Lipkin model (2.37) with $N = 10$ at (a) the first-order QPT ($\lambda = 0.6$, $\chi = 0$) and (b) the second-order QPT ($\lambda = 0.2$, $\chi = 0$). Randomly chosen decay-inducing eigenvectors $|\phi_j\rangle$, $j = 1, 2$ are the same in both cases (a) and (b). The dashed red lines indicate the spectrum of the clean QPT configuration. The EPs are associated with the avoided crossings in the level dynamics using the procedure commented in Section 4.1.

differ if the unperturbed Hamiltonian is critical or generic. The results are shown and thoroughly discussed in Appendix G.

To conclude this section, the NHSR has had applications in many-body systems that exhibit decay or resonance phenomena, such as nuclei, atoms, molecules, atomic clusters or generic gain-loss systems [188, 190–192], and the current contribution can play an important role in the decaying system undergoes a QPT.

4.3 Quantum tunnelling

The last topic covered in this chapter will be the semiclassical theory of quantum tunnelling through general onedimensional multibarrier potential. Whereas the previous two sections deal with systems that are described by non-Hermitian Hamiltonians, this section addresses complex extensions of inherently real quantities, such as quantum level density or classical time delay. We show a tight connection between these quantities and demonstrate ESQPT-like singularities associated with stationary points of the tunnelling potential.

The level density of quantum bound systems is given by the sum of Dirac δ functions sitting at the discrete eigenenergies (2.7), or equivalently and somewhat

more abstractly,

$$\rho(E) = -\frac{1}{\pi} \lim_{\epsilon \to 0} \text{Im Tr} \left[\hat{\mathsf{G}}(E + i\epsilon) \right], \tag{4.9}$$

where

$$\hat{\mathsf{G}}(E) = \frac{1}{E - \hat{\mathsf{H}}} \tag{4.10}$$

is the Green operator associated with the system's Hamiltonian $\hat{\mathsf{H}}$. The level density (4.9) diverges if applied to a system with a continuous spectrum. However, if we subtract another "infinity" given by the level density of a noninteracting system described by Hamiltonian $\hat{\mathsf{H}}_0$ with Green operator $\hat{\mathsf{G}}_0$,

$$\delta\rho(E) = -\frac{1}{\pi} \lim_{\epsilon \to 0} \text{Im Tr} \left[\hat{\mathsf{G}}(E + i\epsilon) - \hat{\mathsf{G}}_0(E + i\epsilon) \right], \tag{4.11}$$

we obtain a finite number used as the continuum level density in scattering theory [193, 194].

Instead of real energy E, we switch to complex eigenvalues $\mathcal{E} = E_k - \frac{i}{2}\Gamma_k$ corresponding to resonance states with widths Γ_k. Technically, the resonances can be found, for instance, using the complex-scaling method [167], which reveals discrete resonances up to a certain width, while the rest remains in the so-called rotated continuum. Combined with confining the system into a box with arbitrarily large dimensions, the number of resonances will be large but countable and we can reformulate the continuous level density as

$$\Delta\rho(\mathcal{E}) = \frac{i}{\pi} \text{Tr} \frac{1}{\mathcal{E} - \hat{\mathsf{H}}} - \frac{i}{\pi} \text{Tr} \frac{1}{\mathcal{E} - \hat{\mathsf{H}}_0}, \tag{4.12}$$

where $\mathcal{E}_k$ and $\mathcal{E}_k^{(0)}$ represent poles of $\hat{\mathsf{H}}$ and $\hat{\mathsf{H}}_0$, respectively. Note that $\Delta\rho$ is in general a complex variable.

A 1D scattering problem is usually described by Hamiltonian in the standard form

$$\hat{\mathsf{H}} = \hat{\mathsf{H}}_0 + \hat{\mathsf{V}}, \tag{4.13}$$

where $\hat{\mathsf{H}}_0 \equiv \hat{\mathsf{T}} = \hat{\mathsf{p}}^2/(2m)$ is the kinetic term and $\hat{\mathsf{V}}$ is the coordinate-dependent tunnelling potential, assumed to be practically nonzero only inside a certain finite interval $q \in (a, b)$. A stationary solution of the Schrödinger equation is

$$\psi(q) = \begin{cases} e^{\frac{i}{\hbar}pq} + R(E)\, e^{-\frac{i}{\hbar}pq} & q < a, \\ T(E)\, e^{\frac{i}{\hbar}pq} & q > b, \end{cases} \tag{4.14}$$

where $p = \sqrt{2ME}$ is the momentum of the particle, $R(E)$ is the reflection amplitude and $T(E)$ the transmission amplitude. The complex transmission amplitude can be written as

$$T(E) = |T(E)|\, e^{i\phi(E)} = e^{i\Phi(E)}, \tag{4.15}$$

where $\phi(E)$ is the real phase shift of the transmitted wave and $\Phi(E)$ is a corresponding complex phase.

The real continuum level density (4.11) is connected to the phase shift $\phi(E)$ [195] via relation

$$\delta\rho(E) = \frac{1}{\pi}\frac{\mathrm{d}}{\mathrm{d}E}\phi(E). \tag{4.16}$$

Extended to the complex level density and complex phase, it reads

$$\Delta\rho(E) = \frac{1}{\pi}\frac{\mathrm{d}}{\mathrm{d}E}\Phi(E) = \frac{1}{\pi}\phi(E) - \frac{\mathrm{i}}{\pi}\frac{\mathrm{d}}{\mathrm{d}}\ln|T(E)| \tag{4.17}$$

and provides a link from the level density to the observable quantities $\phi(E)$ and $T(E)$.

The phase shift can be also related to a properly defined time or "time delay". For instance, the Eisenbud-Wigner time [196],

$$\delta t(E) = \hbar\frac{\mathrm{d}}{\mathrm{d}E}\phi(E) \tag{4.18}$$

gives a time shift $\delta t \approx \hbar/\Gamma_k$ near the centre of a single resonance of width Γ_k, proportional to the average lifetime, whereas it vanishes away from the resonance. A complex extension of the time delay will naturally be

$$\Delta t(E) = \hbar\frac{\mathrm{d}}{\mathrm{d}E}\Phi(E) = \hbar\pi\,\Delta\rho(E). \tag{4.19}$$

Since the complex level density has a strongly oscillating component, similar to its real sibling (2.8), we shall focus on the smoothed values $\Delta\bar{\rho}(E)$, $\bar{\Phi}(E)$ and $\Delta\bar{t}(E)$ only.

The smooth time shift Δt can be understood from the semiclassical Wentzel-Kramers-Brillouin approximation, which gives for the transmitted wave

$$\bar{T}(E)\,\mathrm{e}^{\frac{\mathrm{i}}{\hbar}pb} = \mathrm{e}^{\frac{\mathrm{i}}{\hbar}pa}\,\mathrm{e}^{\frac{\mathrm{i}}{\hbar}\int_a^b \mathrm{d}q\sqrt{2M[E-V(q)]}+c}, \tag{4.20}$$

where c is the phase accumulated at the turning points between the classically allowed and forbidden regions in (a, b) [197].

By putting everything together, the real part of the complex time delay will be

$$\mathrm{Re}\,\Delta\bar{t}(E) = \int_a^b \mathrm{d}q\,\Theta(E-V(q))\sqrt{\frac{M}{2[E-V(q)]}} - \frac{M}{2E}(b-a), \tag{4.21a}$$

and, similarly, the imaginary component

$$\mathrm{Im}\,\Delta\bar{t}(E) = \int_a^b \mathrm{d}q\,\Theta(V(q)-E)\sqrt{\frac{M}{2[V(q)-E]}}, \tag{4.21b}$$

where Θ is the Heaviside step function that guarantees that the integrals are taken across all the classically allowed (forbidden) regions for the real (imaginary) part of $\Delta\bar{t}(E)$, which can include several coordinate intervals for a multibarrier tunnelling potential.

The theory is demonstrated on a Hamiltonian with a polynomial potential supported by a Gaussian function,

$$\hat{\mathsf{H}} = \frac{\hat{\mathsf{p}}^2}{2m} + \mathrm{e}^{-\eta\hat{\mathsf{q}}^2}\sum_j c_j\hat{\mathsf{q}}^j, \tag{4.22}$$
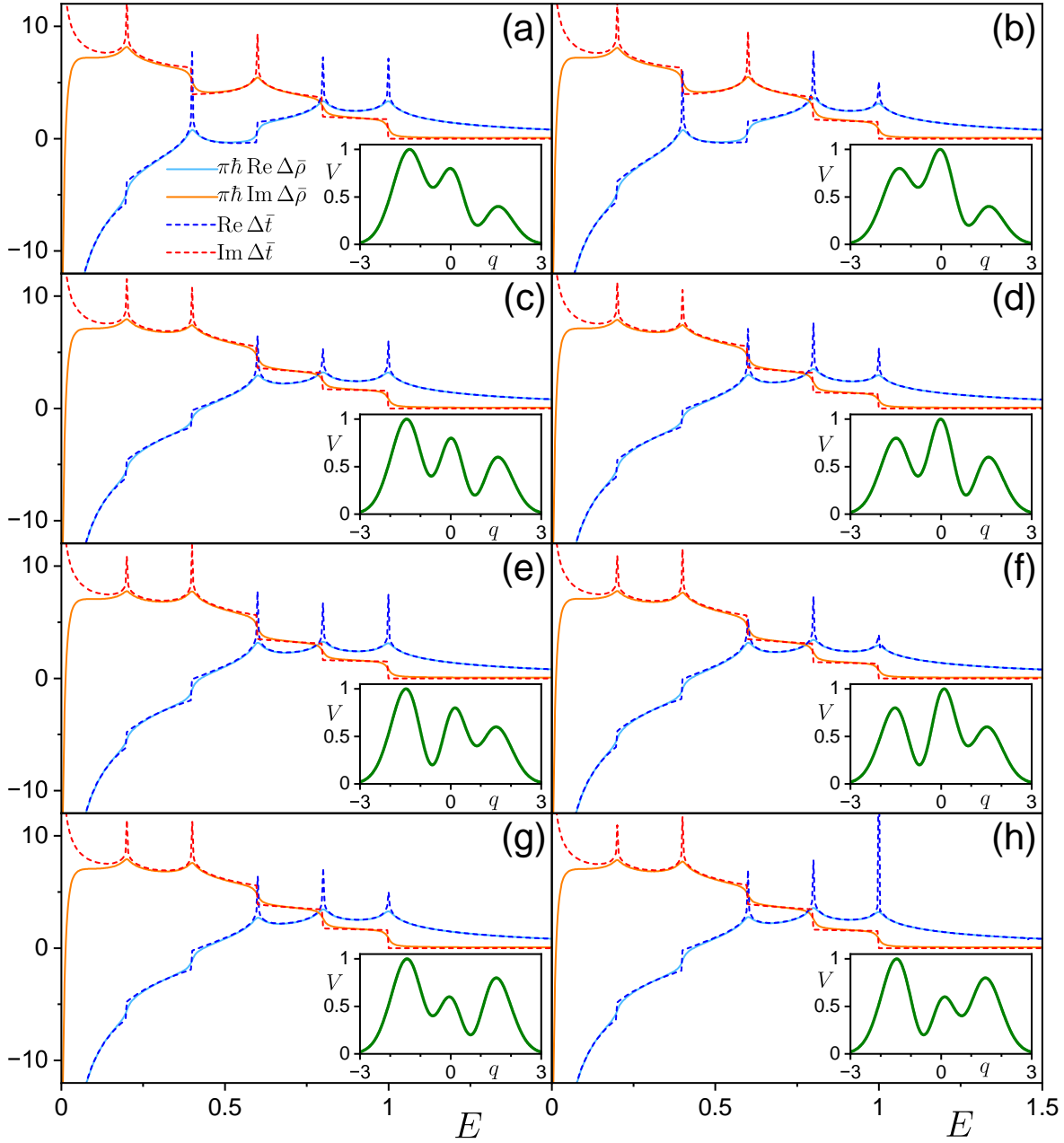
Figure 4.4: The smooth continuum level density $\Delta\bar\rho$ calculated for a finite size ("classicality") parameter $\mathcal{N} = 200$ (2.25) (characteristic energy and characteristic lengths are taken as $E_{ch} = 1$, $q_{ch} = 1$) is shown by light blue and orange solid curves for the real and imaginary part, respectively. The semiclassical time delay $\Delta\bar{t}$ (4.21), is plotted by dark blue and red dash curves.

where $\eta > 0$ characterises the width of the potential and c_j are tunable parameters modelling the tunnelling barriers and wells. Figure 4.4 shows the smooth complex level density and the complex time delay for all eight possible configurations of the multibarrier potential (4.22) with three local quadratic maxima and two local quadratic minima [the polynomial in (4.22) is of the fourth-order]. The potentials are plotted

in the insets. The parameters c_j are chosen in such a way that all the local extremes of the potential sit at $V = 0.2, 0.4, 0.6, 0.8$ and the global maximum is situated at $V = 1$. Following the theory given in Chapter 2, one expects singularities in the level density—analogues of the ESQPTs in the discrete spectra of bound systems—at the energies of the stationary points. The stationary points of the 1D tunnelling system can only have indices $r = 0$ (quadratic minimum) and $r = 1$ (quadratic maximum), leading to upward jumps and upward-pointing logarithmic divergencies in the real part of the level density, respectively. A novelty here is that the singularities appear also in the imaginary part of the level density, but they have an opposite character: a downward jump for the potential maximum and a logarithmic divergence for the potential maximum. In general, the singularities in the imaginary part of the level density follow the same ESQPT theory as in the real part, but one has to analyse the indices of the stationary points of the Hamiltonian turned "upside down", $-H(p, q)$, instead of $H(p, q)$. It means that the potential minimum has index $r = 2$ for $-H$, whereas the potential maximum has index $r = 1$ for $-H$ (the kinetic term of the negative Hamiltonian is a local maximum). Note that the opposite character of the singularities in $\text{Im}\,\bar{\rho}(E)$ can also be deduced from Formulae (4.21).

The theory is fully developed in Appendices J and K, where the reader can also find technical details about the calculations, more numerical examples of tunnelling potentials and extensive discussion. The Appendices further discuss a possible complex extension of classical mechanics that offers a straightforward interpretation of the complex tunnelling time: the particle moves forward in the real time in classically allowed regions of the potential, but they tunnel in the imaginary time with imaginary momentum through the classically forbidden regions. The position of the tunnelling particle stays real in all regions.

Chapter 5

Summary and Outlook

This thesis presented the main three branches of our ongoing research in collective many-body physics: critical phenomena (quantum phase transitions and excited-state quantum phase transitions), classical-quantum correspondence in chaos theory and non-Hermitian extensions of quantum mechanics. The intention was to give a brief but clear and summarising introduction to the individual areas and demonstrate how these areas are interconnected and how one can help to understand the other, which is usually not possible in specialised papers. However, the main text is firmly based on and tightly related to the selection of published works reprinted in the Appendices, which give thorough rigorous analyses of specific problems.

Each of the three main lines of research is still being developed and pushed further. Let us conclude this thesis by mentioning some open questions and directions for further development.

Concerning the ESQPTs, an interesting open question is how these critical phenomena are connected to other recently introduced concepts, such as the Dynamical Quantum Phase Transitions (DQPTs). There are some indications that there is, indeed, a relation, especially between the ESQPTs and the DQPTs of type I [198]. However, the connection can be more profound and can be fruitfully studied by the complex extension of the survival probability [54]. Another field of study stems from the fact that so far, it has been shown that ESQPTs can practically be observed only if the effective number of degrees of freedom is low (the ESQPT singularities appear in low derivatives of the level density and other affected quantities), which is often connected with a high degree of collectivity in the dynamics. However, would there be any way to extend the ESQPT concept into non-collective many-body systems, often without a classical limit? Active current research by our group also tries to elucidate what could be the optimal quantum driving (adiabatic or nonadiabatic) in the presence of the QPTs or ESQPTs. We are also working on the classification of ESQPT singularities connected with the boundary of the compact phase space in algebraic collective models, where the compactness can be related to the existence of an additional integral of motion. One can also ask whether the analogues of ESQPTs exist in periodic lattice systems or in periodically driven systems. And what happens if the system with an ESQPT is not isolated, but interacts with an environment and decoheres? How does the presence of the ESQPTs affect thermodynamics, especially canonical thermodynamics?

In the area of quantum chaos, we are currently elaborating on the theory of relative asymptotic oscillations and plan to extend the analysis to (i) many-body systems with

local interaction, and (ii) other than microcanonical OTOCs, especially the OTOCs in coherent states, which is highly relevant experimentally. Also, there have been introduced recently the concept of quantum many-body scars [199]—an extension of quantum scars as an increased localisation of some wave functions around classically unstable periodic orbits [200]—so a natural question arises how the scarring is imprinted in the OTOCs. Some case studies are already known [156, 162]

Finally, the complex extensions and non-Hermitian approach to quantum mechanics offer a profound theoretical tool that has not been fully exploited yet. We plan to focus on the distribution of zeros in the survival probability extended for complex times, which seems promising for understanding the connection between the ESQPTs and DQPTs.

List of Author's Publications

(In chronological order)

[1] P. Cejnar and P. Stránský, "Regular and chaotic vibrations of deformed nuclei with increasing γ rigidity", Physical Review Letters **93**, 102502 (2004).

[2] P. Cejnar, M. Macek, P. Stránský, and M. Kurian, "Regular and chaotic nuclear vibrations", in Capture gamma-ray spectroscopy and related topics: 12th international symposium, Vol. 819, edited by A. Woehr and A. Aprahamian, AIP Conference Proceedings (2006), pp. 487–492.

[3] P. Stránský, M. Kurian, and P. Cejnar, "Classical chaos in the geometric collective model", Physical Review C **74**, 014306 (2006).

[4] M. Macek, P. Stránský, P. Cejnar, S. Heinze, J. Jolie, and J. Dobeš, "Classical and quantum properties of the semiregular arc inside the Casten triangle", Physical Review C **75**, 064318 (2007).

[5] P. Stránský, P. Cejnar, and M. Macek, "Order and chaos in the geometric collective model", Physics of Atomic Nuclei **70**, 1572–1576 (2007).

[6] M. Macek, P. Stránský, and P. Cejnar, "Order and chaos in the interacting boson model", Physics of Atomic Nuclei **70**, 1592–1596 (2007).

[7] P. Cejnar and P. Stránský, "Impact of quantum phase transitions on excited-level dynamics", Physical Review E **78**, 031130 (2008).

[8] P. Cejnar, P. Stránský, and M. Macek, "Quantum phase transitions and nuclear structure", International Journal of Modern Physics E **18**, 965–974 (2009).

[9] M. Macek, P. Stránský, and P. Cejnar, "Peres lattices in nuclear structure", International Journal of Modern Physics E **18**, 1058–1061 (2009).

[10] P. Stránský, P. Hruška, and P. Cejnar, "Quantum chaos in the nuclear collective model: Classical-quantum correspondence", Physical Review E **79**, 046202 (2009).

[11] P. Stránský, P. Hruška, and P. Cejnar, "Quantum chaos in the nuclear collective model: II. Peres lattices", Physical Review E **79**, 066201 (2009).

[12] P. Cejnar and P. Stránský, "Quantum phase transitions for excited states", in Capture gamma-ray spectroscopy and related topics: 13th international symposium, Vol. 1090, edited by A. Blazhev, J. Jolie, N. Warr, and A. Zilges, AIP Conference Proceedings (2009), pp. 169–173.

[13] P. Stránský, M. Macek, P. Cejnar, and J. Dobeš, "Peres lattices in nuclear structure and beyond", in Capture gamma-ray spectroscopy and related topics: 13th international symposium, Vol. 1090, edited by A. Blazhev, J. Jolie, N. Warr, and A. Zilges, AIP Conference Proceedings (2009), pp. 174–178.

[14] M. Macek, J. Dobeš, P. Stránský, and P. Cejnar, "Regularity-induced separation of intrinsic and collective dynamics", Physical Review Letters 105, 072503 (2010).

[15] P. Stránský, M. Macek, P. Cejnar, A. Frank, R. Fossion, and E. Landa, "Chaotic dynamics in collective models of nuclei", in XXXIII symposium on nuclear physics, Vol. 239, edited by L. Barrón-Palos, R. Bijker, R. Fossion, and D. Lizcano, Journal of Physics: Conference Series (July 2010), p. 012002.

[16] R. Fossion, E. Landa, P. Stránský, V. Velázquez, J. C. L. Vieyra, I. Garduño, D. García, and A. Frank, "Scale invariance as a symmetry in physical and biological systems: listening to photons, bubbles and heartbeats", in Symmetries in nature: symposium in memoriam Marcos Moshinsky, Vol. 1323, edited by L. Benet, P. O. Hess, J. M. Torres, and K. B. Wolf, AIP Conference Proceedings (2010), pp. 74–90.

[17] P. Cejnar, P. Stránský, and M. Macek, "Regular and chaotic collective modes in nuclei", Nuclear Physics News 21, 22–27 (2011).

[18] I. O. Morales, E. Landa, P. Stránský, and A. Frank, "Improved unfolding by detrending of statistical fluctuations in quantum spectra", Physical Review E 84, 016203 (2011).

[19] E. Landa, I. O. Morales, R. Fossion, P. Stránský, V. Velázquez, J. C. L. Vieyra, and A. Frank, "Criticality and long-range correlations in time series in classical and quantum systems", Physical Review E 84, 016224 (2011).

[20] P. Cejnar, M. Macek, and P. Stránský, "Symmetry vs. chaos in collective dynamics", International Journal of Modern Physics E 20, 213–218 (2011).

[21] E. Landa, I. O. Morales, P. Stránský, R. Fossion, V. Velázquez, J. C. L. Vieyra, and A. Frank, "Scale invariance in chaotic time series: Classical and quantum examples", in Chaos theory: Modeling, simulation and application, edited by C. H. Skiadas, I. Dimotikalis, and C. Skiadas (May 2011), pp. 247–254.

[22] P. Stránský, M. Macek, P. Cejnar, A. Frank, R. Fossion, and E. Landa, "Manifestation of chaos in collective models of nuclei", in Chaos theory: Modeling, simulation and application, edited by C. H. Skiadas, I. Dimotikalis, and C. Skiadas (May 2011), pp. 406–413.

[23] P. Stránský, A. Frank, and R. Bijker, "On prolate shape predominance in nuclear deformation", in XXXIV symposium on nuclear physics, Vol. 322, edited by L. Barrón-Palos and R. Bijker, Journal of Physics: Conference Series (Oct. 2011), p. 012018.

[24] M. J. Ermamatov, P. C. Srivastava, P. R. Fraser, P. Stránský, and I. O. Morales, "Coriolis contribution to excited states of deformed ^{163}Dy and ^{173}Yb nuclei with multiple mass parameters", Physical Review C 85, 034307 (2012).

[25] M. J. Ermamatov, P. C. Srivastava, P. R. Fraser, and P. Stránský, "Ground-state, β and $K = 11/2^-$ γ bands in ^{163,165}Er", The European Physical Journal A 48, 123 (2012).

[26] E. Landa, I. O. Morales, P. Stránský, and A. Frank, "Manifestation of scale invariance in the spectral fluctuations of random matrices", Physical Review E **87**, 032919 (2013).

[27] P. Stránský, R. Bijker, and A. Frank, "Collective description of the prolate shape predominance in nuclear deformation", in Capture gamma-ray spectroscopy and related topics, edited by P. E. Garrett and B. Hadinia (Apr. 2013), pp. 21–26.

[28] P. Cejnar and P. Stránský, "Understanding chaos via nuclei", in Latin-American school of physics Marcos Moshinsky ELAF: Nonlinear dynamics in Hamiltonian systems, Vol. 1575, edited by R. Bijker, O. Castaños, R. Jáuregui, R. Lemus, and O. Rosas-Ortiz, AIP Conference Proceedings (2014), pp. 23–49.

[29] P. Stránský, M. Macek, and P. Cejnar, "Excited-state quantum phase transitions in systems with two degrees of freedom: Level density, level dynamics, thermal properties", Annals of Physics **345**, 73–97 (2014).

[30] P. Stránský, M. Macek, A. Leviatan, and P. Cejnar, "Excited-state quantum phase transitions in systems with two degrees of freedom: II. Finite-size effects", Annals of Physics **356**, 57–82 (2015).

[31] P. Stránský and P. Cejnar, "Study of a curvature-based criterion for chaos in Hamiltonian systems with two degrees of freedom", Journal of Physics A: Mathematical and Theoretical **48**, 125102 (2015).

[32] P. Stránský and P. Cejnar, "Geometric criterion for chaos in collective dynamics of nuclei", Physica Scripta **90**, 114014 (2015).

[33] P. Cejnar, P. Stránský, and M. Kloc, "Excited-state quantum phase transitions in finite many-body systems", Physica Scripta **90**, 114015 (2015).

[34] P. Stránský and P. Cejnar, "Classification of excited-state quantum phase transitions for arbitrary number of degrees of freedom", Physics Letters A **380**, 2637–2643 (2016).

[35] P. Cejnar and P. Stránský, "Quantum phase transitions in the collective degrees of freedom: nuclei and other many-body systems", Physica Scripta **91**, 083006 (2016).

[36] P. Cejnar and P. Stránský, "Heat capacity for systems with excited-state quantum phase transitions", Physics Letters A **381**, 984–990 (2017).

[37] M. Kloc, P. Stránský, and P. Cejnar, "Quantum phases and entanglement properties of an extended Dicke model", Annals of Physics **382**, 85–111 (2017).

[38] M. Kloc, P. Stránský, and P. Cejnar, "Monodromy in Dicke superradiance", Journal of Physics A: Mathematical and Theoretical **50**, 315205 (2017).

[39] P. Stránský, M. Kloc, and P. Cejnar, "Excited-state quantum phase transitions and their manifestations in an extended Dicke model", in Nuclei and mesoscopic physics, Vol. 1912, edited by P. Danielewicz and V. Zelevinsky, AIP Conference Proceedings (2017), p. 020018.

[40] P. Stránský, M. Dvořák, and P. Cejnar, "Exceptional points near first- and second-order quantum phase transitions", Physical Review E **97**, 012112 (2018).

[41] M. Kloc, P. Stránský, and P. Cejnar, "Quantum quench dynamics in Dicke superradiance models", Physical Review A **98**, 013836 (2018).

[42]J. Chávez-Carlos, B. López-del-Carpio, M. A. Bastarrachea-Magnani, P. Stránský, S. Lerma-Hernández, L. F. Santos, and J. G. Hirsch, "Quantum and classical Lyapunov exponents in atom-field interaction systems", Physical Review Letters **122**, 024101 (2019).

[43]M. Macek, P. Stránský, A. Leviatan, and P. Cejnar, "Excited-state quantum phase transitions in systems with two degrees of freedom. III. Interacting boson systems", Physical Review C **99**, 064323 (2019).

[44]P. Stránský and P. Cejnar, "Superradiance in finite quantum systems randomly coupled to continuum", Physical Review E **100**, 042119 (2019).

[45]P. Cejnar, P. Stránský, M. Kloc, and M. Macek, "Static vs. dynamic phases of quantum many-body systems", in Symmetries and order: algebraic methods in many body systems, Vol. 2150, edited by R. Maruyama, AIP Conference Proceedings (2019), p. 020017.

[46]M. Macek, P. Cejnar, P. Stránský, J. Dobeš, and A. Leviatan, "Order, chaos and (quasi-) dynamical symmetries across 1-st order quantum phase transitions in nuclei", in Symmetries and order: algebraic methods in many body systems, Vol. 2150, edited by R. Maruyama, AIP Conference Proceedings (2019), p. 050001.

[47]S. Pilatowsky-Cameo, J. Chávez-Carlos, M. A. Bastarrachea-Magnani, P. Stránský, S. Lerma-Hernández, L. F. Santos, and J. G. Hirsch, "Positive quantum Lyapunov exponents in experimental systems with a regular classical limit", Physical Review E **101**, 010202 (2020).

[48]P. Stránský, M. Šindelka, M. Kloc, and P. Cejnar, "Complex density of continuum states in resonant quantum tunneling", Physical Review Letters **125**, 020401 (2020).

[49]P. Cejnar, P. Stránský, M. Macek, and M. Kloc, "Excited-state quantum phase transitions", Journal of Physics A: Mathematical and Theoretical **54**, 133001 (2021).

[50]M. Kloc, D. Šimsa, F. Hanák, P. R. Kaprálová-Žďánská, P. Stránský, and P. Cejnar, "Quasiclassical approach to quantum quench dynamics in the presence of an excited-state quantum phase transition", Physical Review A **103**, 032213 (2021).

[51]P. Stránský, M. Šindelka, and P. Cejnar, "Continuum analogs of excited-state quantum phase transitions", Physical Review A **103**, 062207 (2021).

[52]P. Stránský, P. Cejnar, and R. Filip, "Stabilization of product states and excited-state quantum phase transitions in a coupled qubit-field system", Physical Review A **104**, 053722 (2021).

[53]F. Matus, J. Střeleček, P. Stránský, and P. Cejnar, "Search for optimal driving in finite quantum systems with precursors of criticality", Physical Review A **107**, 012216 (2023).

[54]Á. L. Corps, P. Stránský, and P. Cejnar, "Mechanism of dynamical phase transitions: The complex-time survival amplitude", Physical Review B **107**, 094307 (2023).

[55]M. Šindelka, P. Stránský, and P. Cejnar, "Equations of motion governing the dynamics of the exceptional points of parameterically dependent nonhermitian Hamiltonians", Journal of Physics A: Mathematical and Theoretical **56**, 145201 (2023).

[56]P. Cejnar, P. Stránský, J. Střeleček, and F. Matus, "Decoherence-assisted quantum driving", Physical Review A **107**, L030603 (2023).

[57]J. Novotný and P. Stránský, "Relative asymptotic oscillations of the out-of-time-ordered correlator as a quantum chaos indicator", Physical Review E **107**, 054220 (2023).

Bibliography

[58]R. Filip, *Private communication*, 2020.

[59]S. Sachdev, *Quantum Phase Transitions*, 2nd ed. (Cambridge University Press, Cambridge, 2011).

[60]L. Carr, *Understanding quantum phase transitions*, edited by L. Carr (CRC Press, Nov. 2011), p. 728.

[61]G. Jaeger, "The Ehrenfest Classification of Phase Transitions: Introduction and Evolution", Archive for History of Exact Sciences **53**, 51–81 (1998).

[62]A. Polkovnikov, K. Sengupta, A. Silva, and M. Vengalattore, "Colloquium: Nonequilibrium dynamics of closed interacting quantum systems", Reviews of Modern Physics **83**, 863–883 (2011).

[63]W. Huang, M. Wang, F. Kondev, G. Audi, and S. Naimi, "The AME 2020 atomic mass evaluation (i). evaluation of input data, and adjustment procedures", Chinese Physics C **45**, 030002 (2021).

[64]M. Wang, W. Huang, F. Kondev, G. Audi, and S. Naimi, "The AME 2020 atomic mass evaluation (II). tables, graphs and references", Chinese Physics C **45**, 030003 (2021).

[65]C. F. v. Weizsäcker, "Zur Theorie der Kernmassen", de, Zeitschrift für Physik **96**, 431–458 (1935).

[66]A. E. L. Dieperink, O. Scholten, and F. Iachello, "Classical Limit of the Interacting-Boson Model", Physical Review Letters **44**, 1747–1750 (1980).

[67]N. J. Stone, "Table of nuclear magnetic dipole and electric quadrupole moments", Atomic Data and Nuclear Data Tables **90**, 75–176 (2005).

[68]P. Cejnar, J. Jolie, and R. F. Casten, "Quantum phase transitions in the shapes of atomic nuclei", Reviews of Modern Physics **82**, 2155–2212 (2010).

[69]P. Cejnar, M. Macek, S. Heinze, J. Jolie, and J. Dobeš, "Monodromy and excited-state quantum phase transitions in integrable systems: collective vibrations of nuclei", Journal of Physics A: Mathematical and General **39**, L515 (2006).

[70]M. Caprio, P. Cejnar, and F. Iachello, "Excited state quantum phase transitions in many-body systems", Annals of Physics **323**, 1106–1135 (2008).

[71]K. Baumann, C. Guerlin, F. Brennecke, and T. Esslinger, "Dicke quantum phase transition with a superfluid gas in an optical cavity", Nature **464**, 1301–1306 (2010).

[72]M. P. Baden, K. J. Arnold, A. L. Grimsmo, S. Parkins, and M. D. Barrett, "Realization of the Dicke Model Using Cavity-Assisted Raman Transitions", Physical Review Letters **113**, 020408 (2014).

[73]R. J. Lewis-Swan, A. Safavi-Naini, J. J. Bollinger, and A. M. Rey, "Unifying scrambling, thermalization and entanglement through measurement of fidelity out-of-time-order correlators in the dicke model", Nature Communications **10**, 10.1038/s41467-019-09436-y (2019).

[74]M. A. Quiroz-Juárez, J. Chávez-Carlos, J. L. Aragón, J. G. Hirsch, and R. d. J. León-Montiel, "Experimental realization of the classical Dicke model", Physical Review Research **2**, 033169 (2020).

[75]X. Li, D. Dreon, P. Zupancic, A. Baumgärtner, A. Morales, W. Zheng, N. R. Cooper, T. Donner, and T. Esslinger, "First order phase transition between two centro-symmetric superradiant crystals", Physical Review Research **3**, L012024 (2021).

[76]M. Heyl, "Dynamical quantum phase transitions: a review", Reports on Progress in Physics **81**, 054001 (2018).

[77]F. Haake, *Quantum signatures of chaos* (Springer Berlin Heidelberg, 2010).

[78]V. Ivrii, "100 years of Weyl's law", Bulletin of Mathematical Sciences **6**, 379–452 (2016).

[79]M. C. Gutzwiller, *Chaos in classical and quantum mechanics* (Springer New York, 1990).

[80]M. Morse, *Calculus of variations in the large*, Vol. 18, Colloquium Publications (American Mathematical Society, 1934), p. 368.

[81]J. Milnor, *Morse theory*, Vol. 51, Annals of Mathematic Studies (Princeton University Press, 1963), p. 160.

[82]M. Pettini, *Geometry and topology in hamiltonian dynamics and statistical mechanics*, Interdisciplinary Applied Mathematics (Springer, 2007), p. 456.

[83]M. Audin and M. Damian, *Morse theory and floer homology*, Universitext 1, Original French edition published by EDP Sciences, Les Ulis Cedex A, France, 2010 (Springer London, 2014).

[84]M. Kastner, "Phase transitions and configuration space topology", Reviews of Modern Physics **80**, 167–187 (2008).

[85]B. Dietz, F. Iachello, and M. Macek, "Algebraic Theory of Crystal Vibrations: Localization Properties of Wave Functions in Two-Dimensional Lattices", Crystals **7**, 246 (2017).

[86]I. Stewart, "Catastrophe theory in physics", Reports on Progress in Physics **45**, 185 (1982).

[87]S. C. Creagh and N. D. Whelan, "Complex Periodic Orbits and Tunneling in Chaotic Potentials", Physical Review Letters **77**, 4975–4979 (1996).

[88]P. Stránský, *Dynamics of the Creagh-Whelan potential*, https://pavelstransky.cz/cw.php, [online].

[89] H. J. Lipkin, N. Meshkov, and A. J. Glick, "Validity of many-body approximation methods for a solvable model: (I). Exact solutions and perturbation theory", Nuclear Physics **62**, 188–198 (1965).

[90] N. Meshkov, A. J. Glick, and H. J. Lipkin, "Validity of many-body approximation methods for a solvable model: (II). Linearization procedures", Nuclear Physics **62**, 199–210 (1965).

[91] A. J. Glick, H. J. Lipkin, and N. Meshkov, "Validity of many-body approximation methods for a solvable model: (III). Diagram summations", Nuclear Physics **62**, 211–224 (1965).

[92] F. Iachello, *Lie algebras and applications*, Lecture Notes in Physics (Springer Berlin Heidelberg, 2015), p. 272.

[93] F. Iachello and A. Arima, *The interacting boson model*, Cambridge Monographs on Mathematical Physics (Cambridge University Press, Cambridge, Aug. 1987).

[94] E. Ising, "Beitrag zur Theorie des Ferromagnetismus", de, Zeitschrift für Physik **31**, 253–258 (1925).

[95] A. Zymin, "Quasispin models in quantum physics", Bachelor thesis (Faculty of Mathematics and Physics, Charles University, Prague, Czech Republic, 2019).

[96] J. P. Blaizot and E. R. Marshalek, "Boson expansions and quantization of time-dependent self-consistent fields (I). Particle-hole excitations", Nuclear Physics A **309**, 422–452 (1978).

[97] P. S. Jakub Novotný Pavel Cejnar, In preparation.

[98] F. Iachello, *Algebraic theory of molecules* (Oxford University Press, Apr. 1995), p. 243.

[99] F. Iachello and S. Oss, "Algebraic approach to molecular spectra: two-dimensional problems", The Journal of Chemical Physics **104**, 6956–6963 (1996).

[100] D. Larese, F. Pérez-Bernal, and F. Iachello, "Signatures of quantum phase transitions and excited state quantum phase transitions in the vibrational bending dynamics of triatomic molecules", Journal of Molecular Structure **1051**, 310–327 (2013).

[101] F. Pérez-Bernal and F. Iachello, "Algebraic approach to two-dimensional systems: shape phase transitions, monodromy, and thermodynamic quantities", Physical Review A **77**, 032115 (2008).

[102] J. Khalouf-Rivera, F. Pérez-Bernal, and M. Carvajal, "Anharmonicity-induced excited-state quantum phase transition in the symmetric phase of the two-dimensional limit of the vibron model", Physical Review A **105**, 032215 (2022).

[103] M. Rautenberg and M. Gärttner, "Classical and quantum chaos in a three-mode bosonic system", Physical Review A **101**, 053604 (2020).

[104] C. S. Gerving, T. M. Hoang, B. J. Land, M. Anquez, C. D. Hamley, and M. S. Chapman, "Non-equilibrium dynamics of an unstable quantum pendulum explored in a spin-1 Bose–Einstein condensate", Nature Communications **3**, 1169 (2012).

[105] P. Kunkel, M. Prüfer, H. Strobel, D. Linnemann, A. Frölian, T. Gasenzer, M. Gärttner, and M. K. Oberthaler, "Spatially distributed multipartite entanglement enables EPR steering of atomic clouds", Science **360**, 413–416 (2018).

[106]F. Iachello and R. D. Levine, "Algebraic approach to molecular rotation-vibration spectra. i. diatomic molecules", The Journal of Chemical Physics **77**, 3046–3055 (1982).

[107]M. M. Estévez-Fregoso and R. Lemus, "Connection between the su(3) algebraic and configuration spaces: bending modes of linear molecules", Molecular Physics **116**, 2374–2395 (2018).

[108]E. Wigner, "On the quantum correction for thermodynamic equilibrium", Physical Review **40**, 749–759 (1932).

[109]M. Hillery, R. F. O'Connell, M. O. Scully, and E. P. Wigner, "Distribution functions in physics: Fundamentals", Physics Reports **106**, 121–167 (1984).

[110]D. F. Walls and G. J. Milburn, *Quantum optics*, edited by D. Walls and G. J. Milburn (Springer Berlin Heidelberg, 2008), p. 350.

[111]L. E. Reichl, *A Modern Course in Statistical Physics* (Wiley, 2016).

[112]M. A. Bastarrachea-Magnani, S. Lerma-Hernández, and J. G. Hirsch, "Thermal and quantum phase transitions in atom-field systems: a microcanonical analysis", en, Journal of Statistical Mechanics: Theory and Experiment **2016**, 093105 (2016).

[113]P. Pérez-Fernández and A. Relaño, "From thermal to excited-state quantum phase transition: The Dicke model", Physical Review E **96**, 012121 (2017).

[114]P. Stránský, "Classical and quantum chaos in atomic nuclei", PhD thesis (Faculty of Mathematics and Physics, Charles University, Prague, Czech Republic, June 2009).

[115]M. Tabor, *Chaos and integrability in nonlinear dynamics, An introduction* (Wiley, 1989), p. 364.

[116]L. E. Reichl, *The transition to chaos* (Springer New York, 2004).

[117]W. B. Hayes, "Is the outer Solar System chaotic?", Nature Physics **3**, 689–691 (2007).

[118]J. Laskar and M. Gastineau, "Existence of collisional trajectories of Mercury, Mars and Venus with the Earth", Nature **459**, 817–819 (2009).

[119]G. Brown and H. Rein, "A Repository of Vanilla Long-term Integrations of the Solar System", Research Notes of the AAS **4**, 221 (2020).

[120]E. N. Lorenz, *The Essence of Chaos* (University of Washington Press, 1995).

[121]A. N. Kolmogorov, "Preservation of conditionally periodic movements with small change in the Hamilton function", en, in Stochastic Behavior in Classical and Quantum Hamiltonian Systems, Vol. 93, edited by G. Casati and J. Ford, Lecture Notes in Physics (1979), pp. 51–56.

[122]J. Moser, "On invariant curves of area-preserving mappings of an annulus", Nachrichten der Akademie der Wissenschaften zu Göttingen, Mathematisch-Physikalische Klasse **1962**, 1–20 (1962).

[123]V. I. Arnol'd, "Proof of a theorem of A.N. Kolmogorov on the invariance of quasi-periodic motions under small perturbations of the Hamiltonian", Russian Mathematical Surveys **18**, 9 (1963).

[124]M. V. Berry and M. Robnik, "Semiclassical level spacings when regular and chaotic orbits coexist", Journal of Physics A: Mathematical and General **17**, 2413 (1984).

[125] G. Contopoulos and M. Harsoula, "Stickiness effects in conservative systems", International Journal of Bifurcation and Chaos **20**, 2005–2043 (2010).

[126] B. Mandelbrot, "How long is the coast of britain? statistical self-similarity and fractional dimension", Science **156**, 636–638 (1967).

[127] A. Husain, J. Reddy, D. Bisht, and M. Sajid, "Fractal dimension of coastline of australia", Scientific Reports **11**, 10.1038/s41598-021-85405-0 (2021).

[128] J. J. Duistermaat, "On global action-angle coordinates", Communications on Pure and Applied Mathematics **33**, 687–706 (1980).

[129] N. W. Evans, "Superintegrability in classical mechanics", Physical Review A **41**, 5666–5676 (1990).

[130] O. Bohigas, M. J. Giannoni, and C. Schmit, "Characterization of chaotic quantum spectra and universality of level fluctuation laws", Physical Review Letters **52**, 1–4 (1984).

[131] M. L. Mehta, *Random matrices, volume 142, third edition (pure and applied mathematics)* (Elsevier, Academic Press, 2004), p. 706.

[132] M. V. Berry, "Semiclassical theory of spectral rigidity", Proceedings of the Royal Society of London. A. Mathematical and Physical Sciences **400**, 229–251 (1985).

[133] A. Relaño, J. M. G. Gómez, R. A. Molina, J. Retamosa, and E. Faleiro, "Quantum chaos and 1/f noise", Physical Review Letters **89**, 244102 (2002).

[134] C. E. Porter, *Statistical theories of spectra fluctuations, Fluctuations* (Academic Press, 1965).

[135] M. Berry, "Quantum chaology, not quantum chaos", Physica Scripta **40**, 335 (1989).

[136] S. Weigert, "The problem of quantum integrability", Physica D: Nonlinear Phenomena **56**, 107–119 (1992).

[137] P. Šeba, "Wave chaos in singular quantum billiard", Physical Review Letters **64**, 1855–1858 (1990).

[138] A. Relaño, J. Dukelsky, J. M. G. Gómez, and J. Retamosa, "Stringent numerical test of the poisson distribution for finite quantum integrable hamiltonians", Physical Review E **70**, 026208 (2004).

[139] E. P. Wigner, "On the statistical distribution of the widths and spacings of nuclear resonance levels", Mathematical Proceedings of the Cambridge Philosophical Society **47**, 790–798 (1951).

[140] E. P. Wigner, "Characteristic Vectors of Bordered Matrices With Infinite Dimensions", Annals of Mathematics **62**, 548–564 (1955).

[141] E. P. Wigner, "Characteristics Vectors of Bordered Matrices with Infinite Dimensions II", Annals of Mathematics **65**, 203–207 (1957).

[142] J. M. G. Gómez, R. A. Molina, A. Relaño, and J. Retamosa, "Misleading signatures of quantum chaos", Physical Review E **66**, 036209 (2002).

[143] R. Fossion, G. T. Vargas, and J. C. L. Vieyra, "Random-matrix spectra as a time series", Physical Review E **88**, 060902 (2013).

[144]Y. Y. Atas, E. Bogomolny, O. Giraud, and G. Roux, "Distribution of the ratio of consecutive level spacings in random matrix ensembles", Physical Review Letters **110**, 084101 (2013).

[145]Y. Y. Atas, E. Bogomolny, O. Giraud, P. Vivo, and E. Vivo, "Joint probability densities of level spacing ratios in random matrices", Journal of Physics A: Mathematical and Theoretical **46**, 355204 (2013).

[146]J. Maldacena, S. H. Shenker, and D. Stanford, "A bound on chaos", Journal of High Energy Physics **2016**, 106 (2016).

[147]D. A. Roberts and B. Swingle, "Lieb-Robinson Bound and the Butterfly Effect in Quantum Field Theories", Physical Review Letters **117**, 091602 (2016).

[148]E. M. Fortes, I. García-Mata, R. A. Jalabert, and D. A. Wisniacki, "Gauging classical and quantum integrability through out-of-time-ordered correlators", Physical Review E **100**, 042201 (2019).

[149]K. Hashimoto, K. Murata, and R. Yoshii, "Out-of-time-order correlators in quantum mechanics", Journal of High Energy Physics **2017**, 138 (2017).

[150]A. Larkin and Y. Ovchinnikov, "Quasiclassical method in the theory of superconductivity", Soviet Journal of Experimental and Theoretical Physics **28**, 1200 (1969).

[151]S. H. Shenker and D. Stanford, "Black holes and the butterfly effect", Journal of High Energy Physics **2014**, 67 (2014).

[152]B. Swingle, "Unscrambling the physics of out-of-time-order correlators", Nature Physics **14**, 988–990 (2018).

[153]B. Yan, L. Cincio, and W. H. Zurek, "Information scrambling and loschmidt echo", Physical Review Letters **124**, 160603 (2020).

[154]F. Borgonovi and F. M. Izrailev, "Emergence of correlations in the process of thermalization of interacting bosons", Physical Review E **99**, 012115 (2019).

[155]R. A. Kidd, A. Safavi-Naini, and J. F. Corney, "Saddle-point scrambling without thermalization", Physical Review A **103**, 033304 (2021).

[156]D. Yuan, S.-Y. Zhang, Y. Wang, L.-M. Duan, and D.-L. Deng, "Quantum information scrambling in quantum many-body scarred systems", Physical Review Research **4**, 023095 (2022).

[157]X. Mi, P. Roushan, C. Quintana, S. Mandrà, J. Marshall, C. Neill, F. Arute, K. Arya, J. Atalaya, R. Babbush, J. C. Bardin, R. Barends, J. Basso, A. Bengtsson, S. Boixo, A. Bourassa, M. Broughton, B. B. Buckley, D. A. Buell, B. Burkett, N. Bushnell, Z. Chen, B. Chiaro, R. Collins, W. Courtney, S. Demura, A. R. Derk, A. Dunsworth, D. Eppens, C. Erickson, E. Farhi, A. G. Fowler, B. Foxen, C. Gidney, M. Giustina, J. A. Gross, M. P. Harrigan, S. D. Harrington, J. Hilton, A. Ho, S. Hong, T. Huang, W. J. Huggins, L. B. Ioffe, S. V. Isakov, E. Jeffrey, Z. Jiang, C. Jones, D. Kafri, J. Kelly, S. Kim, A. Kitaev, P. V. Klimov, A. N. Korotkov, F. Kostritsa, D. Landhuis, P. Laptev, E. Lucero, O. Martin, J. R. McClean, T. McCourt, M. McEwen, A. Megrant, K. C. Miao, M. Mohseni, S. Montazeri, W. Mruczkiewicz, J. Mutus, O. Naaman, M. Neeley, M. Newman, M. Y. Niu, T. E. O'Brien, A. Opremcak, E. Ostby, B. Pato, A. Petukhov, N. Redd, N. C. Rubin, D. Sank, K. J. Satzinger, V. Shvarts, D. Strain,

M. Szalay, M. D. Trevithick, B. Villalonga, T. White, Z. J. Yao, P. Yeh, A. Zalcman, H. Neven, I. Aleiner, K. Kechedzhi, V. Smelyanskiy, and Y. Chen, "Information scrambling in quantum circuits", Science **374**, 1479–1483 (2021).

[158]J. M. Deutsch, "Quantum statistical mechanics in a closed system", Physical Review A **43**, 2046–2049 (1991).

[159]M. Srednicki, "Chaos and quantum thermalization", Physical Review E **50**, 888–901 (1994).

[160]E. B. Rozenbaum, S. Ganeshan, and V. Galitski, "Lyapunov Exponent and Out-of-Time-Ordered Correlator's Growth Rate in a Chaotic System", Physical Review Letters **118**, 086801 (2017).

[161]E. B. Rozenbaum, S. Ganeshan, and V. Galitski, "Universal level statistics of the out-of-time-ordered operator", Physical Review B **100**, 035112 (2019).

[162]S. Pilatowsky-Cameo, D. Villaseñor, M. A. Bastarrachea-Magnani, S. Lerma-Hernández, L. F. Santos, and J. G. Hirsch, "Ubiquitous quantum scarring does not prevent ergodicity", Nature Communications **12**, `10.1038/s41467-021-21123-5` (2021).

[163]J. Novotný, "Řád a chaos v jednoduchém modelu molekulárních vibrací", MA thesis (Faculty of Mathematics and Physics, Charles University, Prague, Czech Republic, 2020).

[164]E. B. Rozenbaum, L. A. Bunimovich, and V. Galitski, "Early-time exponential instabilities in nonchaotic quantum systems", Physical Review Letters **125**, 014101 (2020).

[165]P. Pérez-Fernández, P. Cejnar, J. M. Arias, J. Dukelsky, J. E. García-Ramos, and A. Relaño, "Quantum quench influenced by an excited-state phase transition", Physical Review A **83**, 033802 (2011).

[166]J. von Neumann and E. P. Wigner, "Über das verhalten von eigenwerten bei adiabatischen prozessen", Physik Zeitschrift **30**, 465 (1929).

[167]N. Moiseyev, *Non-hermitian quantum mechanics* (Cambridge University Press, 2011), p. 394.

[168]M. R. Zirnbauer, J. J. M. Verbaarschot, and H. A. Weidenmüller, "Destruction of order in nuclear spectra by a residual GOE interaction", Nuclear Physics A **411**, 161–180 (1983).

[169]Plato, *The republic* (Penguin Classics, 2007), p. 480.

[170]P. Cejnar, *Private communication*, 2008.

[171]C. M. Bender and S. Boettcher, "Real Spectra in Non-Hermitian Hamiltonians Having PT Symmetry", Physical Review Letters **80**, 5243–5246 (1998).

[172]C. M. Bender, S. Boettcher, and P. N. Meisinger, "Pt-symmetric quantum mechanics", Journal of Mathematical Physics **40**, 2201–2229 (1999).

[173]A. G. Anderson, C. M. Bender, and U. I. Morone, "Periodic orbits for classical particles having complex energy", Physics Letters A **375**, 3399–3404 (2011).

[174]W. D. Heiss, "Exceptional points of a Hamiltonian and phase transitions in finite systems", Zeitschrift für Physik A Atomic Nuclei **329**, 133–138 (1988).

[175] W. D. Heiss and M. Müller, "Universal relationship between a quantum phase transition and instability points of classical systems", Physical Review E **66**, 016217 (2002).

[176] D. I. Borisov, F. Ružička, and M. Znojil, "Multiply Degenerate Exceptional Points and Quantum Phase Transitions", International Journal of Theoretical Physics **54**, 4293–4305 (2015).

[177] M. Šindelka, L. F. Santos, and N. Moiseyev, "Excited-state quantum phase transitions studied from a non-Hermitian perspective", Physical Review A **95**, 010103 (2017).

[178] C. N. Yang and T. D. Lee, "Statistical Theory of Equations of State and Phase Transitions. I. Theory of Condensation", Physical Review **87**, 404–409 (1952).

[179] T. D. Lee and C. N. Yang, "Statistical Theory of Equations of State and Phase Transitions. II. Lattice Gas and Ising Model", Physical Review **87**, 410–419 (1952).

[180] S. Grossmann and W. Rosenhauer, "Temperature dependence near phase transitions in classical and quant. mech. canonical statistics", Zeitschrift für Physik **207**, 138–152 (1967).

[181] S. Grossmann and W. Rosenhauer, "Phase transitions and the distribution of temperature zeros of the partition function", Zeitschrift für Physik A Hadrons and nuclei **218**, 437–448 (1969).

[182] S. Grossmann and V. Lehmann, "Phase transitions and the distribution of temperature zeros of the partition function", Zeitschrift für Physik A Hadrons and nuclei **218**, 449–459 (1969).

[183] P. Cejnar, S. Heinze, and M. Macek, "Coulomb Analogy for Non-Hermitian Degeneracies near Quantum Phase Transitions", Physical Review Letters **99**, 100601 (2007).

[184] M. Dvořák, "Prekursory fázových přechodů v kvantových systémech", Master thesis (Faculty of Mathematics and Physics, Charles University, Prague, Czech Republic, 2015).

[185] H. Feshbach, "Unified theory of nuclear reactions", Annals of Physics **5**, 357–390 (1958).

[186] H. Feshbach, "A unified theory of nuclear reactions. II", Annals of Physics **19**, 287–313 (1962).

[187] P. Kleinwachter and I. Rotter, "Spectroscopic properties of highly excited states", Physical Review C **32**, 1742–1744 (1985).

[188] N. Auerbach and V. Zelevinsky, "Super-radiant dynamics, doorways and resonances in nuclei and other open mesoscopic systems", Reports on Progress in Physics **74**, 106301 (2011).

[189] R. H. Dicke, "Coherence in Spontaneous Radiation Processes", Physical Review **93**, 99–110 (1954).

[190] I. Rotter, "A continuum shell model for the open quantum mechanical nuclear system", Reports on Progress in Physics **54**, 635 (1991).

[191]C. Liu, A. Di Falco, and A. Fratalocchi, "Dicke Phase Transition with Multiple Superradiant States in Quantum Chaotic Resonators", Physical Review X **4**, 021048 (2014).

[192]I. Rotter and J. P. Bird, "A review of progress in the physics of open quantum systems: theory and experiment", Reports on Progress in Physics **78**, 114001 (2015).

[193]A. Kruppa, "Calculation of the continuum level density", Physics Letters B **431**, 237–241 (1998).

[194]A. T. Kruppa and K. Arai, "Resonances and the continuum level density", Phys. Rev. A **59**, 3556–3561 (1999).

[195]R. D. Levine, *Quantum mechanics of molecular rate processes* (Clarendon P., 1969), p. 335.

[196]E. P. Wigner, "Lower Limit for the Energy Derivative of the Scattering Phase Shift", Physical Review **98**, 145–147 (1955).

[197]M. V. Berry and K. E. Mount, "Semiclassical approximations in wave mechanics", Reports on Progress in Physics **35**, 315–397 (1972).

[198]Á. L. Corps and A. Relaño, "Dynamical and excited-state quantum phase transitions in collective systems", Physical Review B **106**, 024311 (2022).

[199]M. Serbyn, D. A. Abanin, and Z. Papić, "Quantum many-body scars and weak breaking of ergodicity", Nature Physics **17**, 675–685 (2020).

[200]E. J. Heller, "Bound-state eigenfunctions of classically chaotic hamiltonian systems: scars of periodic orbits", Physical Review Letters **53**, 1515–1518 (1984).

Appendix A

Excited-state quantum phase transitions in systems with two degrees of freedom: Level density, level dynamics, thermal properties

Abstract: Quantum systems with a finite number of freedom degrees f develop robust singularities in the energy spectrum of excited states as the system's size increases to infinity. We analyze the general form of these singularities for low f, particularly $f = 2$, clarifying the relation to classical stationary points of the corresponding potential. Signatures in the smoothed energy dependence of the quantum state density and in the flow of energy levels with an arbitrary control parameter are described along with the relevant thermodynamical consequences. The general analysis is illustrated with specific examples of excited-state singularities accompanying the first-order quantum phase transition.

The full text of the paper is not included in this version.

Appendix B

Excited-state quantum phase transitions in systems with two degrees of freedom: II. Finite-size effects

Pavel Stránský, Michal Macek, Amiram Leviatan, and Pavel Cejnar, Annals of Physics 356, 57–82 (2015).

Abstract: This article extends our previous analysis Stránský et al. (2014) of Excited-State Quantum Phase Transitions (ESQPTs) in systems of dimension two. We focus on the oscillatory component of the quantum state density in connection with ESQPT structures accompanying a first-order ground-state transition. It is shown that a separable (integrable) system can develop rather strong finite-size precursors of ESQPT expressed as singularities in the oscillatory component of the state density. The singularities originate in effectively 1-dimensional dynamics and in some cases appear in multiple replicas with increasing excitation energy. Using a specific model example, we demonstrate that these precursors are rather resistant to proliferation of chaotic dynamics.

The full text of the paper is not included in this version.

Appendix C

Excited-state quantum phase transitions in systems with two degrees of freedom. III. Interacting boson systems

Michal Macek, **Pavel Stránský**, Amiram Leviatan, and Pavel Cejnar, Physical Review C 99, 064323 (2019).

Abstract: The series of articles [Ann. Phys. **345**, 73 (2014) and **356**, 57 (2015)] devoted to excited-state quantum phase transitions (ESQPTs) in systems with $f = 2$ degrees of freedom is continued by studying the interacting boson model of nuclear collective dynamics as an example of a truly many-body system. The intrinsic Hamiltonian formalism with angular momentum fixed to $L = 0$ is used to produce a generic first-order ground-state quantum phase transition with an adjustable energy barrier between the competing equilibrium configurations. The associated ESQPTs are shown to result from various classical stationary points of the model Hamiltonian, whose analysis is more complex than in previous cases because of (i) a nontrivial decomposition to kinetic and potential energy terms and (ii) the boundedness of the associated classical phase space. Finite-size effects resulting from a partial separability of both degrees of freedom are analyzed. The features studied here are inherent in a great majority of interacting boson systems.

The full text of the paper is not included in this version.

Appendix D

Classification of excited-state quantum phase transitions for arbitrary number of degrees of freedom

Abstract: Classical stationary points of an analytic Hamiltonian induce singularities of the density of quantum energy levels and their flow with a control parameter in the system's infinite-size limit. We show that for a system with f degrees of freedom, a non-degenerate stationary point with index r causes a discontinuity (for r even) or divergence (r odd) of the $(f-1)$ th derivative of both density and flow of the spectrum. An increase of flatness for a degenerate stationary point shifts the singularity to lower derivatives. The findings are verified in an $f = 3$ toy model.

The full text of the paper is not included in this version.

Appendix E

Heat capacity for systems with excited-state quantum phase transitions

Abstract: Heat capacities of model systems with finite numbers of effective degrees of freedom are evaluated using canonical and microcanonical thermodynamics. Discrepancies between both approaches, which are observed even in the infinite-size limit, are particularly large in systems that exhibit an excited-state quantum phase transition. The corresponding irregularity of the spectrum generates a singularity in the microcanonical heat capacity and affects smoothly the canonical heat capacity.

The full text of the paper is not included in this version.

Appendix F

Exceptional points near first- and second-order quantum phase transitions

Abstract: We study the impact of quantum phase transitions (QPTs) on the distribution of exceptional points (EPs) of the Hamiltonian in the complex-extended parameter domain. Analyzing first- and second-order QPTs in the Lipkin-Meshkov-Glick model we find an exponentially and polynomially close approach of EPs to the respective critical point with increasing size of the system. If the critical Hamiltonian is subject to random perturbations of various kinds, the averaged distribution of EPs close to the critical point still carries decisive information on the QPT type. We therefore claim that properties of the EP distribution represent a parametrization-independent signature of criticality in quantum systems.

The full text of the paper is not included in this version.

Appendix G

Superradiance in finite quantum systems randomly coupled to continuum

Abstract: We study the effect of superradance in open quantum systems, i.e., the separation of short- and long-living eigenstates when a certain subspace of states in the Hilbert space acquires an increasing decay width. We use several Hamiltonian forms of the initial closed system and generate their coupling to continuum by means of the random matrix theory. We average the results over a large number of statistical realizations of an effective non-Hermitian Hamiltonian and relate robust features of the superradance process to the distribution of its exceptional points. We show that the superradance effect is enhanced if the initial system is at the point of quantum criticality.

The full text of the paper is not included in this version.

Appendix H

Quantum and Classical Lyapunov Exponents in Atom-Field Interaction Systems

Jorge Chávez-Carlos, B. López-del-Caprio, Miguel A. Bastarrache-Magnani, **Pavel Stránský**, Sergio Lerma-Hernández, Lea F. Santos, and Jorge G. Hirsch, Physical Review Letters 122, 024101 (2019).

Abstract: The exponential growth of the out-of-time-ordered correlator (OTOC) has been proposed as a quantum signature of classical chaos. The growth rate is expected to coincide with the classical Lyapunov exponent. This quantum-classical correspondence has been corroborated for the kicked rotor and the stadium billiard, which are one-body chaotic systems. The conjecture has not yet been validated for realistic systems with interactions. We make progress in this direction by studying the OTOC in the Dicke model, where two-level atoms cooperatively interact with a quantized radiation field. For parameters where the model is chaotic in the classical limit, the OTOC increases exponentially in time with a rate that closely follows the classical Lyapunov exponent.

The full text of the paper is not included in this version.

Appendix I

Positive quantum Lyapunov exponents in experimental systems with a regular classical limit

Saúl Pilatowsky-Cameo, Jorge Chávez-Carlos, Miguel A. Bastarrache-Magnani, **Pavel Stránský**, Sergio Lerma-Hernández, Lea F. Santos, and Jorge G. Hirsch, Physical Review E 101, 010202(R) (2020).

Abstract: Quantum chaos refers to signatures of classical chaos found in the quantum domain. Recently, it has become common to equate the exponential behavior of out-of-time order correlators (OTOCs) with quantum chaos. The quantum-classical correspondence between the OTOC exponential growth and chaos in the classical limit has indeed been corroborated theoretically for some systems and there are several projects to do the same experimentally. The Dicke model, in particular, which has a regular and a chaotic regime, is currently under intense investigation by experiments with trapped ions. We show, however, that for experimentally accessible parameters, OTOCs can grow exponentially also when the Dicke model is in the regular regime. The same holds for the Lipkin-Meshkov-Glick model, which is integrable and also experimentally realizable. The exponential behavior in these cases are due to unstable stationary points, not to chaos.

The full text of the paper is not included in this version.

Appendix J

Complex Density of Continuum States in Resonant Quantum Tunneling

Abstract: We introduce a complex-extended continuum level density and apply it to one-dimensional scattering problems involving tunneling through finite-range potentials. We show that the real part of the density is proportional to a real "time shift" of the transmitted particle, while the imaginary part reflects the imaginary time of an instantonlike tunneling trajectory. We confirm these assumptions for several potentials using the complex scaling method. In particular, we show that stationary points of the potentials give rise to specific singularities of both real and imaginary densities which represent close analogues of excited-state quantum phase transitions in bound systems.

The full text of the paper is not included in this version.

Appendix K

Continuum analogs of excited-state quantum phase transitions

Abstract: Following our work [Phys. Rev. Lett. 125, 020401 (2020)], we discuss a semiclassical description of one-dimensional quantum tunneling through multibarrier potentials in terms of complex time. We start by defining a complex-extended continuum level density of unbound systems and show its relation to a complex time shift of the transmitted wave. While the real part of the level density and time shift describes the passage of the particle through classically allowed coordinate regions, the imaginary part is connected with an instantonlike picture of the tunneling through forbidden regions. We describe singularities in the real and imaginary parts of the level density and time shift caused by stationary points of the tunneling potential, and show that they represent a dual extension of excited-state quantum phase transitions from bound to continuum systems. Using the complex scaling method, we numerically verify the predicted effects in several tunneling potentials.

The full text of the paper is not included in this version.

Appendix L

Relative asymptotic oscillations of the out-of-time-ordered correlator as a quantum chaos indicator

Abstract: A detailed numerical study reveals that the asymptotic values of the standard-deviation-to-mean ratio of the out-of-time-ordered correlator in energy eigenstates can be successfully used as a measure of the quantum chaoticity of the system. We employ a finite-size fully connected quantum system with two degrees of freedom, namely, the algebraic u(3) model, and demonstrate a clear correspondence between the energy-smoothed relative oscillations of the correlators and the ratio of the chaotic part of the volume of phase space in the classical limit of the system. We also show how the relative oscillations scale with the system size and conjecture that the scaling exponent can also serve as a chaos indicator.

The full text of the paper is not included in this version.